Mar 30, 2022

Hydrogeological mapping for Climate Resilient WASH in Ethiopia

Target sites Tselemt woreda, Tigray

Final report




ውኃና ኢነርጂ ሚኒስቴር
MINISTRY OF WATER AND ENERGY

ACACIA WATER

aquacon

UHL

Foreign, Commonwealth & Development Office

Colophon

Document title	.	Hydrogeological mapping for Climate Resilient WASH in Ethiopia – LOT 1
Client	.	Ministry of Water and Energy
Status	.	Final report
Date	.	Mar 30, 2022
Project number	.	201150
Authors	.	dr. Tarekegn Tadesse, dr. Dessie Nedaw, dr. Sirak Tekleab, dr. Shimelis Fisseha, dr. Maarten Waterloo, Vince Uhl
Reference		
Peer review		Jiri Sima
Released by		dr. Arjen de Vries

Table of contents

1 Introduction

The Ministry of Water and Energy has received funding from DFID for a three-year project entitled "Delivering Climate Resilient Water, Sanitation and Hygiene in Ethiopia". As agreed by an MOU between DFID and the Government of Ethiopia, two of the four programs are being implemented by the Ministry.

This project, which runs to 31 March 2022, is part of the UK government's aid strategy to support the poorest people in adapting to climate change, specifically on building climate resilience in water and sanitation services that contributes to achieving Sustainable Development Goal 6. The project complements DFID and Ethiopia's significant programming on water and sanitation and supports effective delivery of the Government of Ethiopia's strategy for sustainable water supply in drought affected areas. A key feature of this program involves funding for groundwater mapping and improvement of groundwater data management.

1.1 Objectives

Overall objective

The objective of this project is to increase access to safe and sustainable water for the people in drought affected regions by producing hydrogeological maps at the Woreda level and recommend drilling sites which the Government of Ethiopia and other partners can use for developing groundwater.

Specific objectives

A first step of this project is the initial identification of target areas for borehole drilling. The focus of this project is:

- Create detailed groundwater potential maps for each Woreda;
- Identify one optimal drilling site and one alternative (optional) drilling site per Woreda, using the groundwater potential maps and geophysical field investigation results, and recommend the type of drilling methodology(s) to be employed;
- Build the capacity of the former Water Development Commission (WDC), former Basins Development Authority (BDA), regional governments, and NGOs to use/apply overlay analysis techniques for groundwater potential mapping and borehole siting in Ethiopia.

1.2 Phases of the Project

The project is designed in 3 phases:

- Phase I (Inception Phase)
- Phase II (Mapping Phase)

- Phase III (Siting Phase)

Phase I has been completed in August 2021, Phase II in December 2021 and this report covers the work for Phase III. The siting phase (Phase III) started in December 2021, after the results from Phase II. have been validated.

The main outputs of Phase I were:

- Creation of the project team, including changes in team composition as a reaction on recent character of the project;
- Collection of basic data about existing geological and hydrogeological maps, reports, water quality and quantity data, meteorological information, demographic data, socio-economic maps produced before project started;
- Compilation of hydrogeological map at scale 1:1,000,000 and 1 : 250 000 showing hydrogeological condition of each Woreda;
- Developing conceptual hydrogeological models to complement data scarcity;
- Compilation of demographic map (1:1,000,000) showing demographic data for each Woreda;
- Preparation of field survey and investigation plans and base maps with information to be used for the Type 3a layers.

The main outputs of Phase II were:

- Groundwater potential map for every Woreda at scale 1:100,000;
- Conceptual hydrogeological models for every Woreda;
- Ground truthing and water point inventories;
- Water demand estimation in target Woredas;
- Selection of target areas (2 per Woreda);
- Risk Mitigation Strategy Document (general document).

The main outputs of Phase III are:

- A more detailed geological unit distribution, including structural details in appropriate scale, based on higher resolution images;
- Hydrogeological operational maps (1:50,000);
- Detailed geological, hydrogeological, and geophysical (including existing data and satellite geophysics) study in each target area;
- Determination of target drilling sites in the target areas, including drilling sites maps (1:5,000) and geophysical profiles;
- Phase III final report per target area, including climate resilience;
- Capitalisation report and knowledge dissemination activities in a workshop provided by the project team towards the end of the project;
- Minutes of the training on Groundwater Mapping Methodology provided by the project team;
- Inclusion water of water quality maps will be taken into account for final target area selection.

Due to the security constrains in the project area, the workplan for phase III. has been revised. The project team cannot travel to the field to carry out hydrogeological or geophysical studies. Instead, we must rely on existing data and remote sensing products. Because fieldwork is essential for updates on the actual water demand and gap analysis, geological and hydrogeological conditions, and geophysical surveys, we can only propose target sites with a certain tolerance radius, not exact drilling sites.

1.3 Project areas

The overall project covers a total of 53 Woredas throughout the country which is subdivided into four lots. The current project deals with the 13 Woredas from Lot 1 in the Tigray, Afar and Amhara Regions (Figure 1). It include 5 woredas in Afar (Afdera, Berahle, Kori Yalo and Megale); 7 woredas in Tigray (Erob, Tsadamba, Merbe Leke, Hawzien, Kola Tembian, Tselmti and Ofla) and, 1 woreda in Amahara (Beyeda) (Fig.1.). These Project locations can be accessed through the main roads to the administrative centers of the Regional states from which usually all weather, often gravel; in some cases tarred roads link the Woreda centers with the regional and zonal administrative centers (Figure 1.1). Target areas are located close to settlements (Kebeles and villages) and are also connected with the Woredas administrative centers by dry weather roads and can be accessed by four-wheel drive vehicles.

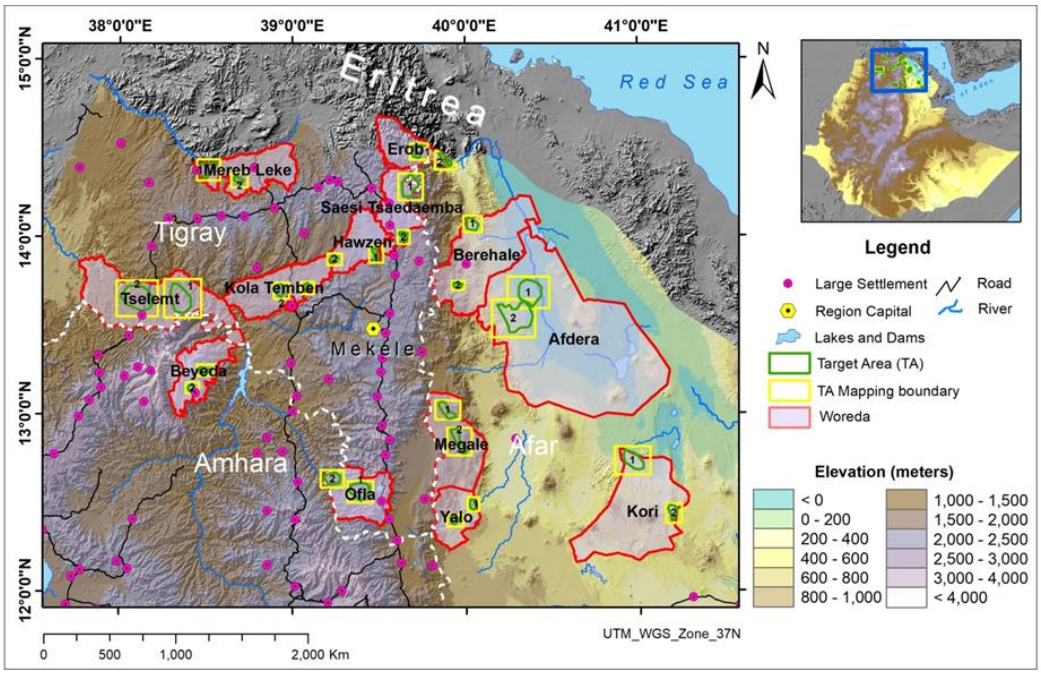

Figure 1.1. Location of the 13 selected Woredas for Lot 1 (including indication of target areas in each Woreda).

Physiography and climate of the project areas

Physiographically, the project areas have a varied nature. While the target areas in Amhara and Tigray regions fall within the Western Ethiopian Plateau; areas in Afar fall partly within the Afar rift lowland and partly along the rift margins. The Beyeda Woreda in Amhara region is situated on the top of Ras Dashan volcanic mountain at elevations of 3000 m amsl and is characterized by cold climatic condition (Dega climatic zone). This area receives relatively high annual rainfall and rivers and streams have dendritic pattern, cut deep gorges and drain to the Tekeze River in the north.

Across Tekeze river valley, Woredas within Southern, South-western Tigray and part of northern Tigray (Merb Lehe Woreda) are generally characterized by rugged, NNE-SSW trending ridges alternating with narrow low land or valley topographies ranging in elevation from 1000 to 2000 m amsl. The topography of these areas is controlled by NE-SW basement structural grain. Most of the rivers and stream in the Southern part of

Tigray drain to the Tekeze River, while areas close to the Mereb River drain to that. These areas have arid (Kola type) climatic condition with mean annual temperature and receive mean annual rain fall.

Woredas and areas in North-eastern Tigray and western Afar are also characterized by ragged, NNE-SSW trending topography controlled by Red Sea rift related fault structure. The areas have elevations ranging from about 300 up to greater than 1000 m amsl. These areas generally have arid to semi-arid climatic conditions, and receive low annual rainfall. Rivers and streams have dendritic pattern and all drain to the rift floor.

Woredas within the Afar Region are mostly situated east of the rift escarpment, belong to the rift valley physiographic zone and characterized by rugged NW-SE grabens and horsts along the rift shoulder and relatively low laying topography with elevations ranging from below sea level at the floor of the rift up to 1000 m amsl close to the escarpment and around tectonically elevated horst structures within the rift valley. The area receives low annual rainfall and is characterized by arid to desert type of climatic condition. Rivers and streams usually flow to the base of the rift having parallel drainage pattern controlled by tectonic structures (lineaments and faults). At the base of the slopes these rivers drop large quantity of fan shaped sheet flood deposits.

Regional Geology of the project areas

The geology of northern and north-eastern Ethiopia, in which the project areas are situated, was previously mapped at different scales and studied by various researchers. The mapping of the region at a scale of 1:250,000 by the Geological survey of Ethiopia including Adigrat map sheet (Garland, 1972); Mekele map sheet (Beyth, 1972), Axum map sheet (Tadesse, 1997), Adi Arkay map Sheet (Tsegaye, 1974) and, compilation work of geology of Afar area at a scale of 1:100,000 (UNICEF report) are sources of major geological information. These works have identified and described a succession of rock formations ranging in age from Precambrian up to Quaternary. The Precambrian metamorphic rocks include low grade metavolcanic and metasedimentary rocks. The metavolcanic rocks cover relatively larger part of the metamorphic terrain of northern Ethiopia and is regionally known as the Tsaliet Group (Beyth, 1972, Garland, 1972, Tefera et. al., 1996). This is uncomformably overlain by poorly metamorphosed and weakly deformed younger silciclastic and carbonate units of slates and limestone known as the Tembian Group (Beyth, 1972, Grland, 1972). These slate-carbonate succession are contained in a series of NE-SW, often overturned pairs of synclinal and anticlinal structures. These rocks together with mafic to felsic intrusive bodies of variable size and composition in the region belong to the Arabian Nubain Shield component of East African Orogen (Stern, 1994, Tadesse, 1997; Tadesse et. al,. 1999, 2000, Asrat et al., 2003) and are thought to be the product of plat tectonic process that involved subduction, build-up of intraoceanic island arcs, lateral accretion of the arcs associated with the convergence and subsequent collusion between East and West Gondwana during the Neoproterozoic (900-550 Ma., Stern 1994, Fritz 2013).

These Neo-Proterozoic metamorphic rocks of the region are unconformable overlain by Palaeozoic (Ordovician) tillites (Edaga Arbi Galcials) which is laterally inter-fingered with carbonate cemented, white clastic Enticho Sandstone (Graland, 1972; Beyth, 1972). These rocks, where not covered by the later Jurassic sedimentary and Tertiary volcanic sequence or eroded deep, they represent potential ground water aquifers of the region. Following the Ordovician deposit, intra-continental rifting in Permian initiated the break-up of Gondwana and led to continental mass subsidence and subsequent transgression

of Indian Ocean (Hunegaw et al., 1998; Boselline et al., 2001). The transgression lain down thick clastic, passive continental margin deposit followed by shallow and deep marine sedimentary deposits during the Jurassic (Hunegnaw et al., 1998; Bosellini et al., 2001). The base of transgression event was marked by the deposition of clastic lower sandstone known as the Adigrat Sandstone in the northern Ethiopia; followed upwards by scission of limestone marl, and shale and ended when the region was uplifted by mantle plum under the Afro-Arbain plate (Mohr and Zanettin, 1988). The up-doming resulted in the withdrawal of the Indian Ocean and deposition of regressive facies; marine sediments caped by clastic sedimentary rock (the upper Sandstone or Abaradam sandstone (Hunegnaw et al., 1998; Bosellini et al., 2001).

Plum related voluminous Tertiary Flood basalt eruption between 42-29Ma on the top of Mesozoic Sedimentary succession is believed to be approximately coeval with northeast-directed extension in the southern Red Sea and Gulf of Aden (Ebinger et al., 1993; Baker et al., 1996; Hofman et al., 1997; Ayalew et al., 2002; Ayalew & Yirgu, 2003). The volcanics are made up repeating sequences of thick (up to 2km) basaltic lava flows overlain by rhyolites including ignimbrites, air fall tuffs and lavas. These volcanic rocks cover much of the NW and SE Ethiopian Plateau. The edge of Afar depression is made of heavily faulted and weathered Eocene to early Miocene (25-15Ma) Trap basaltic volcanic rocks (Beyene & Abdelsalam, 2005). The most extensive volcanic sequence covering about two thirds of the NW-SE Afar Depression is the Pliocene-Pleistocene Afar Stratoid Series of up to 1500 m thick (Barberi & Varet, 1977; Hayward & Ebinger, 1996; Hofstetter & Beyth, 2003). These and overlying younger sequences are believed to be controlled by the NW-SE rifting parallel to the Red Sea rift axis. East and west of the Afar depression, Transverse volcanics of mainly basaltic composition occur (Barberi & Varet, 1977; Hayward & Ebinger, 1996; Hofstetter & Beyth, 2003). The axial zone of the Afar Depression is covered by Quaternary Axial Volcanic Ranges and are characterized by fault controlled fissure eruptions and shield volcanoes with basaltic flows and alkaline and per-alkaline silicic rocks. They occur along northwest-southeast trending narrow rift zones ((e.g. Mohr and Zanettine, 1988)). The Quaternary sediments of the Afar Region are mostly fluvial/ or lacustrine In origin, commonly thin, often terrace forming but occasionally thick pile of sediments occur in deeply faulted narrow grabens.

Regional hydrogeology of the project areas

The hydrogeological characteristics and groundwater potential of the areas are highly affected by the complexity of the geology, physiography, climate and geological structures. The classification of different lithological units is based on the qualitative and quantitative parameters of the hydrogeological characteristics of various rocks. Since quantitative data such as permeability, yield, aquifer thickness and transmissivity are not sufficient or evenly distributed throughout the area, it was essential to apply a qualitative approach in order to achieve a complete and detailed potential classification. Qualitative investigation includes field observations of the geological, hydrogeological, geomorphological, physical and geographical setup. Hence, the lithological units are characterized as having porous or fissured permeability, or they are impermeable.

Based on the hydrogeological character of the lithological units and their topographical position, the study area can be divided into aquifers – non aquifers with different occurrences of groundwater, as follows:

- Porous aquifers developed in Quaternary alluvial and eluvial sediments;
- Fissured and karstic aquifers in limestone, fossiliferous and sandy limestone;

- Fissured aquifers developed in Paleozoic to Mesozoic sedimentary rocks (non-karstic), Tertiary and Quaternary volcanic rocks;
- Fissured aquifers developed in Precambrian basement rocks;
- Aquitards and aquicludes.

The hydrogeology map shows aquifers defined based on the character of groundwater flow (pores, fissures) and the yield of springs, boreholes and dug wells found during the desk and field water point inventory. The following aquifers were defined:

Highly productive porous aquifers (T = 10.1 – 100 m^2/d, q = 1.1 – 10 l/s*m, Q = 5 – 25 l/s for wells and/or springs) or locally extremely productive aquifers consisting of:

Plateau/escarpment	Afar
Quaternary high fluvial terraces with gravel and sandstone and alluvial / colluvial sediment in Maychew graben	Upper Pleistocene continental conglomerate and Red Series (Garsat / Danakil Formation) with conglomerate, sandstone, silt and clay

These aquifers are shown on the hydrogeological map in dark blue color.

Moderately productive porous aquifers (T = 1.1 – 10 m^2/d, q = 0.011 – 1 l/s*m, Q = 0.51 – 5 l/s for wells and/or springs) or local or discontinuous but highly productive aquifers consisting of:

Plateau/escarpment	Afar
Quaternary alluvium and lacustrine deposits and undifferentiated cover with clayey and sand and gravel	Quaternary alluvium with silt, clay, sand and dunes and Afdera bed with limestone and diatomite

These aquifers are shown on the hydrogeological map in light blue color.

Highly productive fissured / karst aquifers (T = 10.1 – 100 m^2/d, q = 1.1 – 10 l/s*m, Q = 5 – 25 l/s for wells and/or springs) or locally extremely productive aquifers consisting of sedimentary and volcanic rocks of:

Plateau/escarpment	Afar
Antalo limestone and limestone and slates where karstified and Upper basalts and trachyte (Tarmaber-Megezez formation and Dessie basalt)	Stratoid vesicular basalts and Aphenatic and Vesicular basalts

These aquifers are shown on the hydrogeological map in dark green color.

Moderately productive fissured aquifers (T = 1.1 – 10 m^2/d, q = 0.011 – 1 l/s*m, Q = 0.51 – 5 l/s for wells and/or springs) or local or discontinuous but highly productive aquifers consisting of sedimentary and volcanic rocks of:

Plateau / escarpment	Afar
Limestones (Antalo, Tsedia, Maikenetal, Asseam), dolomite (Didikama) and sandstone (Enticho, Adigrat, Amba Aradom) and trap volcanics and Mekele dolerite	Picritic basalts, lavas of intermediate composition, basic lava (submarine) flow and related spatter cones mainly of basaltic composition, Quaternary and recent Afar basalt

These aquifers are shown on the hydrogeological map in light green color.

Moderately productive aquifers with alternating layers of fissured and porous permeability (T = 1.1 – 10 m^2/d, q = 0.011 – 1 l/s*m, Q = 0.51 – 5 l/s for wells and/or springs) consisting of Dalha Formation of basalt flows and layers of lacustrine sediments. The aquifers are shown on the hydrogeological map in dark violet.

Low productive fissured aquifers (T = 0.11 – 1 m^2/d, q = 0.0011 – 0.01 l/s.m, Q = 0.051 - 0.5 l/s for wells and/or springs) in which flow is mainly developed in irregular system of fissures and weathered mantle of a crystalline rock consisting of:

Plateau/escarpment	Afar
Phillite and slate (Weri slates, Tsalient group, Amota slate, Arekwa), metavolcanoclastic and metasediments and syenite and granite	Epimetamorphic basement of Danakil Alps and granite

These aquifers are shown on the hydrogeological map in light violet color.

Aquitards, minor aquifers with local and limited groundwater resources (T = 0.01 – 0.1 m^2/d, q = 0.0001 – 0.001 l/s*m, Q = 0.005 – 0.055 l/s) consisting of sedimentary and volcanic rocks of:

Plateau/escarpment	Afar
Agula shale, Edaga Arabi glacials and Hamsho tufite, alkali trachyte and rhyolite and tuff	Zagira formation of with dominating gypsum and Dallol formation / Evaporite with dominating halite and Trachyte and rhyolite, silicic lavas of Afera volcano and silicic centers and domes

These aquifers are shown on the hydrogeological map in light brown color.

Aquicludes: formation with essentially no groundwater resources consisting of dome forming phonolite/trachyte and gabbro and metagabbro and metapyroxinite (aquifuge – solid rocks/blind rocks). These aquifers are shown on the hydrogeological map in dark brown color.

As a result of these evaluations potential target areas have been selected for each Kebele with alternative options for prioritization during the actual field verifications and geophysical surveys. A total of 26 target areas have been selected with the three regions (Afar, Amhara and Tigray).

2 Tselemt Woreda description

The 1:50,000 scale geological mapping of the target areas has been completed by using a combination of methods. These include interpretation of enhanced and transformed high resolution Landsat images of appropriate bandwidth and existing geological maps of different scales. Five Landsat 8 OLI images of the project areas acquired on December 07, 14 and 30, 2021, were used for the geological mapping. The Satellite images were enhanced using band ration enhancement techniques. Accordingly, a color combination of band ratios of 7/5, 6/3 and 4/3 was found to be the best for our mapping. The image interpretation is controlled by data from 1:250,000 scale geological maps produced by Geological survey of Ethiopia and 1:100,000 geological maps (compiled by UNICEF-UNESCO project for Afar region) as a base and reference maps. Lithological unit naming and stratigraphic succession of each target area, therefore, are following the data and legends of geological maps and accompanying report. However, the enhanced Landsat images allowed the tracing of geological boundaries and structural features (including faults, lineaments and folds) reasonably well. As a result, in some cases, our detailed mapping using a combination of enhanced Landsat images have significantly improved the pre-existing maps. Where records are available on the maps of previous works, dip and strike of the metamorphic rocks and dip direction of faults have been adopted.

2.1 Geology

Tselemt Woreda is located in western zone of the Tigray Region and has an area of 2,656 km^2. Physigraphically, the Woreda is located at the Western Plateau (highlands) and slopes to the north where it is bounded by the Tekeze River. Basement rocks outcrops along the Tekeze River at the North and are overlain by Adigrat sandstone and Tertiary basalts to southern border of the Woreda.

2.2 Geomorphology and Hydrogeology

Tselemt Woreda and the subsequent target area falls in near to the main the Tekeze River. The elevation in the Woreda ranges from 772 m amsl. to 3392 m amsl. Generally the topography steeply inclined to the northern side towards the Tekeze River that serves as the Woreda boundary. All small rivers such as Jama and others flow northward to join the main the Tekeze River.

Hydrogeological units with fissured permeability and moderate productivity consist of Adigrat sandstone overlain by Tertiary basalts. It is exposed usually in highly dissected valleys and forms cliffs. The permeability of the sandstone is increased by weathering in addition to closely spaced vertical fissures, fractures and horizontal bedding. This aquifer is recharged from the overlaying aquifers in Tertiary trap basalts, from perennial rivers and from direct rainfall infiltration. Low productive fissured aquifers in Precambrian basement complex consisting of low grade metamorphic rocks (dominantly metavolcanics) penetrated by intrusive (granite). Hamesho units is small it is composed

of tuffaceous sediments, quartzite, arkose and agglomerate and has an impermeable character.

Development of aquifers in basement rocks is by spring development and by drilling mainly 30 to 70 m deep shallow wells. Greater yield of wells can be achieved when siting wells using Remote Sensing structural analysis (identification of faults and lineaments) and geophysical exploration, which seems to be indispensable for basement rocks. The area along the river can be also preferable for well siting. Groundwater resources in sandstone aquifers can be developed mainly by springs and deep wells drilled into fractured aquifer and some fissured zones (faults and lineaments) near to perennial rivers and near contact of sandstone with basement. These structures should be located by combination of Remote Sensing and geophysical. Better chance for groundwater accumulation is near contact of sandstone with underlying basement rocks. Groundwater resources in basalt aquifers can be developed mainly by springs and deep wells drilled into fractured aquifer and some fissured zones near to perennial rivers. These structures should be located by combination of Remote Sensing and geophysical.

An inventory of existing water points (boreholes, hand dug wells, and springs) in the Tselemt woreda has been conducted. The results of this inventory are shown in the table of the Existing Water Points Annex.

Groundwater is soft with TDS between 300 and 500 mg/l and no ions exceeding standards for drinking.

3 Target areas

Using the groundwater potential maps, socio-economic maps, conceptual models and cross sections, target areas have been selected in every Woreda for further study during phase III. The selection of target areas should have been done in consultation with local experts and stakeholders. Due to the security constraints, this could not be realized. Instead, the project team has prepared a prioritized list of 2 to 4 target areas per Woreda where both groundwater potential, and water demand has been considered. It should be noted here that the water demand is derived from secondary data from CSA census, projected population growth, locations of schools, health centers and existing water point inventories. We propose to do the final selection of two target areas per Woreda in consultation with the review committee during the validation workshop of phase II.

In the process of selecting potential target areas, several factors have been considered which include both technical and socio-economic aspects of the areas. These include evaluations on geology and geomorphological settings, general hydrogeological conditions and suitability for groundwater development, access, water demand and presence of social infrastructures in the area with lack of water supply to get priority in selections, etc.

The groundwater potential map used as a basis to select the target areas has been prepared using the overlay analysis methodology which applies the rating and scoring of hydrogeological parameters that controls the occurrence and movement of groundwater in the areas, which considers parameters such as: lithology, lineament and lineament density, drainage, and drainage density, inferred permeability, geomorphology and slope, precipitation, and recharge rate.

Specific drilling site within the selected target area, will be fixed during the actual planning for drilling with additional geophysical survey works to support the present analysis to further detail to determine expected depth of drilling to intercept the inferred potential aquifer formation and indications on the water quality conditions, define drilling methods and preparations of TOR for drilling.

In this phase, the target areas are presented as polygons with reference coordinates to their centers to support in ground control during the geophysical survey and pinpointing the actual drilling sites which will be depicted on the 1:50,000 operational hydrogeological maps during phase III.

Basic information about groundwater characteristics of two proposed target areas in the Tselemt Woreda are shown in Table 3.1.

Table 3.1. Groundwater characteristics of target areas in Tselemt Woreda.

SN	Target Area code	Region	Zone	Woreda	Kebele	Center X	Center Y	Area (km^2)
1	TS2	Tigray	North Western Tigray	Tselemt	May Ayene	403352	1510137	220
Moderately productive fissured aquifers hosted by Adigrat sandstone. Surface and groundwater is flowing to the north to the Tekeze River. Groundwater resources can be developed mainly by springs and deep wells drilled into fractured aquifer along faults and lineaments near to perennial rivers and near contact with basement. Groundwater is soft with TDS between 500 and 1,000 mg/l in several shallow wells nitrate ion exceeding standards for drinking reflecting lack of sanitation.								
2	TS3	Tigray	North Western Tigray	Tselemt	Dima	430032	1509368	165
Moderately productive fissured aquifers hosted by Adigrat sandstone. Surface and groundwater is flowing to the north to the Tekeze River. Groundwater resources can be developed mainly by springs and deep wells drilled into fractured aquifer along faults and lineaments near to perennial rivers and near contact with basement. Groundwater is soft with TDS between 500 and 1,000 mg/l in several shallow wells nitrate ion exceeding standards for drinking reflecting lack of sanitation.								

4 Geology of target areas in the Tselemt Woreda

4.1 Geology and structure of target area 1 (TS2, May Ayene)

The geology of Target area 1 (fig. 4.1) comprises metavolcanics of Tsaliet Group (Pl) which are covered by Jurassic Adigrat sandstone (Ja) followed stratigraphically upwards by Ashangi basalt (Tab).

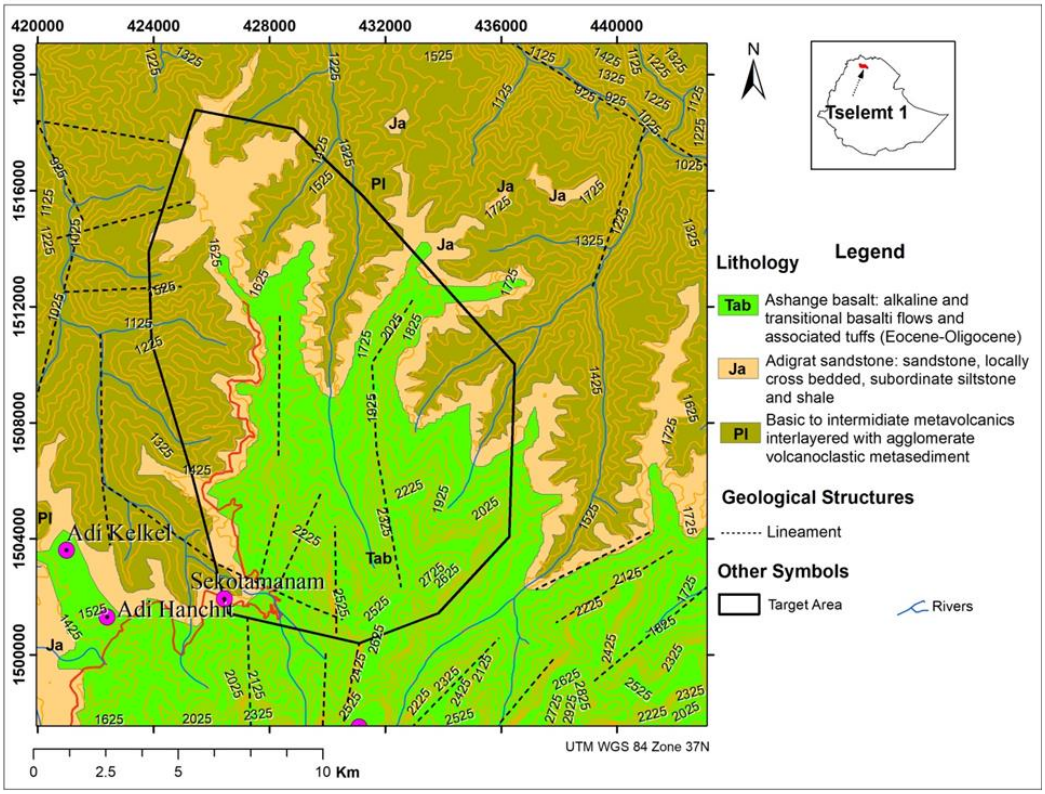

Figure 4.1. Geological map of target area 1 of the Tselemt Woreda.

The Tsaliet Group (Pl): Exposed at the northern, western and eastern part of the target area and is unconformably overlain by Adigrat sandstone. The unit is comprised of low grade, fine grained, greenish and epidotized intermediate to basic metavolcanics associated with volcanoclastic metasediments including metagreywake, metaagglomerate, tuffaceous metasediments (phyllite) and chlorite schist. It is generally foliated, but more intensely schistose along narrow deformational zones which comprises phyllite and chlorite schist. The overall thickness of the unit may over 500m in the target area.

Adigrat Sandstone (Ja): This unit is exposed mainly in the central, south eastern and south western part of the target area forming gentle slopes. It overlies the Tsaliet Group (Pl) low grade metamorphic rocks and itself is overlain by the Ashangi basalt (Tab). It is comprised of yellow to red sandstone, fine to medium-grained; interbedded with variegated siltstone and clay stone. Also includes White, cross bedded, friable sandstone. The Adigrat Sandstone has estimated thickness about 250m.

Ashangi basalt (Tab): This unit covers the southern part of the target area covering the top part high topographic hills. The Ashangi basalt in the target area is composed of basalt with varying proportions of aphanitic basalt, vesicular basalt, and phyric basalt. Characteristically, the exposures of the Ashangi basalt is strongly weathered, intensely fractured and jointed. The flows are horizontally bedded and doleritic dikes commonly inject it. Its estimated thickness is about 1000m.

The major structures seen in the area are N-S and NE-SW lineaments traced from land sat images with topographic breaks across the Trap basalt sequence (Tba), Adigrat sandstone (Ja) and Tsaliet Group (Pl) metavolcanic rocks (Fig. 4.2).

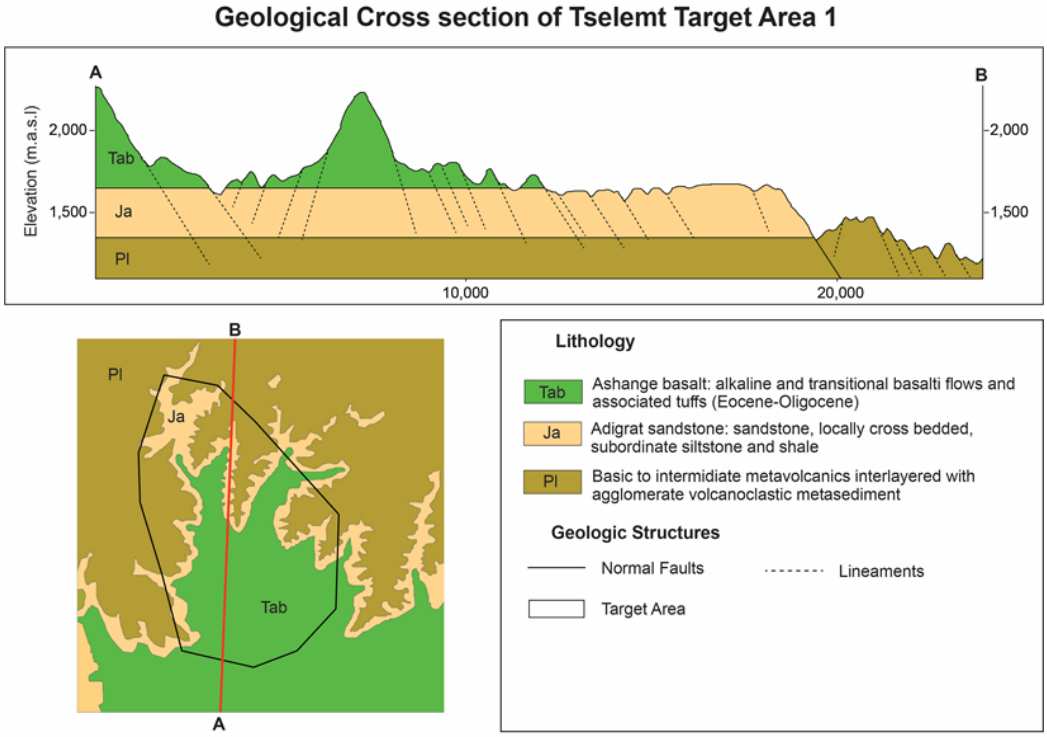

Figure 4.2. Geological cross section of target area 1 of the Tselemt Woreda.

4.2 Geology and structure of target area 2 (TS3, Dima)

Target area 2 (Fig. 4.3) of Tselemt Woreda is mainly covered by low grade metamorphosed Werii slate (Ptw). This metamorphic rock is overlain by Jurassic Adigrat sandstone (Ja) and Ashangi basalt (Tab).

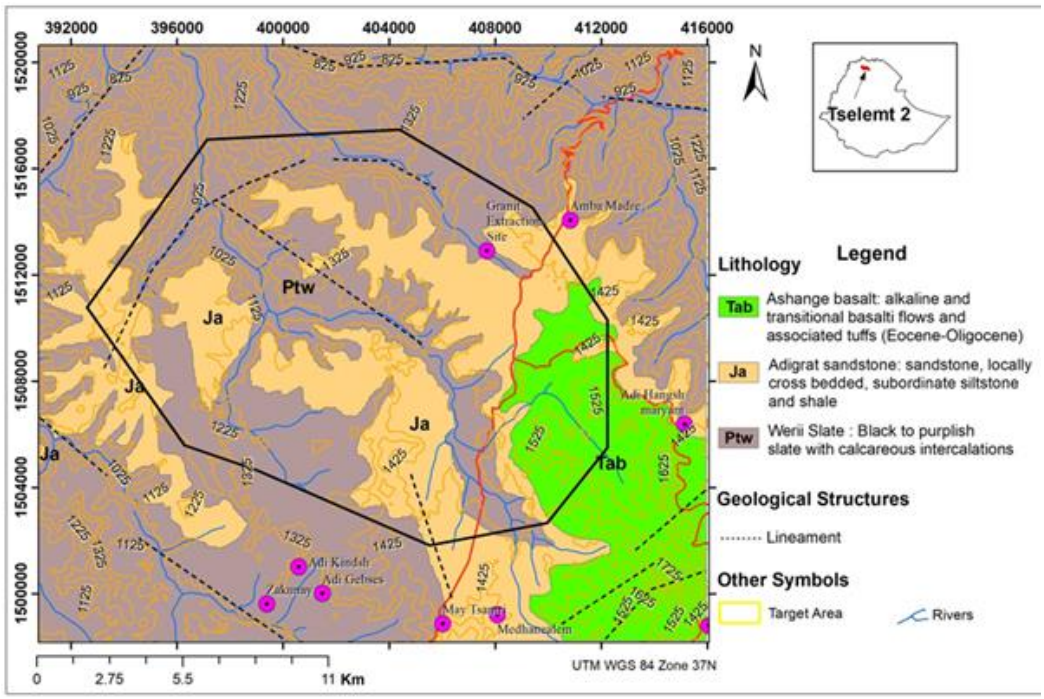

Figure 4.3. Geological map of target area 2 of the Tselemt Woreda.

Werii Slate (Ptw): With the exception of south eastern corner, the Werii slate is exposed almost over the entire width of the target area. It is overlain by the Adigrat sandstone (Ja). The Werii slate is comprised of purplish, green gray to black slates and phyllites intercalated with calcareous slate and black limestone layers. The unit forms generally undulating hills and wide valleys. The unit is generally well cleaved and fissile, commonly closely jointed. This unit represents the lower most stratigraphic unit (the lower slate) of Tembain Group rocks in the region. It has an estimated thickness >300m.

Adigrat Sandstone (Ja): The Adigrat sandstone unit is exposed mainly in the central, western and south eastern part occupying flat plains of the graben and gentle slopes of the hills. It overlies the Werii slate (Ptw) and overlain by the Ashangi basalt (Tab). It is comprised of yellow to red sandstone, fine to medium-grained; interbedded with variegated siltstone and clay stone. Also includes White, cross bedded, friable sandstone. It has an estimated thickness about 100m.

Ashangi basalt (Tab): This unit covers the southern eastern part of the target area covering the top the hills overlying the Adigrat sandstone (Ja). The Ashangi basalt in the target area is composed of basalt with varying proportions of aphanitic basalt, vesicular basalt, and olivine- phyric basalt. Characteristically, the exposures of the Ashangi basalt are strongly weathered, intensely fractured and jointed. The flows are horizontally layered and cut by doleritic dikes. Its estimated thickness is >100m within the limit of the target area.

NW-SE and NE-SW trending normal faults and lineaments traced from land sat images represents the major structural features of the target area. The normal faults formed graben and horst structure (Fig. 4.4).

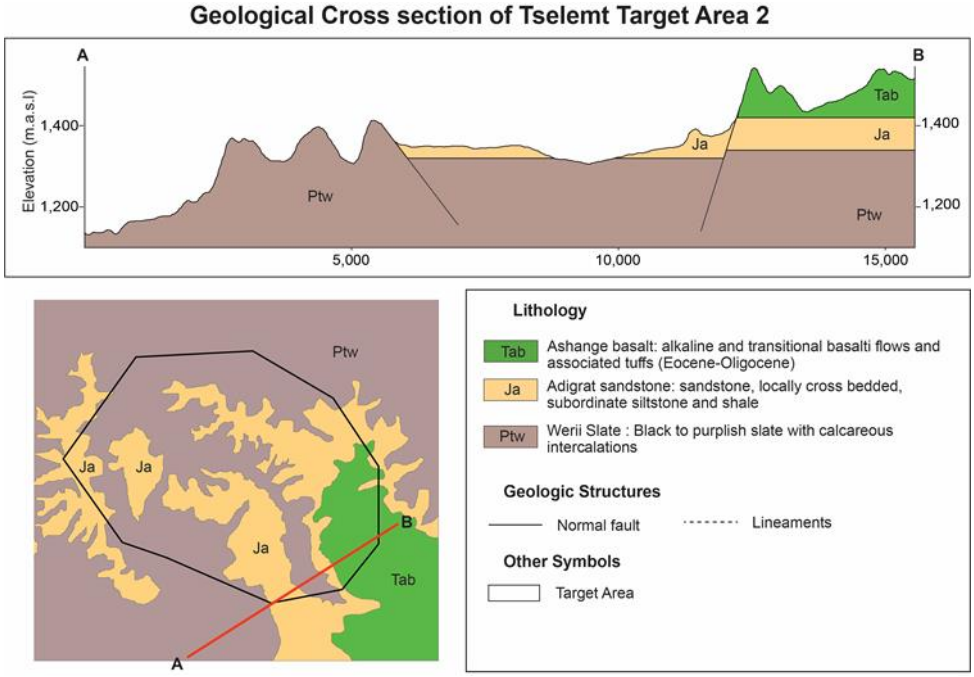

Figure 4.4. Geological cross section across target area 2 of the Tselemt Woreda.

5 Geophysical Exploration

5.1 Objectives, Overview and Limitations

The main objectives of geophysical investigation have been the identifications of structural elements with depth estimates of anomalous subsurface sources using potential data, namely, regional airborne gravity data. The main objective is to delineate all possible structural features and examine their roles on the regional groundwater dynamics of Northern and North-eastern Ethiopia.

Geophysical techniques are routinely used in groundwater mapping programs to assess the physical and chemical properties of soils, rock and interstitial water.

The paramount benefits of geophysical methods, for groundwater exploration come from using them in site characterization process. The methods are typically non-destructive, less risky, cover more area spatially and volumetrically, and require less time and cost than other conventional methods. On the other hand, interpreting the data generated by these methods require profession skill and experience. The indirect nature results (models) creates uncertainties that can only be resolved by use of multiple methods and direct observation. Nevertheless, using geophysical methods in such programs significantly increases cost effectiveness in borehole siting, over “hit or miss” approach.

Overview of geophysical methods being widely used for variety of purposes in groundwater studies, such as:

- Geologic characterization, including assessing types and thicknesses of strata and the topography of the bedrock surface below unconsolidated material, and generating fracture mapping and paleochannels;
- Aquifer characterization, including depth to water table, water quality, hydraulic conductivity;
- Contaminant plume identification, both vertical and horizontal distribution including monitoring changes over time.

There are several geophysical methods that are common to most groundwater studies. The first most important step is collecting high-quality data using the geophysical method or methods that are most likely to provide crucial parameter that can help resolving a particular hydrogeological characterization or monitoring objective and that work well in the given environment. Although the corresponding geophysical properties.

Among all geophysical methods, electrical/resistivity approach is being widely used in characterizing local groundwater occurrence. However, potential methods such as the Gravity and Magnetic methods are considered as the best options for regional basins studies. Various studies have shown that gravity methods are efficient methods for the scale of regional reviews in groundwater exploration.

Maximum effort has been exerted to review of all existing geophysical works within the project area and use the data to assist the ongoing integrated ground water assessment program in Lot 1, which comprised Woredas in Tigray, Afar and Amhara Regions.

The first desirable component, readily available for regional evaluation, was a countrywide Airborne Gravity data. The existing aero-gravity data covering the North and Northeast regions is obtained from the airborne gravity surveys over Ethiopia, acquired in the period from 2006 to 2008, through the collaboration between the Geophysical Observatory (the current IGSSA) of the Addis Ababa University, the Ethiopian Geological Survey, (GSE) and the Danish National Space Centre (DNSC). The flight altitude has been kept as close as possible to the terrain (i.e., from 1490 to 5000 m) and flight line spacing of 10 nautical miles (Figure 5.1).

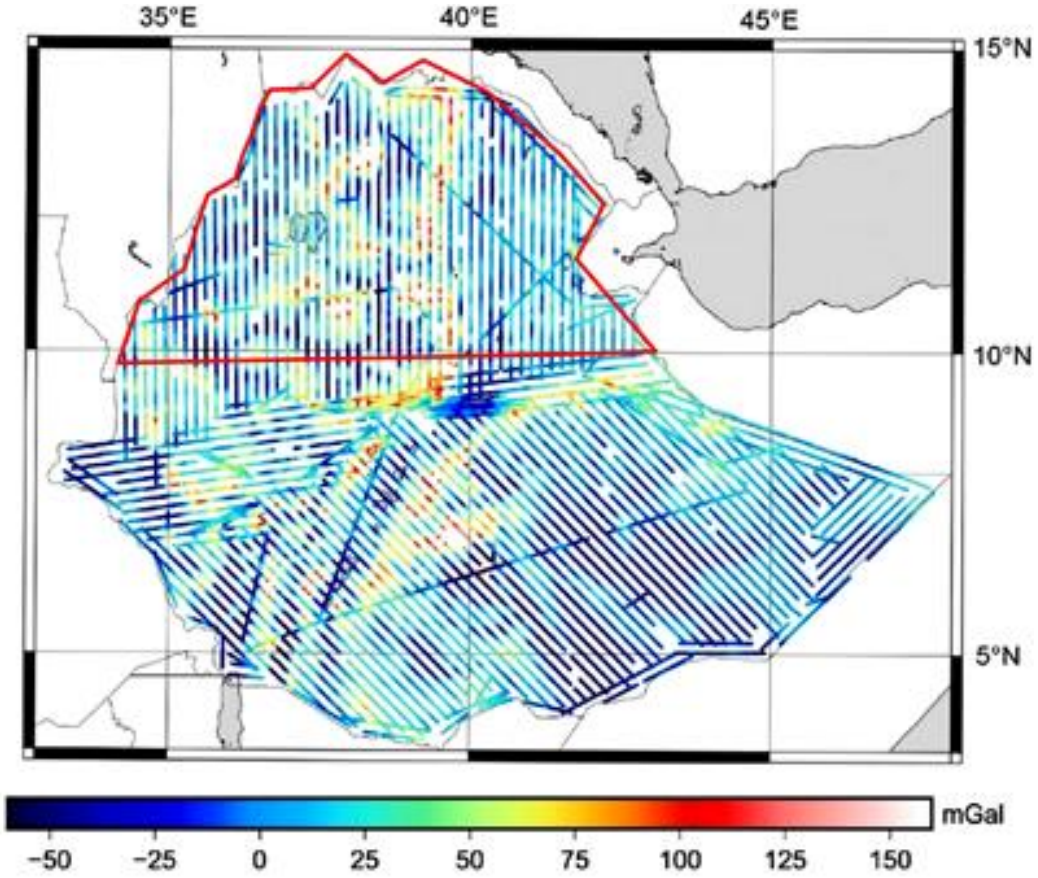

Figure 5.1. Airborne gravity coverage over Ethiopia at the flight attitude which is partly used in the present study.

As a result, homogeneous and high quality airborne gravity anomalies at the flight altitude covering the whole area of Ethiopia were obtained.

The gravity-sensing equipment carried in the aircraft is based on the principle of accelerometers. This complex technology records extremely small variations in Earth's gravity field while operating in a moving aircraft.

The Bouguer gravity anomaly mapping and its derivatives can illustrate regional subsurface condition, especially the basement configuration and main structures that might directly influence the aquifers distribution. Hence, part of this airborne gravity

anomaly data is used, in this work, to study the regional groundwater occurrence in the project area.

The other usable input is that of geoelectric data resulted from previous geophysical works, Vertical Electrical Survey (VES), in the LOT1 project area.

As shown in Figure 5.2, the vast majority number of the sounding points are from east central Tigray regions. A good number of usable VES data were also found from Afar region. Unfortunately, there has not been any VES data from Woredas in the Amhara region.

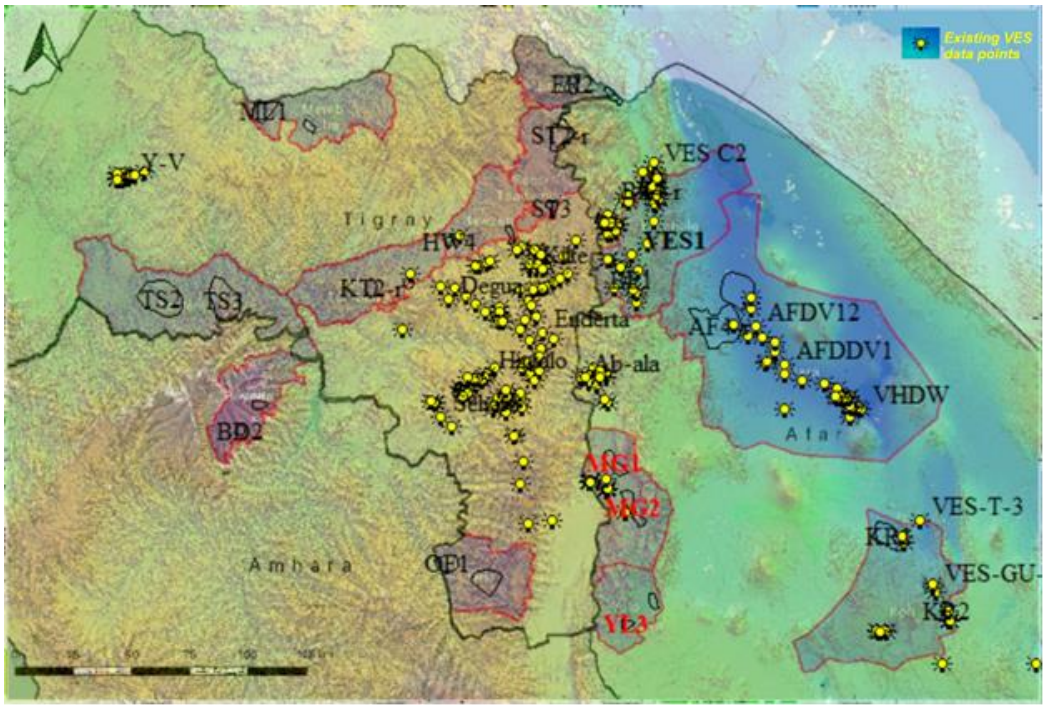

Figure 5.2. Map showing locations of existing VES data which is partly used in the present study.

Those set of geoelectrical data, whose sounding points are within the boundary of the target areas of the current project, would be used for quantitative appraisal of the subsurface layer parameters.

Limitations and shortcomings are related to general as well as specific problems of the area under study. It is well known that, the prolonged lack of peace, security and stability in the northern and Northeastern Ethiopia, has been and still undermining the progress of all developmental projects in those parts of the country. All the target Woredas of LOT 1 of the "Hydrogeological mapping for Climate Resilient WASH in Ethiopia" are within the regions severely affected by this calamitous circumstances. Hence, due to the prevalence of this unfortunate situation, it has not been possible to acquire the planned geophysical data from the project target areas.

Existing geophysical datasets provide a useful, yet highly limited, perspective on geophysical signatures of groundwater occurrence in the project area. This constitutes a major limitation that the subsurface hydro geophysical parameters were sought from the scarce previous works in the area.

5.2 Aero – Gravity study

Gravimetry is one of the classical and well established methods in applied geophysics. It deals with the density distribution of the earth's crust. Advances in theory, technology and application were not only pushed by the need for geophysical exploration, but also by progresses in the field of geodesy.

The variations in gravity readings are related to subsurface mass variations. With the current improvements in the sensitivity of gravity meters, gravimetric studies are used to investigate small changes caused by decreasing water within unconfined aquifers. The term local gravimetry points to the small magnitudes of gravity anomalies that often have to be expected in the context of groundwater geophysics making great demands on instruments, on the layout of field surveys, and on data processing. The successful application of the gravity method in groundwater geophysics is documented in many papers.

Gravity data is composed of signals with many wavelength ranges reflecting sources arising from different depths and entities of various densities. The shorter wavelength components usually correspond to density variations of shallow depth. The medium to longer wavelength components of gravity signals, on the other hand, correspond to deeper variations.

The main objective of using the airborne gravity data is to delineate all possible structural features and examine their roles on the regional groundwater dynamics of Northern and Northeastern Ethiopian. The analysis focuses on the identifications of structural elements with depth estimates of anomalous subsurface sources using potential data namely, regional airborne gravity data.

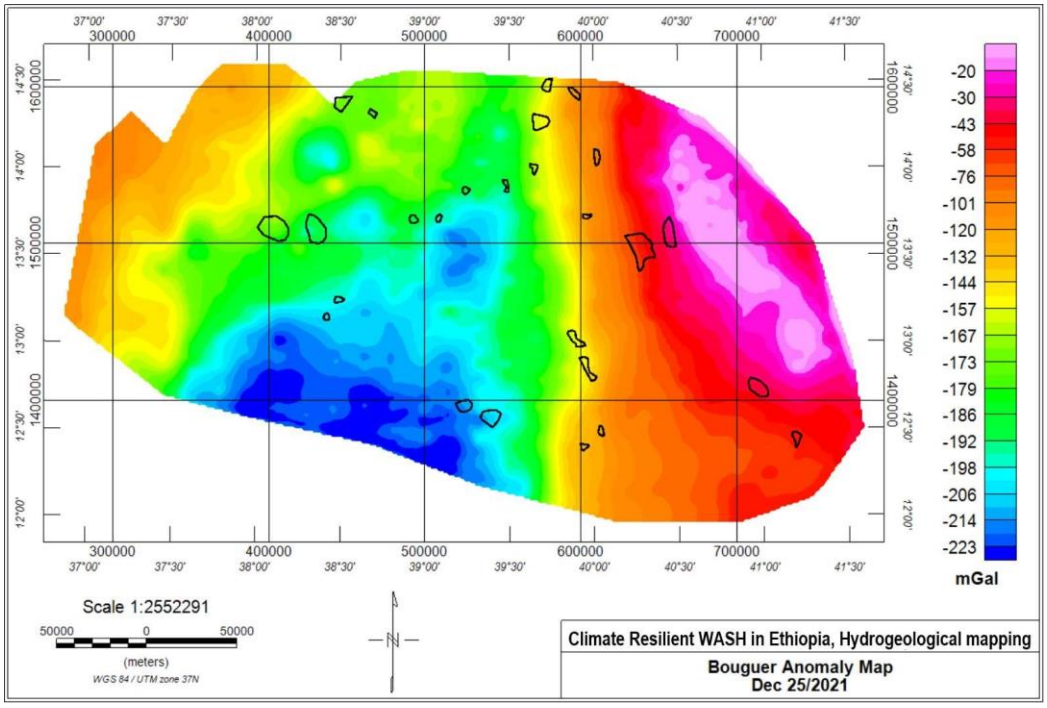

Figure 5.3. Residual gravity anomaly map of the study area, the overlayed polygons are the target areas for investigating groundwater.

Analysis and interpretations of gravity anomaly is carried out by Geosoft Oasis montaj 8.4.0.3285 and QGIS 3.6.0 'Noosa' software. Herein, the Complete Bouguer gravity anomaly map of the study area was produced with a grid spacing of 250.0 m x 250.0 m, which covers an area of 111,556 km^2 (Figure 5.3).

5.2.1 Gravity anomaly separation

The anomalous value of the gravity field at a point is the sum of the gravity effects of widespread and deep-seated mass distributions and smaller, localized mass distributions near the observation point. The interpretation of Bouguer gravity anomalies often involves isolating anomalies of interest (residual gravity anomalies) (Mickus et al., 1991).

The observed Bouguer gravity anomaly field consists of two components: a regional and residual gravity anomaly field that can be expressed by a simple relation:

$$g(x,y) = g_s(x,y) + g_d(x,y) \qquad (5.1)$$

Where g(x,y) is the observed gravity field, s and d refer to the gravity response of shallow and deeper structures, respectively.

Thus, one of the most important issues in potential field data interpretation is the removal of regional trends when dealing with relatively shallower local geological structures (Dobrin, 1976). Therefore, some mathematical methods are required to separate the map data into two components which are the regional nature and the local fluctuations (Davis and Sampson, 1986). Since the study presented herein deals with the shallow geological structures and rift basin architectures of the southern main Ethiopian rift, regional/residual separation process was applied to gravity data-set in order to estimate the amplitude of the regional background.

Upward continuation can be used to separate a regional gravity anomaly resulting from deep sources from the observed gravity. Commonly, the regional Bouguer gravity anomaly is the longer wavelength field due to deep sources, whereas the residual Bouguer gravity anomaly corresponds to short wavelength fields of shallower bodies. However, in practice, the terminology of a regional gravity anomaly varies according to the target of the investigation, In case of this study the target sources are a few kilometers deep, and the regional field is generated by the rocks at the base of the sedimentary columns which is the metamorphic basement rock.

Upward continuation is an operation that shifts the data by a constant height level above the surface of the earth (or the plane of measurements). It is used to estimate the large scale or regional (low frequency or long wave length) trends of the data.
The upward continuation can be formulated as (Blakely, 1995):

$$F[U_u] = F[U] \times e^{-\Delta z.k} \qquad (5.2)$$

Where F[U], F[U_u] is the Fourier transform of the potential field U, upward continued field U_u , $\Delta z>0$ is elevation difference, and $k=\sqrt{k_x^2 + k_y^2}$ is the radial wave number. The transform field is then computed by taking the inverse Fourier transform of F[U_u].

Upward continuation maps are produced at different height of 2, 4, 6, 8 and 10km (Figure 5.4) and profile curves are computed for each map in the SW-NE direction where contrasting anomalies are observed as shown in (Figure 5.5).

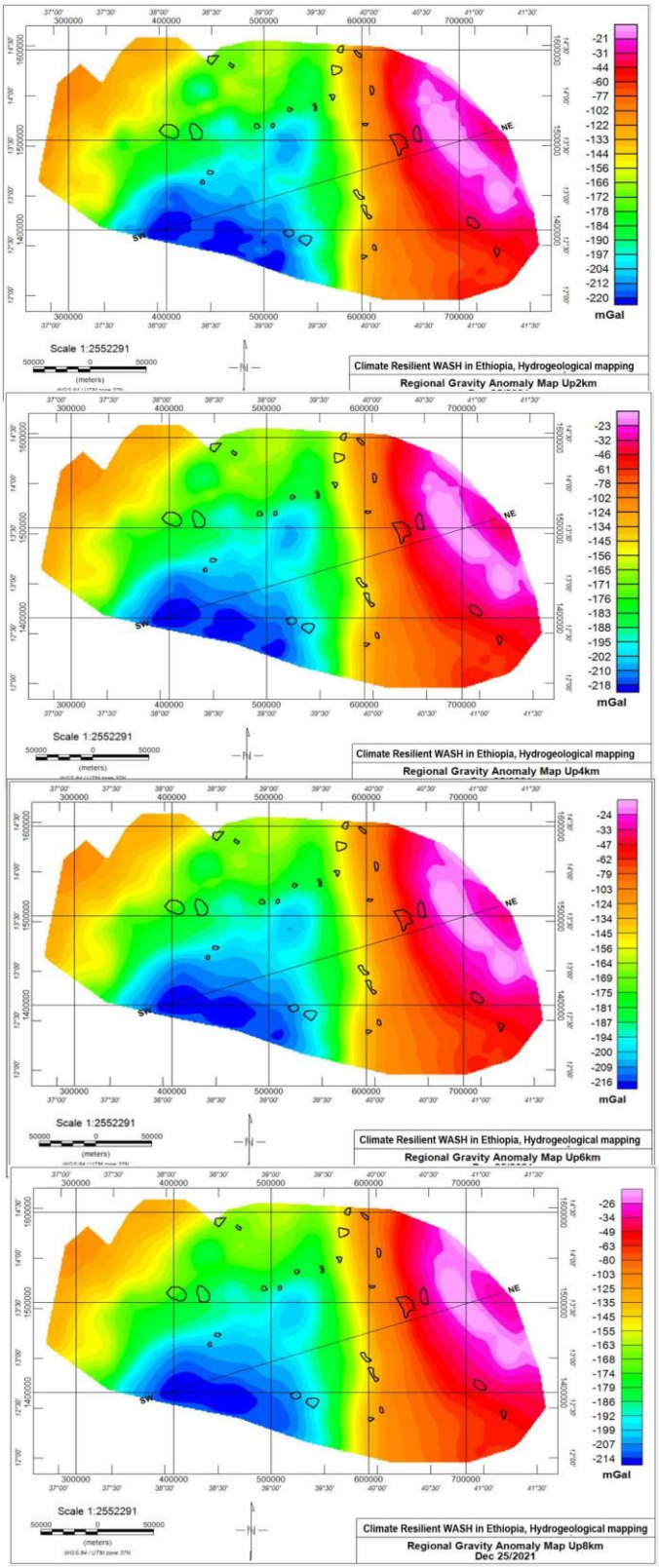

Figure 5.4. Regional gravity background of the study area computed by upward continuation filter of 2, 4, 6 and 8 km.

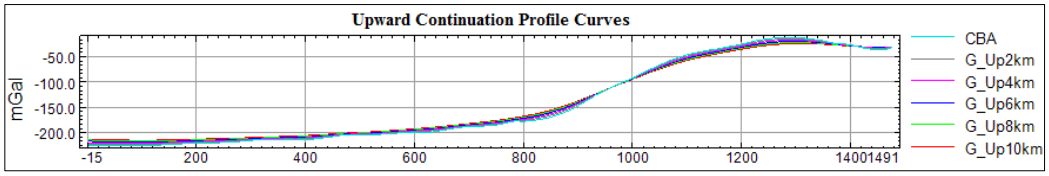

Figure 5.5. Upward continuation profile curves computed at different heights.

Upward continuation can be used to separate a regional gravity anomaly resulting from deep sources from the observed gravity (Kebede and Mammo, 2021; Kebede Hailemichael et al., 2020; Mammo, 2013). This is an operation that shifts the data by a constant height level above the surface of the earth (or the plane of measurements). It is used to estimate the large scale or regional (low frequency or long wave length) trends of the data.

Since the target depth is the basement which is approximately undulating 3km-4km, the data is upward continued at 6km to remove the short wavelength anomalies. Jacobsen (1987) demonstrated that if a potential field is upward continued to a certain height z, then it is possible to focus on sources situated at a depth greater than $z/2$ (see also Lyngsie et al. 2006; Mammo 2010).

The residual gravity anomaly map is computed by removing the regional gravity anomaly map from the complete Bouguer gravity anomaly as shown below:

$$g_s(x,y) = g(x,y) - g_d(x,y) \qquad (5.3)$$

Where g(x, y) is the observed gravity field, s and d refer to the gravity response of shallow and deeper structures, respectively.

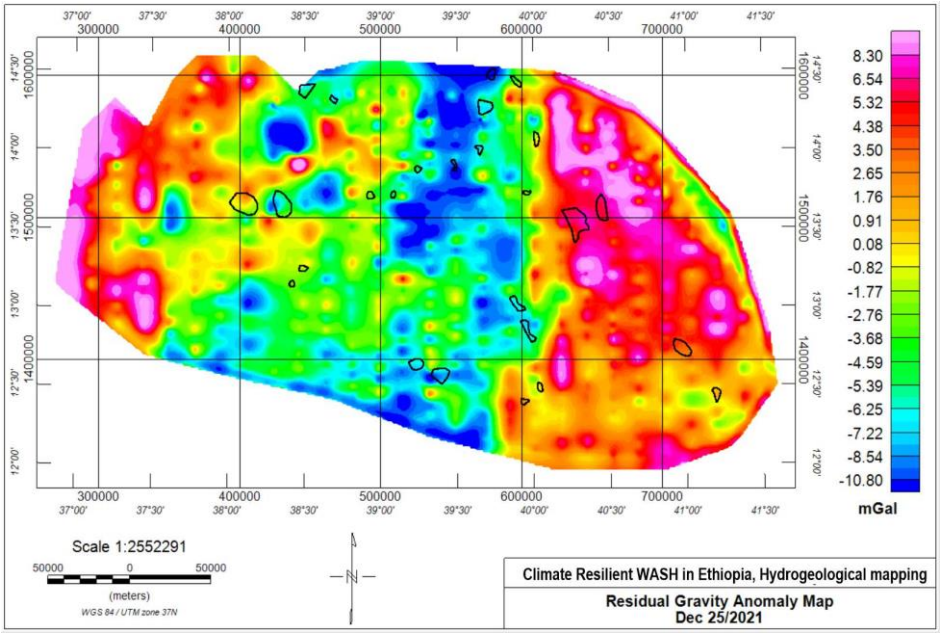

Figure 5.6. Residual gravity anomaly map of the study area.

The residual gravity anomaly (Figure 5.6) have contrasting anomaly -11mGal to more than 9mGal with probable depth of investigations 3 km from the surface target areas

associated with lower anomalies bound to have more groundwater potentials than those with higher anomalies.

5.2.2 Edge Detection and Depth Estimation using a Tilt Angle Map

The tilt angle is the angle computed as the arctangent of ratio of the first vertical derivative to the first horizontal derivatives of the gravity field. Its parameter varies between $-\frac{\pi}{4}$ and $+\frac{\pi}{4}$ where the zero contours locate close to the source-body contact.

Miller and Singh (Miller and Singh, 1994) developed the tilt angle filter (TA). This filter is defined as

$$\theta = \tan^{-1}\left(\frac{\frac{\partial M}{\partial z}}{\sqrt{\left(\frac{\partial M}{\partial x}\right)^2+\left(\frac{\partial M}{\partial y}\right)^2}}\right) \qquad (5.4)$$

Where θ Tilt angle Filter M is the gravity or magnetic field and $\frac{\partial M}{\partial z}, \frac{\partial M}{\partial x}$ and $\frac{\partial M}{\partial y}$ are the first derivatives of the field M in the x, y and z directions. The tilt amplitudes are restricted to values between $-\frac{\pi}{2}$ and $+\frac{\pi}{2}$ according to the nature of the arctangent trigonometric function and respond to a large dynamic range of amplitudes for anomalous sources at the different depths. Its amplitude has three rates: positive over the source, zero at or near the edge of the source, and negative outside the source (Ibraheem et al., 2018).

In the presence of noise, this technique acts as an effective signal discriminator for both shallow and intermediate sources but becomes blurred for sources at considerable depths, where it can not reveal deep-level geologic boundaries(Arisoy and Dikmen 2013). The horizontal derivative of the gravity anomaly is given by

$$\text{HDR} = \sqrt{\left(\frac{\partial M}{\partial x}\right)^2 + \left(\frac{\partial M}{\partial y}\right)^2} \qquad (5.5)$$

Where HDR is the Horizontal Derivative of Bouguer gravity anomaly and its maxima indicates locations of linear anomalous body (Figure 5.7).

The tilt angle technique can be used to estimate depth of the upper end of vertical contact source obtained by measuring the perpendicular distance between contours θ=00 and $\theta=\pm\frac{\pi}{4}$. The distance between zero and $\pm\frac{\pi}{4}$ pairs obtained from the tilt angle map corresponds to the depth to the top of the vertical contact model. Alternatively, the half distance between $-\frac{\pi}{4}$ and $+\frac{\pi}{4}$ radians is equal to the depth to the same model. It can easily be calculated from the reciprocal of horizontal gradient values at the zero contour points. The zero contours estimate the location of abrupt lateral changes in density of basement materials (Figure 5.8).

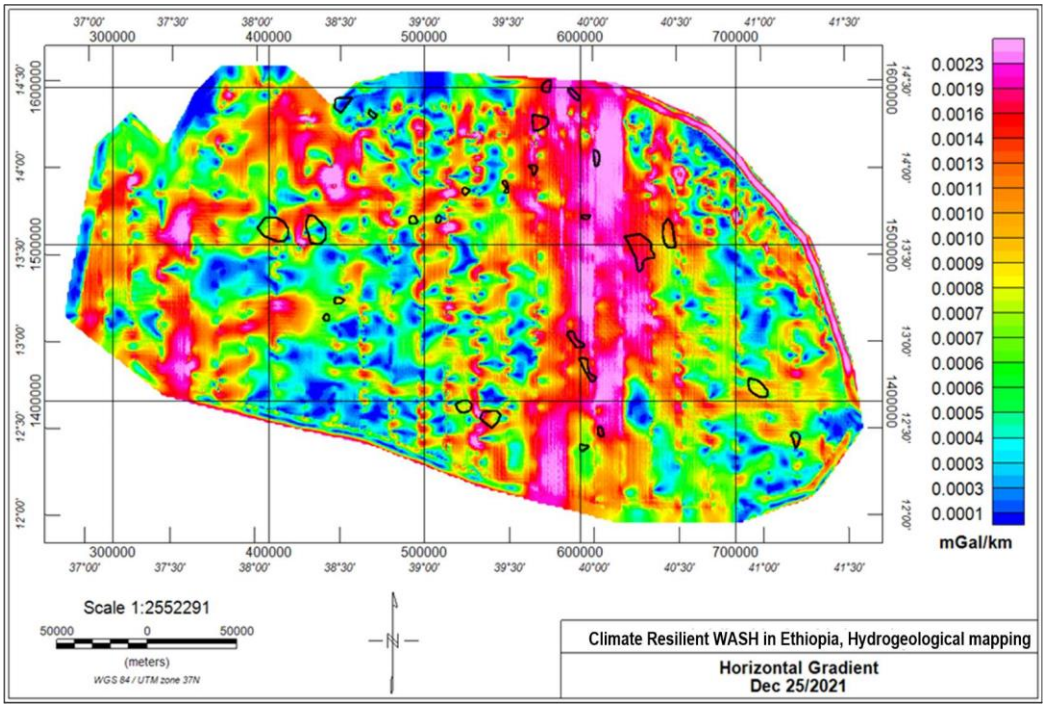

Figure 5.7. Horizontal Gradient map of the study area.

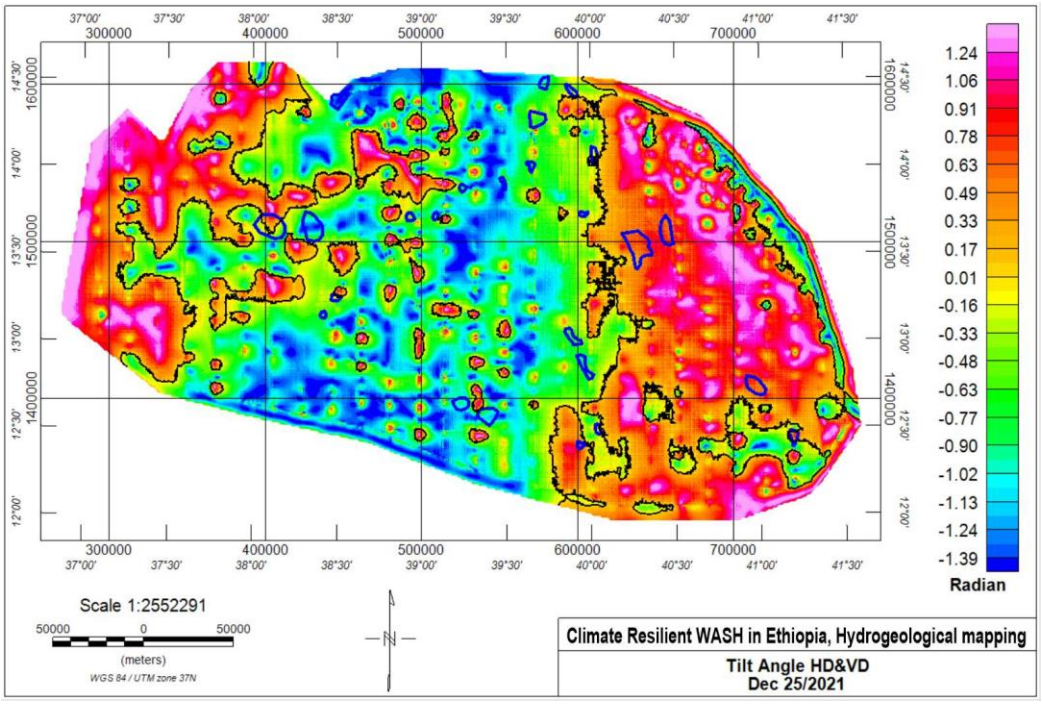

Figure 5.8. Tilt Angle computed from horizontal and vertical derivatives using equation (4).

5.2.3 Tilt Angle from Analytical Signal

Beiki (2010) used an analytic signal approach applied to the gravity data to estimate the source location parameters of simple gravity bodies. The disadvantage of the analytic signal approach is that it is more sensitive to noise than conventional approaches (Figure 5.9).

Tilt angle map is computed using the analytic signal map generated from the gravity gradient data components Gzz, Gxx and Gyy in order to get better structural features of the study area (Figure 5.7). The analytic signal map was generated using Bouguer gravity anomaly components

$$|As(x,y,z)| = \sqrt{\left(\frac{\partial M}{\partial x}\right)^2 + \left(\frac{\partial M}{\partial y}\right)^2 + \left(\frac{\partial M}{\partial z}\right)^2} \qquad (5.6)$$

Where $|As(x,y,z)|$ is analytic signal $\frac{\partial M}{\partial z}, \frac{\partial M}{\partial x}$ and $\frac{\partial M}{\partial y}$ are the first derivatives of the gravity field M in the x, y and z directions.

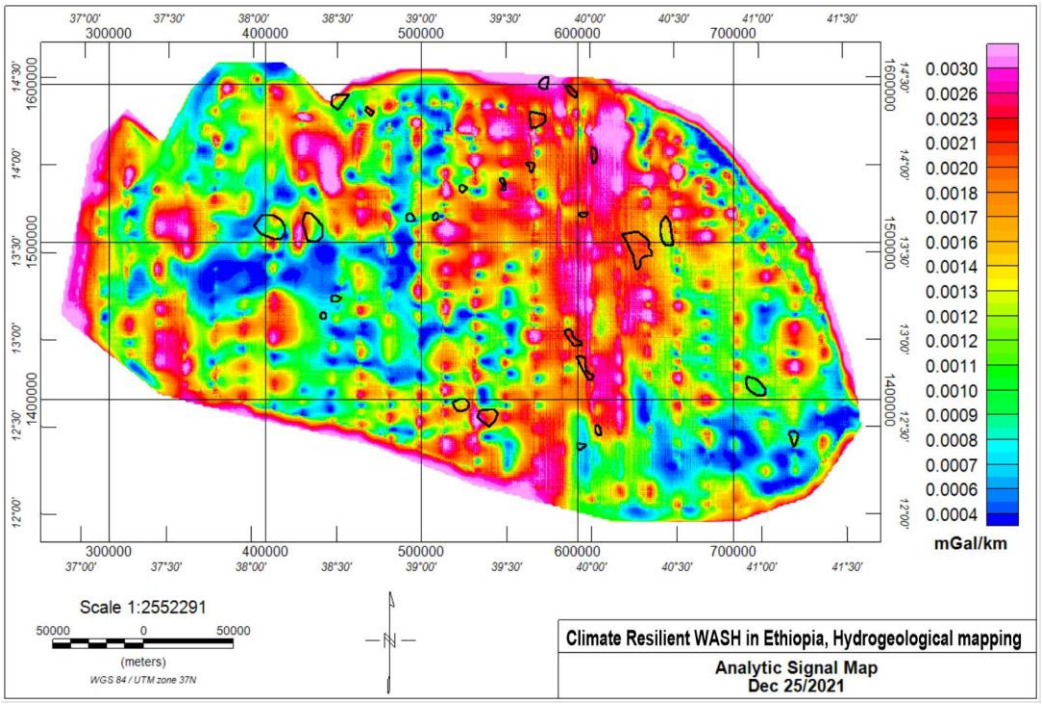

Figure 5.9. Analytical signals.

The tilt angle map is generated using the tilt angle formula (Equation 4) using the analytic signal as an input.

$$\theta_{As} = \tan^{-1}\left[\frac{\frac{\partial|As(x,y,z)|}{\partial z}}{\sqrt{\left(\frac{\partial|As(x,y,z)|}{\partial x}\right)^2 + \left(\frac{\partial|As(x,y,z)|}{\partial y}\right)^2}}\right] \qquad (5.7)$$

Zero counters are extracted from the tilt angle map (Figure 5.10A) and then the lineaments are extracted from zero counters (Figure 5.10B) linear features that show various structural fabrics in the southern main Ethiopian rift.

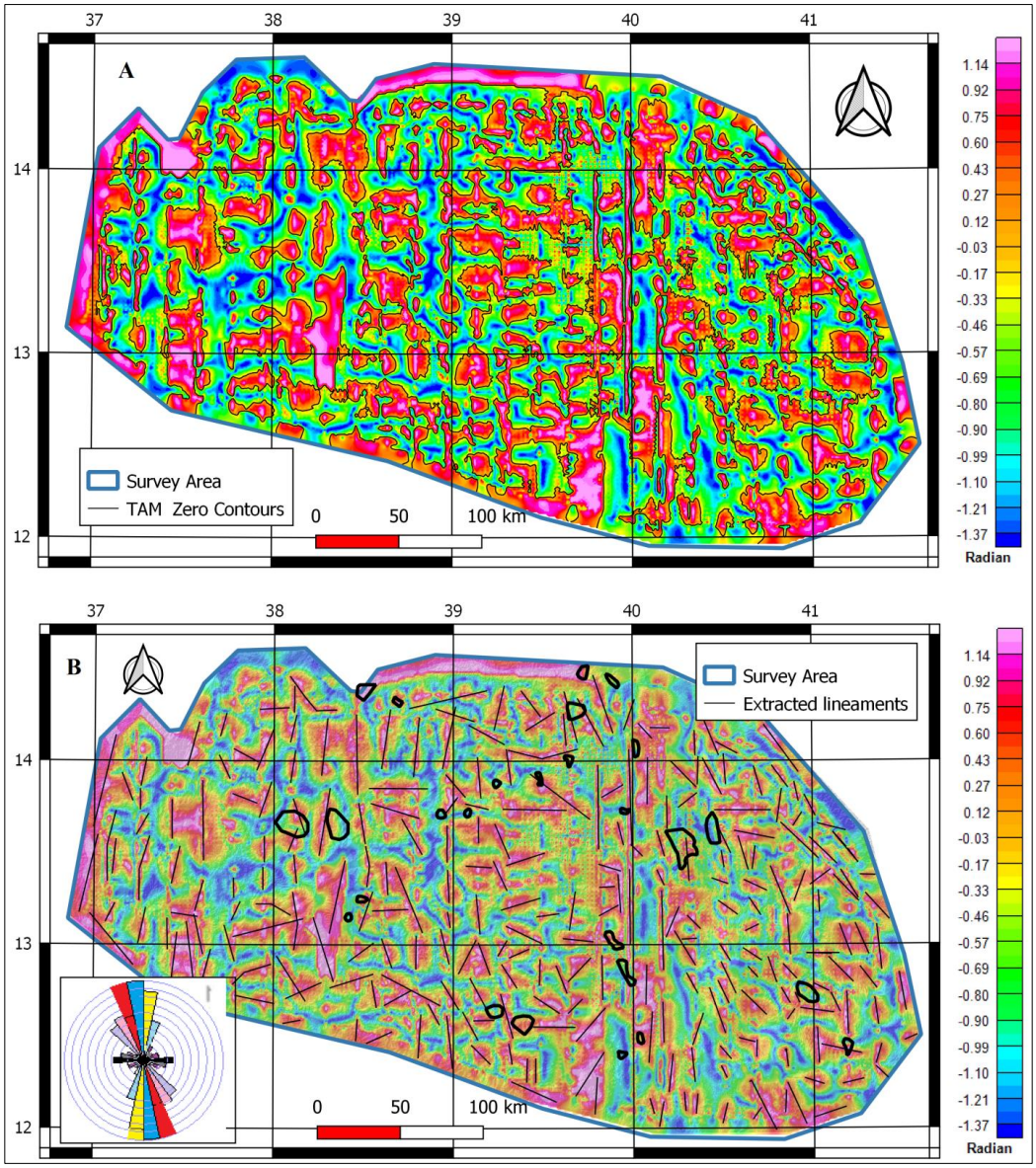

Figure 5.10. (A) Tilt Angle map generated from Analytical Signal Map with zero contours; (B) TAM with extracted lineament and Rose diagram highlighting the orientations of the main trend displayed on SRTM-DEM hillshade.

Directional analyses were done on the extracted lineaments using tilt angle displayed on SRTM-DEM hillshade on (Figure 5.10B) and the rose diagrams highlighting the orientations of the main trend in agreement with the regional fault orientations obtained from Mengesha et al, 1996 (Figure 5.11), the final lineament map of southern main Ethiopian rift (SMER) (Figure 5.12) is generated and the result is presented with reference to fault map of the SMER obtained from geological survey of Ethiopia (Mengesha et al., 1996) as shown in the Figure 5.11.

Both the existing and the extracted lineaments are overlaid on SRTM-DEM hill shade and the directional analysis is performed using the rose diagrams highlighting the orientations of the main trends which is almost identical on both maps as shown in (Figure 5.11 and 5.12).

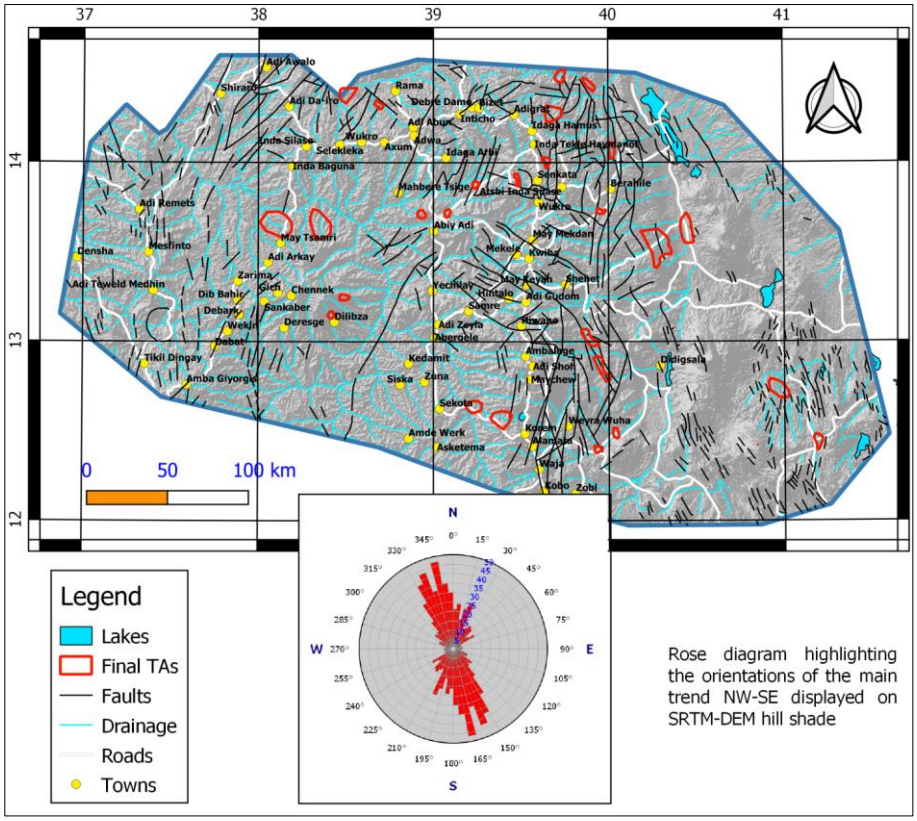

Figure 5.11. Existing faults obtained from the Geological map of Ethiopia (Mengesha et al., 1996).

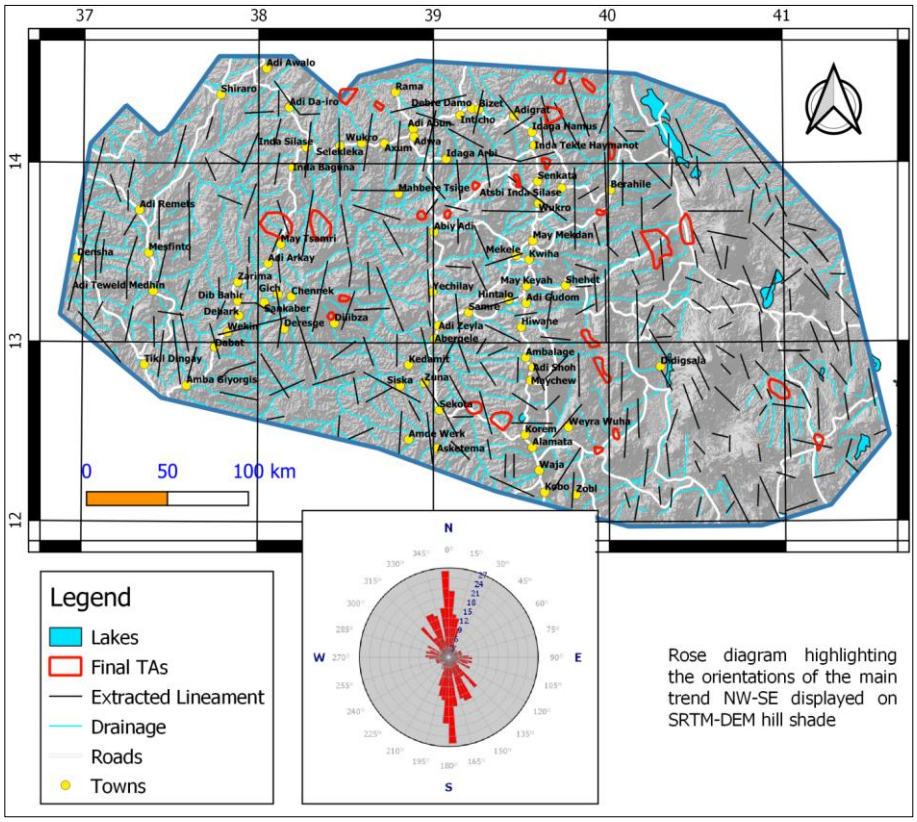

Figure 5.12. Extracted lineament using Bouguer gravity data set displayed on SRTM-DEM hillshade.

5.2.4 Source Depth Estimation

According to Salem et al. (2011) in the case of a thin vertical sheet, we assume that its thickness t is negligible; we therefore apply the approximation that the edges of the sheet correspond to the horizontal location of the source ($h = 0$). The depth to the edge of the horizontal sheet source corresponds to the distance between 0^o and 45^o adaptive tilt angle values ($h = z_c$); this result is similar to vertical contacts from magnetic data described by Salem et al. (2007) shown below;

$$\theta = \tan^{-1}\left[\frac{h}{Z_c}\right] \qquad (5.8)$$

Where h is the horizontal distance from the source, θ tilt angle and z_c is the depth to the contact. Equation-9 indicates the value of the tilt angle above the edges of the contact is 0^o ($h = 0$) and equal to 45^o when $h = z_c$ and -45^o when $h = -z_c$. This suggests that contours of the tilt angle can identify both the location at ($\theta = 0°$) and depth (half the physical distance between $\pm 45^o$contours) of contact-like structures.

Thus, the mapped shape of the zero contours indicates the mapped shape of the causative source, and the horizontal distance between the zero and $\frac{\pi}{4}$ contours provides an estimate of the depth to the top of the linear trends beneath the zero contours. The tilt angle map computed from the gravity components is a very useful interpretation tool since it provides a simple and clean image. The technique tends to enhance mapping of the subtle gravity anomalies, and maximizes characterizing the geometrical contrast of the anomalous sources and the method produces satisfactory depth estimation.

The depth estimation on average varies from 0.9 km to 3.1 km (Figure 5.13).

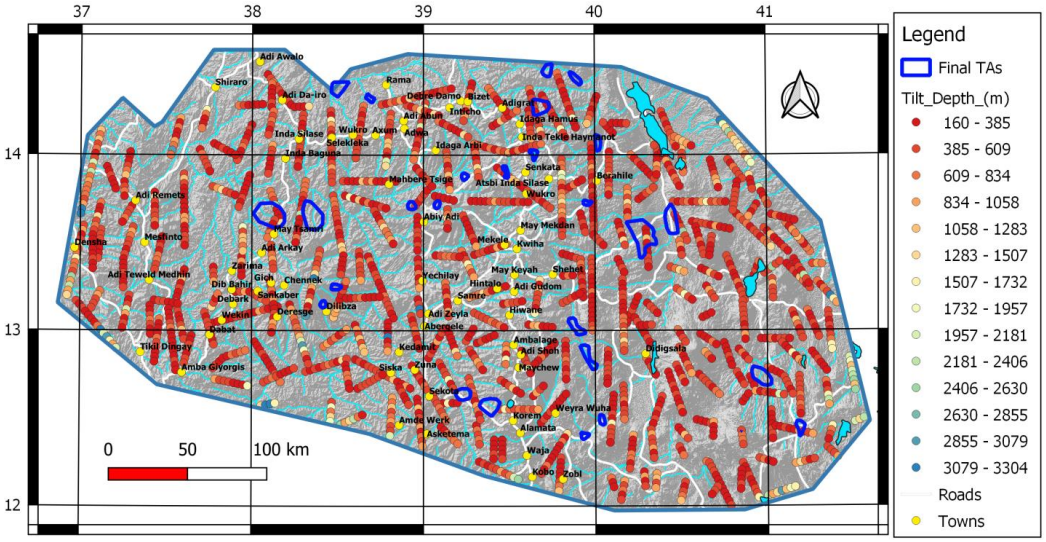

Figure 5.13. Tilt Depth extracted from tilt map prepared by the analytical signal from G_{zz}, G_{xx} and G_{yy} displayed on SRTM-DEM hillshade.

5.2.5 Edge Detection on Tilt Derivative Horizontal (TDX)

Tilt Derivative Horizontal (TDX) proposed by Cooper and Cowan (2006) is the amplitude of the horizontal gradient that is normalized to the absolute value of the vertical derivative. It can be computed by Equation-9 as follows:

$$TDX = \tan^{-1}\left(\frac{\sqrt{\left(\frac{\partial M}{\partial x}\right)^2+\left(\frac{\partial M}{\partial Y}\right)^2}}{\left|\frac{\partial M}{\partial z}\right|}\right) \qquad (5.9)$$

Where TDX Tilt Derivative Horizontal Filter, M is the gravity or magnetic field and $\frac{\partial M}{\partial z}, \frac{\partial M}{\partial x}$ and $\frac{\partial M}{\partial y}$ are the first derivatives of the field M in the x, y and z directions.

The positive peak values in Tilt Derivative Horizontal (TDX) grid are then extracted to locate the source edges using an automatic edge detection method. Tilt Derivative (TDR) works effectively with data from shallow sources, but it is considered relatively ineffective when dealing with data from deep sources. TDX is the inverse of the TDR proposed; as it performs equally well with both shallow and deep sources. Horizontal Tilt Derivative (TDX) (Figure 5.14) and an automatic edge detection (SED) performed on TDX clearly outlined the sub-basins edges. Fault from GSE Ethiopian Geological Map 1:2,000,000 with spectral display are shown in Figure 5.15.

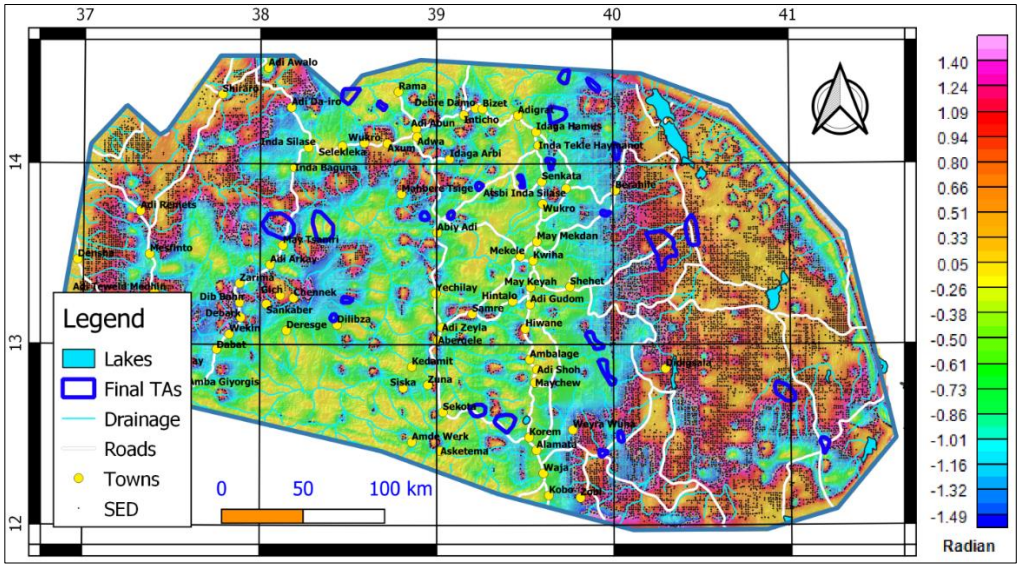

Figure 5.14. TDX Inverse of tilt angle map generated from Analytical Signal Map displayed on SRTM-DEM hillshade.

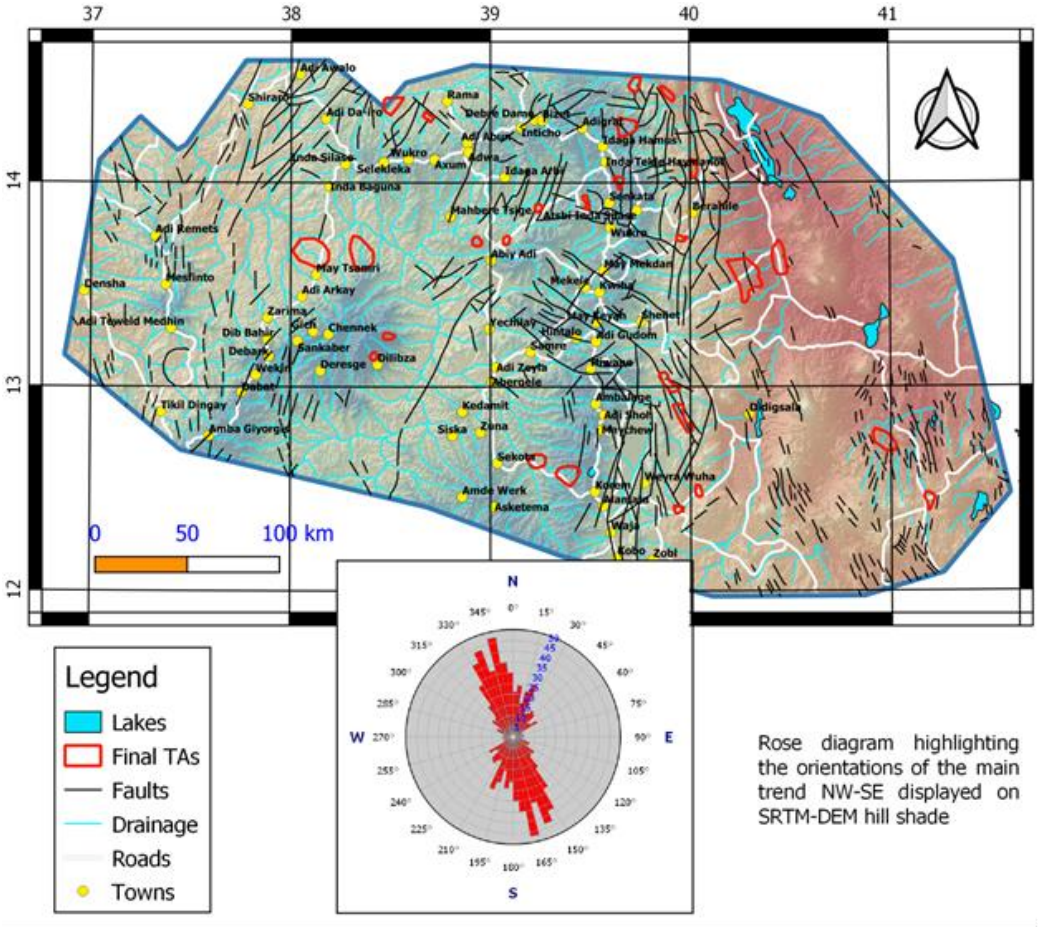

Figure 5.15. Fault from GSE Ethiopian Geological Map 1:2,000,000 with spectral display.

5.2.6 Results and discussion

Mapping lithological units/groups, structures such as contacts, lineaments, faults and dykes are essential processes in structural study. Identifying structural is of great importance to groundwater assessment programs. Length, orientation and density of lineaments are determined for the characterization of potentiality of resources. Tectonic features and lithological boundaries, weak zones, topographic reliefs can be revealed as regional lineaments.

As shown in the preceding sections, the different maps resulted from the numerical analysis of the airborne gravity data provide vital information such as depth of burial, extent, structure, and density and susceptibility properties of rock units.
The main contribution of this regional gravity data analysis is assisting better understanding of the regional tectonic framework of the project area which, in turn, the present and future endeavours of exploration for subsurface water.

The orientations of lineaments are multi-directional may be due to the effect of different tectonic processes. Owing to the broad regional nature of the data used, one should bear in mind that the signals correspond to elements of deeper origins in scale.
The source depth for the lineaments were also estimated on average varies from 900 m to 3100 m, indicating the majority of these signature attributes to shallow crustal fractures.

The residual gravity anomaly (Figure 5.6) shows contrasting anomaly, ranging from -11 mGal (over the central highland area of LOT1) to more than 9 mGal (over the relatively flat regions on the Easter target area) with probable depth of investigations 3km from the surface.

The large positive anomaly in the eastern part of the LOT 1 area is believed to be caused by massive basalt in the area and the low gravity anomaly is interpreted to reflect deeper basement structure, overlain by a low density material. Those target areas associated with lower anomalies bound to have more ground water potentials than those with higher anomalies.

5.3 Electrical method

5.3.1 Methodology

DC Electrical resistivity surveys are based on the response of the subsurface materials to the flow of artificially generated electrical current introduced into the ground by means of a pair of electrodes. The resulting potential differences, measured at the surface across another pair of electrodes provides a means to determine the resistivity that governs the relation between the current density and the gradient of the electrical potential. (Telford et al., 1990; Lowrie 1977). With few exception, most common rock-forming minerals are electrically insulators. Conduction of electricity in rocks and soils is therefore via electrolytes within the pore space which implies the resistivity in the subsurface is largely dependent upon the amount of pore water present, its conductivity, and the manner of its distribution within the material (Guyod, 1964). Hence, the electrical resistivity contrasts existing between lithological sequences in the subsurface is used in the delineation of distinct geoelectric layers which can ultimately be used to understand their physical and mechanical characteristics, such as compositions, moisture/fluid contents as well as degrees of weathering and fracturing.

The practical use of electrical resistivity measurements in studying construction site is related to the fact that the action structural disturbance and intensive weathering alter the soils characteristics such as moisture content, strength and consistency. This results in developing resistivity contrast between the top weathered column and the unaffected mass from the cumulative or separate action of mechanical breakage, weathering and an increase of water content. In such context, the conventional 1D Vertical Electrical Soundings has been used in a wide range of deeper geotechnical investigations including dam sites and helps to establish vertical layer stratifications (Othman 2005, Savvaidis et al 1999, Sharma, 1997),

Vertical Electrical Sounding (VES) is a focused single-point probing approach applied at selected locations to discriminate the subsurface layers. Implementation of this technique is based on the injection of known intensity of electric current (I) into the ground with the help of two stainless steel electrodes (A & B) and measuring the potential field difference (□V) with another two electrodes (M & N). Apparent resistivity (ra) is the parameter computed using the well-known standard formula:

$$\rho_a = k\frac{\Delta V}{I} \qquad (5.10)$$

Where k is the geometric factor (array coefficient) that depends on the mutual arrangement of the current and potential electrodes and it is computed as:

$$\rho_a = k\frac{\Delta V}{I} \qquad (5.11)$$

Where, rAM, rAN, rBM & rBN are distances between the respective electrodes as shown in Figure 5.16.

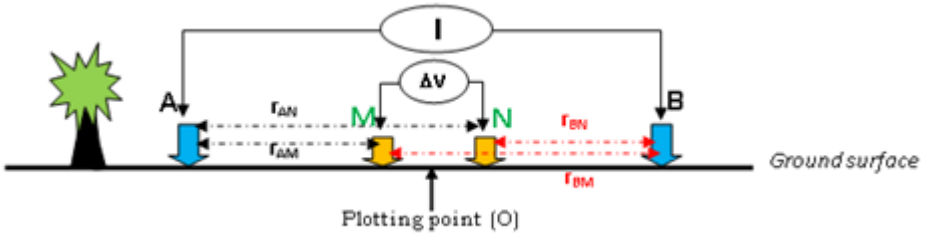

Figure 5.16. Electrode layout for VES surveys.

5.3.2 Data Processing

Whenever the VES points are found aligned along traverse lines, those points are used to construct the apparent resistivity pseudo-depth sections. Such representations are useful in getting an unbiased picture of the subsurface over the survey area and proved expedient in obtaining general but valid pictures of the subsurface.

For quantitative appraisal, a resistivity data processing and analysis software WinResist was used to obtain the final models in terms of the layer parameters (layer resistivity and thicknesses/depths) from the sounding data (Van der Velpen, 2004). The program utilizes an iterative inversion approach to fit the field data to a suitable subsurface model and provides layer parameters beneath each sounding points. During data analysis, a minimum root mean square percentage of error (the discrepancy between the observed data and the model response), ranging from 2 to 4% has been taken as acceptable.

Finally, the formation resistivity and thickness/depths, beneath the sounding point along the traverses have been used to construct a geo-electric section.

5.3.3 Results and discussion

It should be noted that only very few VES points were happened to be within the boundary of the target areas.

6 Hydrology

6.1 Introduction

The hydrological study aims at characterization of catchment areas, streams and rivers within or adjacent to the study areas and assessments on recharge patterns and rates, existence of springs and their hydrogeological implications and surface water and groundwater relationships. The assessment of the hydrology of the target areas is part of the development of Conceptual Models (Phase II) since analyzing the interaction between surface and groundwater is essential to understand the hydrogeology of the area.

The sustainability of groundwater use is a balance between recharge volumes of groundwater in a source area and subsequent extraction for domestic, agricultural and industrial use. Agricultural use of water is related to irrigation, mainly in the dry season. As irrigated water is lost to the atmosphere by evapotranspiration, the extraction of groundwater for irrigation results in increased evapotranspiration, and therefore will affect river runoff if groundwater levels are structurally lowered by the extraction. The water balance equation provides information on the distribution of precipitation over the evapotranspiration, groundwater flow and river runoff components, as shown in Equation 6.1.

$$P = ET + Q_g + Q_s + \Delta S \qquad (6.1)$$

6.1.1 Objectives

The objectives of the surface water balance study were:

- Collection, compilation and review of all existing pertinent data and information from various sources
- Delineation of all surface water bodies including river networks, reservoirs, lakes and ponds and assess their interaction with groundwater;
- To carry out a monthly water balance modelling of the selected 26 target areas;
- Provide groundwater recharge maps for the target areas.

Groundwater recharge is one of key input in the overlay analysis and is investigated using multiple approaches so at to arrive at acceptable values. Recharge is estimated for each woreda based on the recharge generated by validated SWAT models, which has been a proven approach in Ethiopia. The recharge values obtained in this study serve to assess the sustainability and limits of groundwater extraction for use in agriculture or drinking water supply.

6.1.2 Scope

This study is a continuation of Phase I and II of hydrogeological mapping of climate resilient WASH project in Ethiopia. For the surface water hydrological study, meteorological and hydrological data available on daily time scale were collected and analyzed. The study envisages the rainfall-runoff processes with the objective of estimating the water balance components of the target areas on monthly and annual time scales. Groundwater recharge was estimated using the Soil and Water Assessment Tool (SWAT) model at sub-watershed level. The water availability within the target areas for different competing needs, i.e. for domestic, irrigation, industrial and livestock use, have been estimated through accepted techniques. Due to many sources of uncertainties, such as in the temporal input data, spatial data heterogeneities, hydrological model spatial representation and model parameter uncertainties, the estimated water balance components and recharge are subject to a certain degree of uncertainty. Hence, the study first and foremost was limited to use merged rainfall satellite products from the Climate Forecast System Re-analysis (CFSR) and CHIRPS data (Climate Hazards Centre, n.d.; Dinku et al., 2018) as forcing inputs into the SWAT model in order to estimate the water balance components and recharge. However, one could get different outcomes using different forcing inputs, hydrological models and approaches. The other limitation of this study is that the estimated baseflow and the spatio-temporal variation of the water availability have not been validated through field exploration. This could not happen due to the current security issue in the study area.

6.2 Methodology

The determination of the water balance components, including river flow amounts and groundwater recharge estimates, was based application of the Soil Water Assessment Tool (SWAT) model (Arnold et al., 2012; Srinivasan et al., 2010; Tibebe and Bewket, 2011) to a number of catchments in the project area. The modelling data and procedures has been described below.

6.2.1 Hydrological approach to evaluating water balance aspects

The streamflow data are mainly used to understand the rainfall-runoff relationship in the area so as to estimate the water balance and the recharge amount reach to the groundwater storage on monthly and annual time scales. By understanding the data scarcity and time constraints, the streamflow data of the Geba River a tributary of Tekeze from 1998 to 2013 gauged at Adi Kumsi have been used. After calibrating and validating the model the calibrated model parameters are transferred into the bigger catchment area Tekeze gauged at Emba Madre and the target areas. The general methodological framework followed in this study is presented in Figure 6.1.

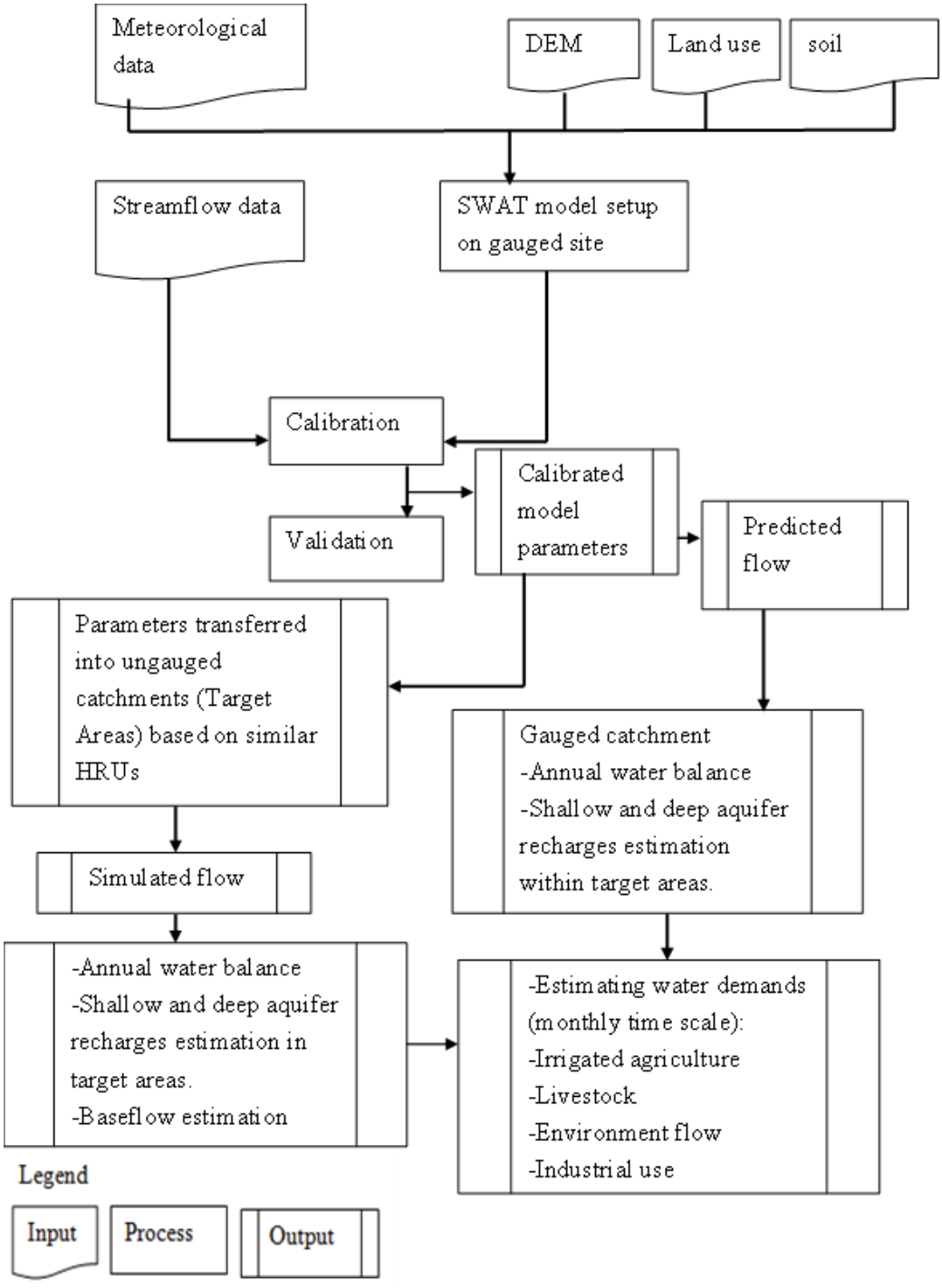

Figure 6.1. Schematic flow diagram for the approach to arrive at water balance estimates in the target areas.

6.2.2 SWAT Model

The internationally widely-used SWAT model (Arnold et al., 2012) calculates water and nutrient cycles, as well as sediment transport and vegetation growth. The model is therefore uniquely suited to quantify the effects of changes in land use, management techniques, and climate on the distribution of water and nutrients in catchments, including groundwater recharge impacts. SWAT combines elevation, land use, and soil

data into so-called Hydrological Response Units (HRUs), which form the basis of the hydrological, biological and biogeochemical calculations. The HRUs are sub-catchment elements, each forming a unique combination of soil, land use and slope, which drain into reaches in a sub-catchment. The sub-catchments together form the main catchment. The distribution of HRUs, sub-catchments and stream channels in the Tekeze River Basin covering a number of project target areas is shown in Figure 6.2. Water is routed through the individual channels that form the (sub)catchment stream network. Calculated water fluxes are calculated for each of the HRUs, sub-catchments, and stream sections. These fluxes were used to estimate the groundwater recharge.

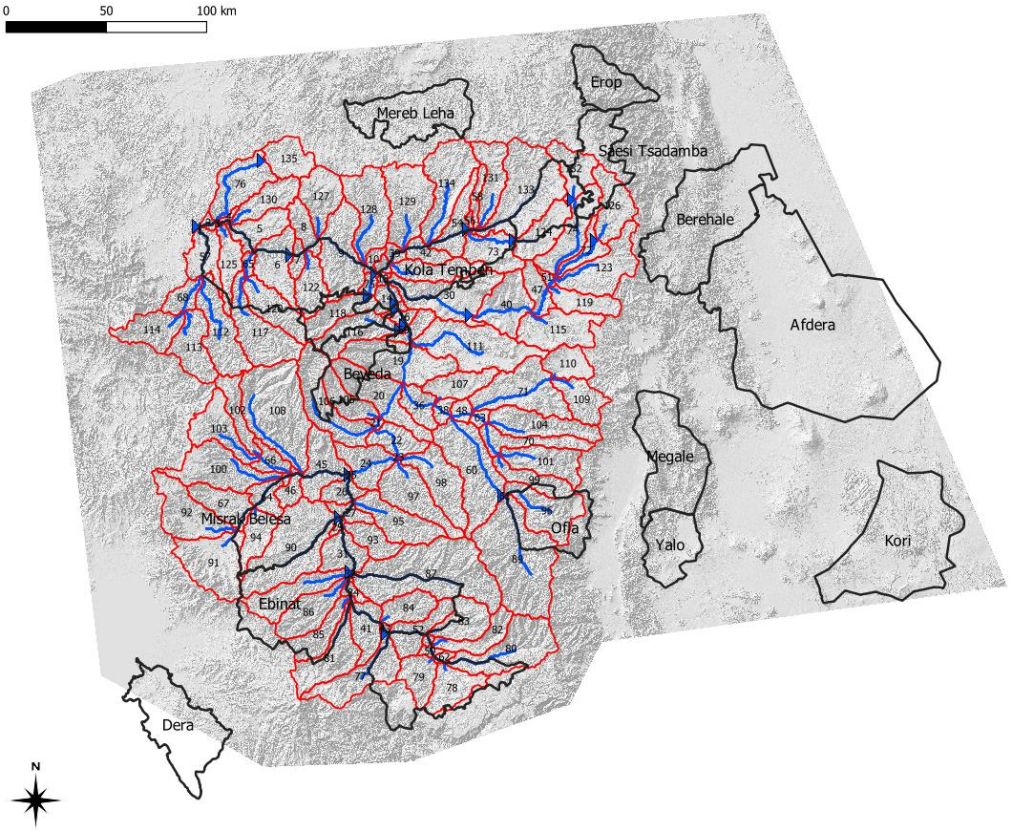

Figure 6.2. SWAT model of the Tekeze River basin including the Embamadre and other river stations. The distribution of subcatchments (red), drainage (blue) and a number of target woredas (black) are shown on a hillshade background.

6.2.3 The SWAT Model application

The rainfall runoff SWAT model has been used to estimate the discharge time series, water balance components and recharge amount in the target areas. Among many methods of prediction discharges at ungauged location, transferability of model parameters to the nearest catchment through spatial proximity method was employed in this study. Consequently, calibrated parameters of Geba River catchment, gauged at Adi-kumsi, with similar unique hydrologic response units as for the larger region was set to predict the streamflow at the ungauged sites where target areas are located. The hydrological cycle, based on the water balance equation (Equation 6.2) is captured in more detail by:

$$SW_t = SW_O + [\sum_{i=1}^{t} R_{day} - Q_{surf} - E_a - W_{seep} - Q_{gw}] \quad (6.2)$$

Where: SW_t is the final soil water content (mm); SW_0 is the initial soil water content on day *i* (mm); *t* is the time (days); and R_{day}, Q_{surf}, *E*a, W_{deep} and Q_{gw} are, respectively, the amounts in mm of precipitation, surface runoff, evapotranspiration, water percolation into the deep aquifer and the amount of groundwater flow on day *i*.

The Natural Resources Conservation Service Curve Number (CN) method was used for the estimation of the surface runoff component in SWAT (USDA-NRCS, 2004). The evapotranspiration was estimated using Penman-Monteith (Equation 6.3) (Monteith, 1965). The Penman-Monteith method, which has been applied successfully in different parts of the world, was compared with other methods and is accepted as the preferred method for computing potential evaporation from meteorological data (Allen et al., 1998; Zhao et al., 2005). The flow routing in the river channels is computed using the variable storage coefficient method (Williams, 1969).

$$\lambda E = \frac{\Delta.(R_n - G) + \rho_{air}.C_p.[e_z^0 - e_z]/r_a}{\Delta + \gamma.(1 + \frac{r_c}{r_a})} \qquad (6.3)$$

Where λE is the latent heat flux density (MJ m^{-2} d^{-1}), E is the evaporation rate (mm d^{-1}), Δ is the slope of the saturation vapor pressure-temperature curve, de/dT (kPa $^{\circ}C^{-1}$), R_n is the net radiation (MJ m^{-2} d^{-1}), G is the heat flux density to the ground (MJ m^{-2} d^{-1}), ρ_{air} is the air density (kg m^{-3}), c_p is the specific heat at constant pressure (MJ kg^{-1} $^{\circ}C^{-1}$), is the saturation vapour pressure of air at height z (kPa), e^o_z and e_z are the water vapour pressures of air at height z (kPa), γ is the psychrometric constant (kPa $^{\circ}C^{-1}$), r_c is the plant canopy resistance (s m^{-1}), and r_a is the diffusion resistance of the air layer (aerodynamic resistance) (s m^{-1}). Further detailed descriptions about the model formulations are found in Neitsch et al. (2011) and Arnold et al. (2012).

The following SWAT model outputs were important for assessing the water balance components and groundwater recharge in the target areas. It should be noted that the target areas do not follow hydrological boundaries and that recharge of target are groundwater may also be in upstream parts of the catchment areas outside of the target area boundaries.

The components listed below are shown on target area maps and the averages were calculated for each area to provide an indication of the average annual totals for the area. The monthly variations in these components are shown in graphs.

Precipitation

Precipitation was based on a Thiessen polygon (Thiessen, 1911) approach in the SWAT model as part of taking into account the spatial distribution of CHIRPS or CFSR precipitation in the larger region.

Evapotranspiration

Potential evaporation values for these grided sites have been estimated using the Hargreaves method. The method is based on air temperature data (Hargreaves and Allen, 2003) and can be used to estimate crop water requirements (Latif and Javed, 1998). Furthermore, actual evapotranspiration (ET_a) estimates for the different hydrological response units was modelled in SWAT using the Penman-Monteith (Monteith, 1965) equation. The modelled ET_a values for the HRUs were used to show the spatial variation within the target areas.

Lateral runoff components

The lateral runoff was simulated with SWAT for each HRU and contributes to the fast flow component of the stream hydrographs.

Groundwater recharge

Groundwater recharge was simulated for every HRU with the SWAT model and forms the dry season baseflow component of the stream hydrographs. In addition, SWAT also models recharge to deep groundwater reservoirs that does not leave the basin as streamflow but contributes to a larger regional system.

6.3 Data Sources

The study relied for input on public data sources, whereas observed data from the Ethiopian authorities were used for verification.

6.3.1 Public data sources

The SWAT model use topography, land cover and soil maps for the generation of the HRUs, whereas meteorological data are used to drive the model.

Topography

The Digital Elevation Model (DEM) used for the SWAT model was the Shuttle Radar Topography Mission (SRTM) with a resolution of 30 m (Farr et al., 2007). The topography of the region is shown in Figure 6.3. Elevation in the region varied between 760 m and 4537 m amsl, with the mean elevation at 1971 m amsl. The cumulative elevation distribution for the area is shown in Figure 6.4. The relatively high elevation impacts on the ambient air temperature and therefore affects evaporation rates.

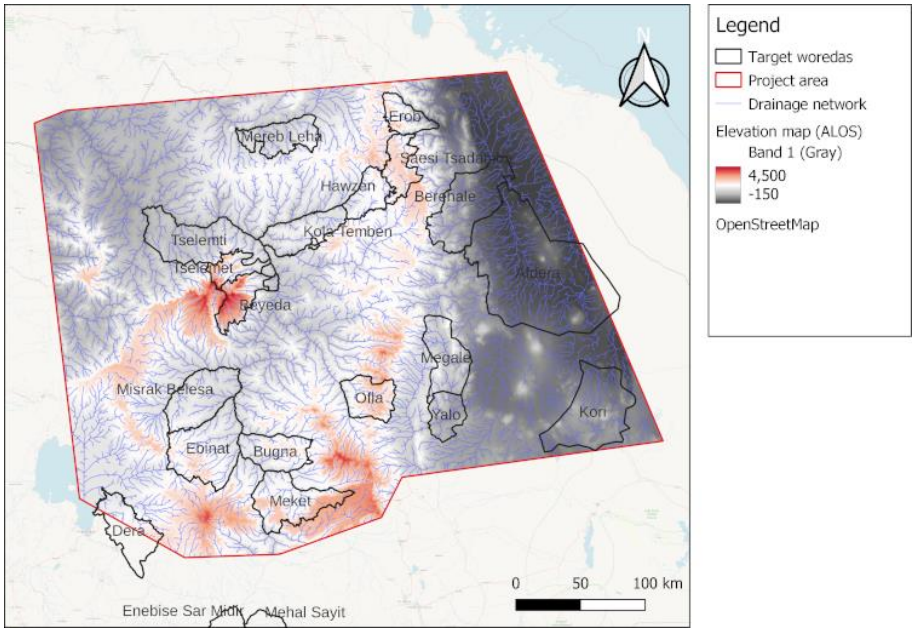

Figure 6.3. Digital elevation map of the project area.

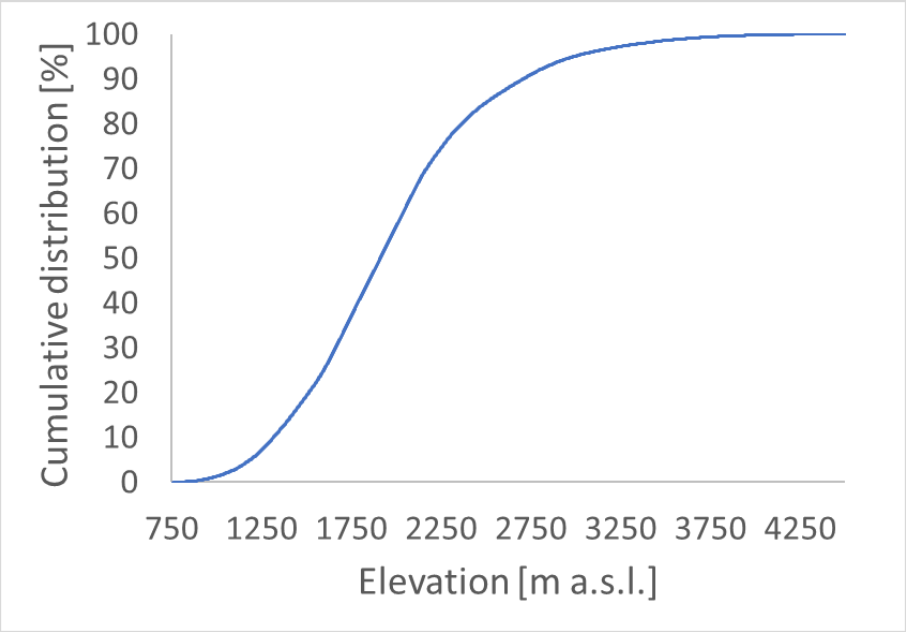

Figure 6.4. Cumulative distribution of the elevation in the Tekeze River basin region.

Land cover

The land cover map was the 100 m resolution Copernicus Global Land Cover Layers: CGLS-LC100 Collection 3 (Buchhorn et al., 2021) which reflects the land cover in 2015. The land cover in the region consisted mainly of cultivated and managed vegetation/agriculture – cropland (42%, AGRL), shrubland (36%, SHRB), herbaceous vegetation (14%, PAST) and closed forests (7%, FOMI). The land cover map is shown in Figure 6.5.

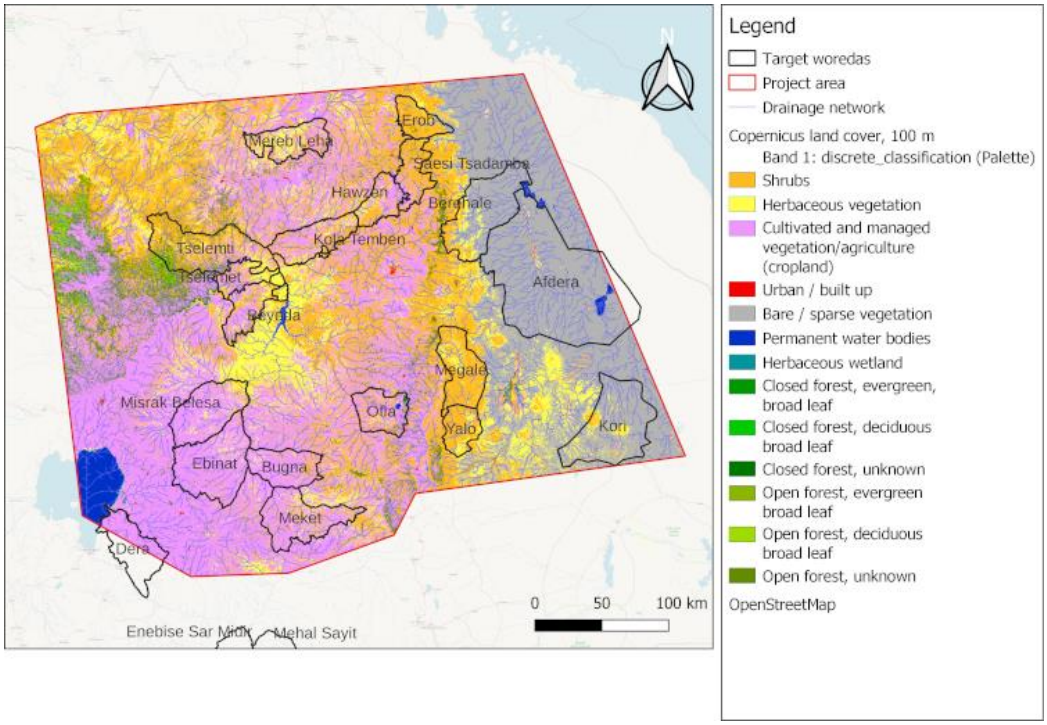

Figure 6.5. Copernicus land cover map of the project area.

Soil

The soil map was a rasterized version, at 100 m resolution, of the Soil Atlas of Africa (Joint Research Centre (European Commission) et al., 2013). The dominant soil was a shallow Lithic Leptosol covering 47% of the area. Eutric Leptosols and Haplic Luvisols covered 19% and 15% of the area, respectively. The soil map of the region is shown in Figure 6.6.

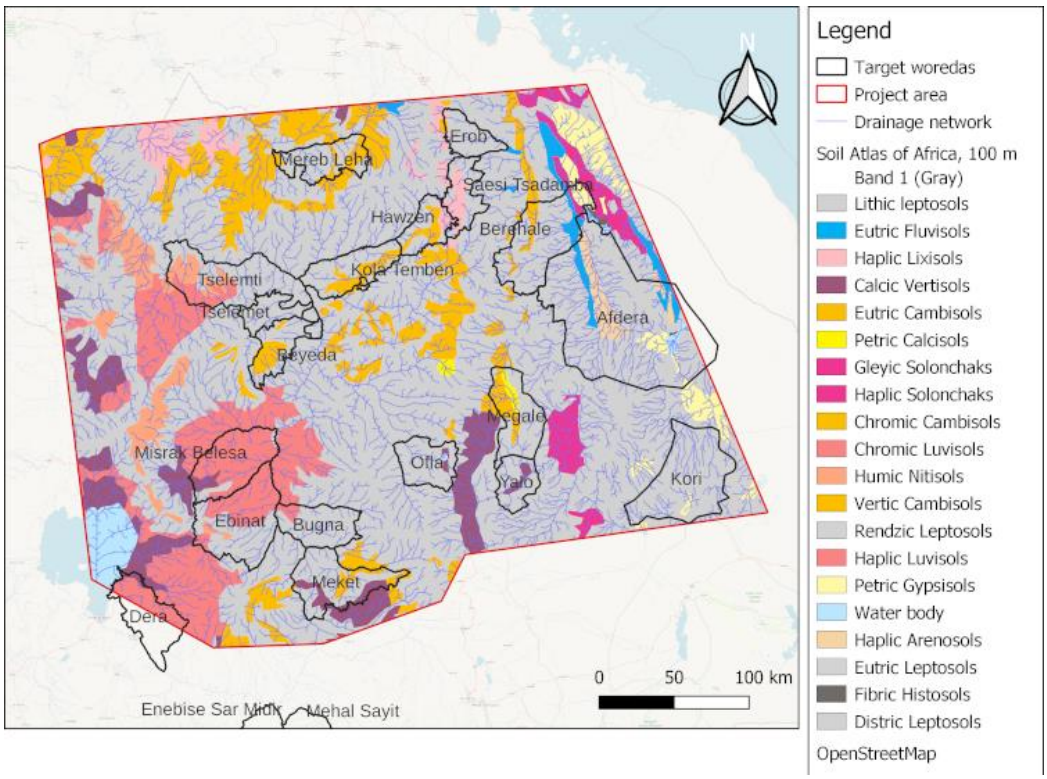

Figure 6.6. Soil Atlas of Africa map of the project area.

Climate

Climate data were obtained from the Climate Forecast System Reanalysis (CFSR) (Saha et al., 2010) for a number of grid points covering the area using the period 1984 – 2013. Gridded Climate Forecast System Reanalysis (CFSR) data (1994-2013) of 109 stations covering the project area were retrieved and processed to serve as input into the SWAT model. The data consisted of daily time series of minimum temperature, maximum temperature, relative humidity, wind speed and solar irradiance. The spatial distribution of the climate data is shown in Figure 6.7. In addition, 29 CHIRPS precipitation data stations (Climate Hazards Centre, n.d.; Dinku et al., 2018) were used to drive the Tekeze Basin study (Figure 6.8) as the CFSR precipitation data was found to underestimate precipitation for some stations.

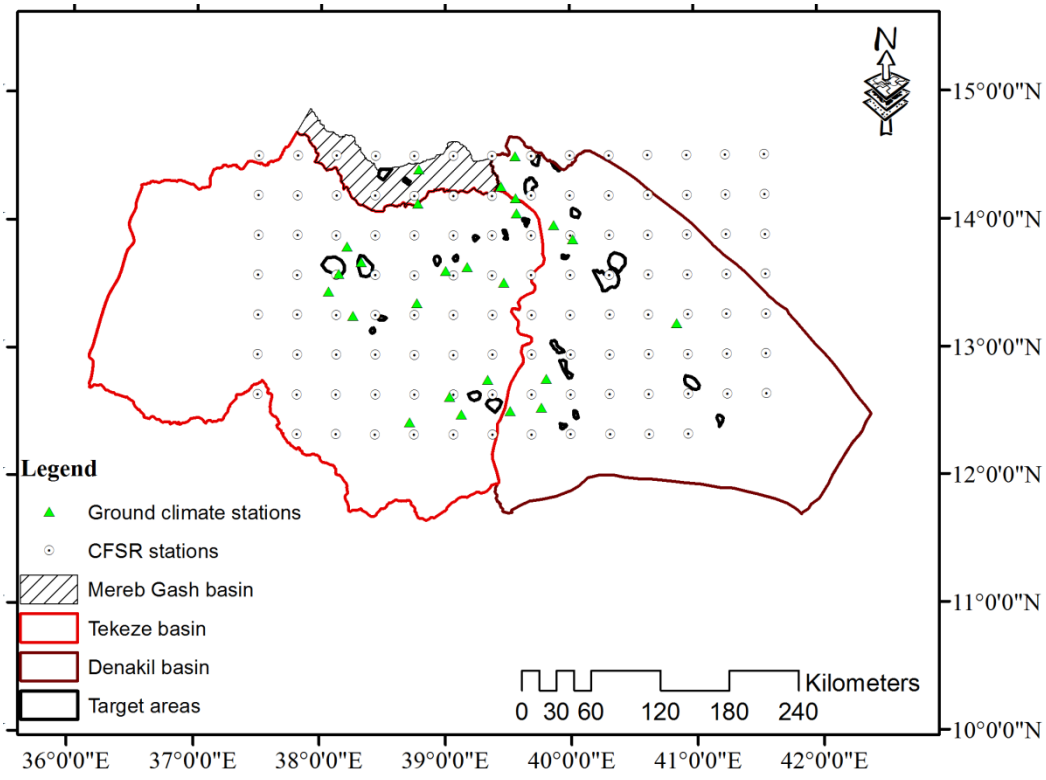

Figure 6.7. Spatial distribution of the CFSR Climate stations in the study area.

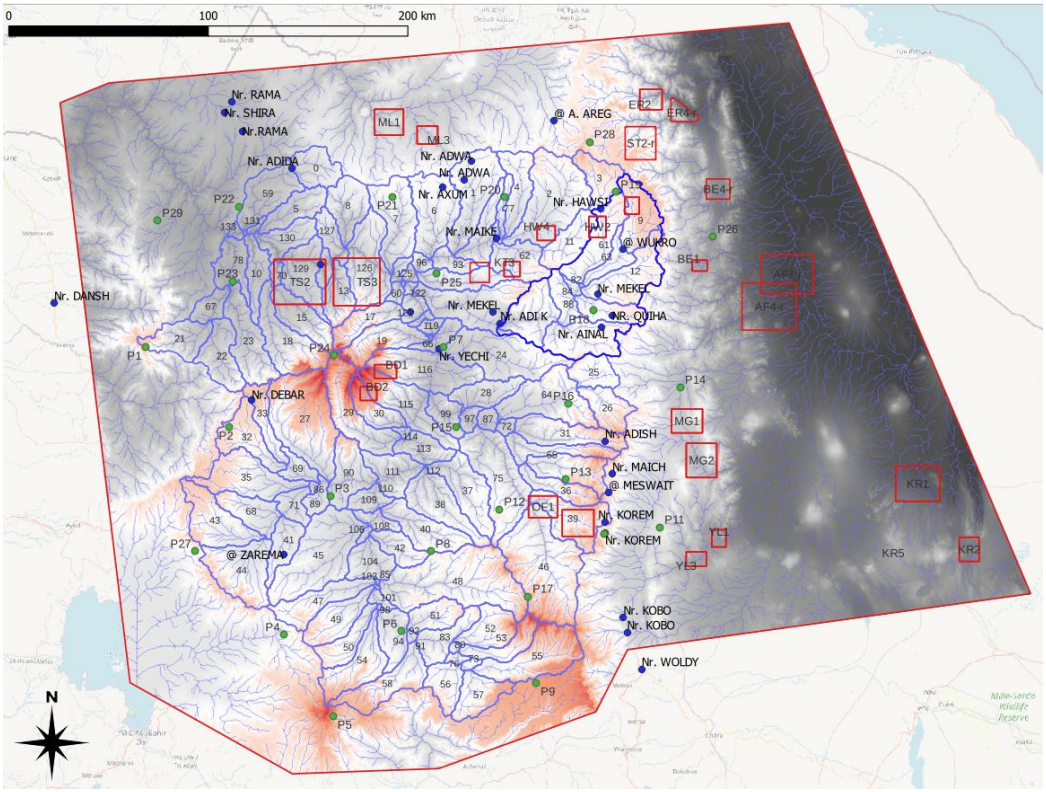

Figure 6.8. SWAT model of the Tekeze River Basin with numbered sub-catchments (light-blue), the Geba catchment (dark-blue) and target areas (red). The CHIRPS precipitation data points (green) and streamflow observation points (blue) are also shown.

6.3.2 Observational data

Both climate and hydrological observational data were provided by the National Meteorological Agency (NMA) and by Ministry of Water and Energy (MoWE). To solve the problem of data scarcity, the CFSR data from 1996 to 2013 have been used. This period was selected because ground climate stations had too many gaps in the recorded data and the streamflow data availability in the study area also forced to use a concurrent dataset.

To validate the input data for the SWAT model, a comparison was made for the public and observational data. In order to use the CFSR data, about 19 ground based climate stations in the study area nearest to the CFSR location were cross checked at least for their spatial correlation. The long-term mean monthly value of rainfall and air temperature has been inspected. For brevity only sample figures showing the seasonal pattern are presented in Figure 6.9. The lists of the climate stations, along with their correlation coefficients, are provided in Table 6.1 and Table 6.2, respectively. The spatial distribution of ground climate and CFSR stations used for cross validation is shown in Figure 6.10.

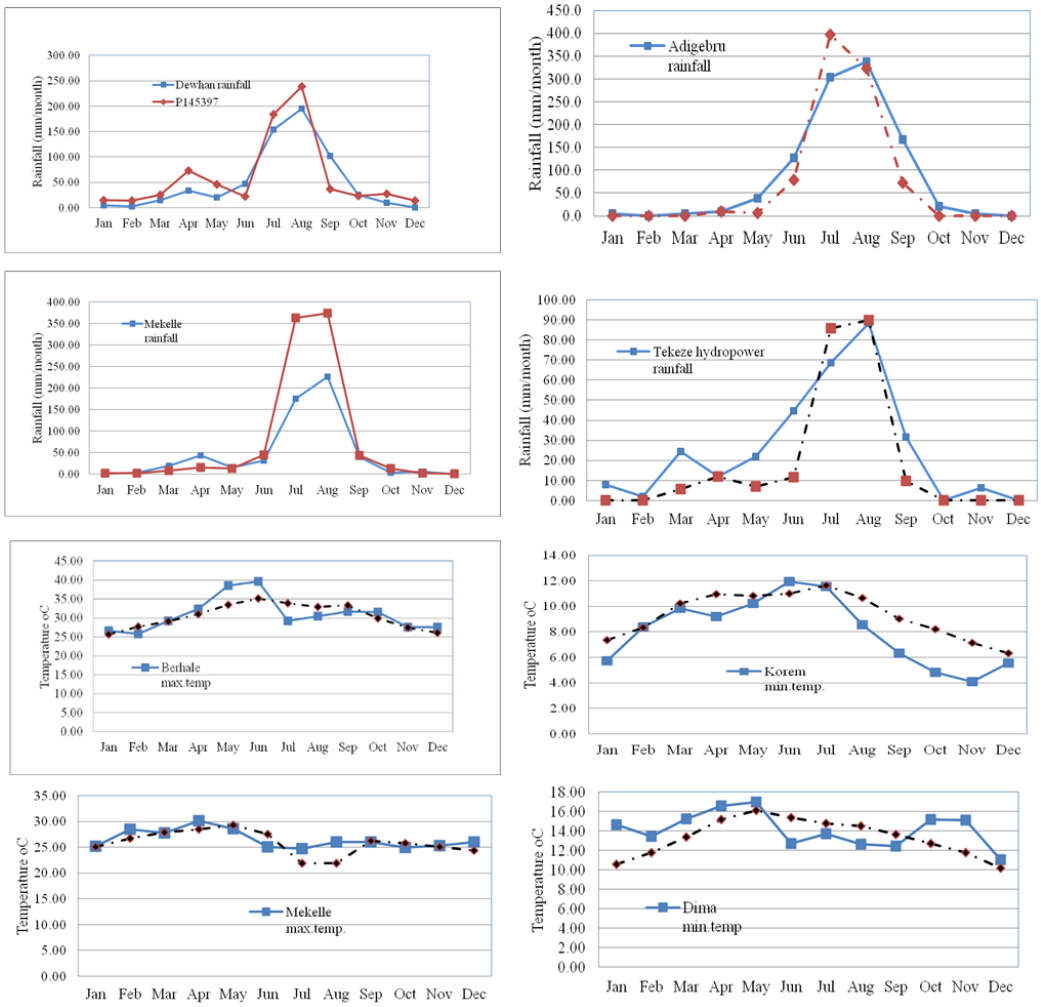

Figure 6.9. Comparison between long-term observed precipitation time series and corresponding CFSR data.

Table 6.1. Correlation of long-term average rainfall of ground climate stations and the corresponding nearby CFSR climate stations.

S. No.	Ground station	CFSR station	Correlation coef. (r)	Data length
1	Abi-Adi	P136391	0.96	1995-2012
2	Adigebru	P139381	0.99	2007-2013
3	Adigrat	P142394	0.92	2002-2013
4	Amedework	P123388	0.99	2009-2012
5	Axum airport	P142388	0.98	2007-2013
6	Berhale	P139400	0.62	2008-2013
7	Chercher	P126397	0.94	2007-2013
8	Dewehan	P145397	0.92	2006-2013
9	Dimma	P136384	0.45	1998-2009
10	Gibana	P123391	0.91	2008-2013
11	Hagere Selam	P136394	0.21	1990-2012
12	Korem	P123394	0.97	1992-2012
13	Matsebre	P136381	0.96	2008-2013
14	Mekelle	P136394	0.98	2004-2013
15	Rama	P142388	0.99	2003-2013
16	Senkata	P136397	0.92	2001-2013
17	Sekota	P126391	0.99	1997-2013
18	Tekeze Hydropower	P133388	0.92	2008-2011
19	Wedisemro	P126394	0.99	2002-2013

Table 6.2. Correlation of long-term mean monthly air temperature of ground climate stations and the corresponding nearby CFSR climate stations.

S. No.	Ground station	CFSR station	Correlation coef. (r) max. temp.	Correlation coef. (r) min. temp.	Data length
1	Abi-Adi	t136391	0.76	0.79	1995-2012
2	Adigrat	t142394	0.50	0.75	1998-2013
3	Axum airport	t142388	0.88	0.82	2007-2013
4	Berhale	t139400	0.76	0.48	2008-2013
5	Chercher	t126397	0.81	0.55	2007-2013
6	Dewehan	t145397	0.83	0.95	2006-2013
7	Dimma	t136384	0.74	0.40	1998-2009
8	Hagere Selam	t136394	0.30	-0.28	1990-2012
9	Korem	t123394	0.40	0.88	1992-2012
10	Kuneba	t139400	0.40	0.30	2008-2013
11	Mekelle	t136394	0.65	0.83	2004-2013
12	Senkata	t136397	0.57	0.90	2001-2013
13	Sekota	126391	0.74	0.71	1995-2013
14	Wedisemro	t126394	0.65	0.36	2002-2013

The spatial variation in the area is large, with low values in the eastern low-elevation parts and high values in the mountain ranges in the West. The variation as obtained from CHIRPS is shown in Figure 6.11.

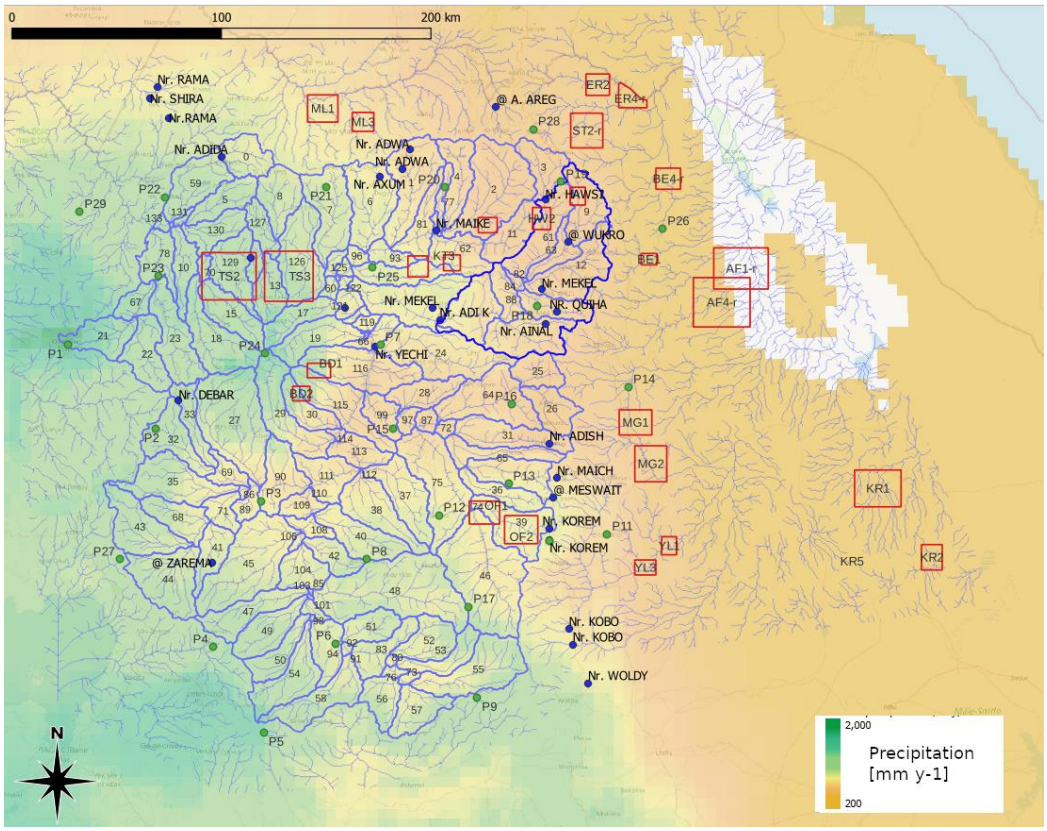

Figure 6.10. Spatial variation in annual precipitation totals as given by CHIRPS (2001-2021).

6.4 Baseflow separation method

To separate baseflow from stormflow, the discharge time series in $m^3 s^{-1}$ was converted to mm d^{-1} units and the natural logarithm was taken to allow separation of fast draining soil reservoirs from slow groundwater reservoir contributions, as characterized by changes in the slopes in the baseflow recession curve (Tallaksen, 1995). When the dam reservoir in the Tekeze River Basin was created and filled from 2008 onwards, this method could not be used anymore as the flow became influenced by the reservoir storage and release operations. A linear increase was assumed for baseflow increase in wet periods and the slope of the baseflow increase was determined from the difference in flow between the start of stormflow and return to the baseflow recession, divided by the time in days.

6.5 SWAT Model setup for Geba catchment

In the process of model setup, the public topographic, land cover and soil maps described above were used to delineate and characterize the catchment Geba river gauged at Adi Kumsi station. The delineated area constitutes about 3,385 km^2, divided into 25 sub-catchments.

The land cover for the catchment is shown in Figure 6.11. All land use parameterizations (e.g. leaf area index, maximum stomatal conductance, maximum root depth, optimal and minimum temperature for plant growth) were assigned on available SWAT land use classes, as shown in Table 6.3.

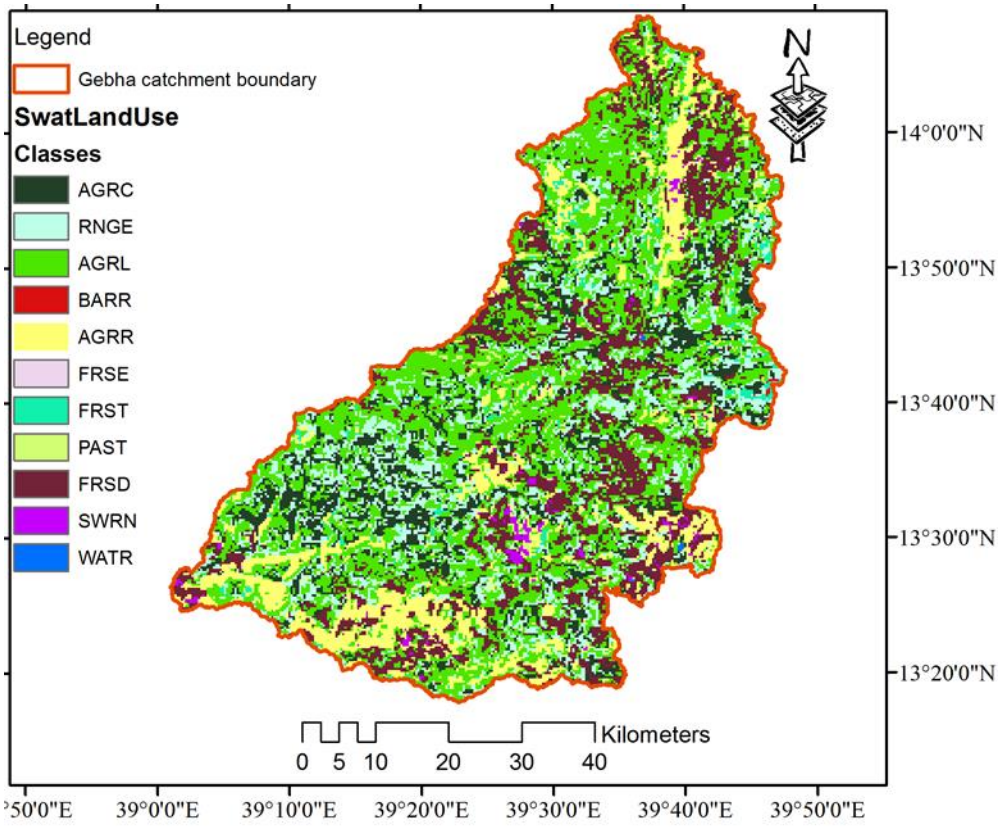

Figure 6.11. Land use map of Geba catchment with outlet at Adi Kumsi.

Table 6.3. Land use/cover types of Geba catchment gauged at Adi Kumsi for SWAT model input.

LU/LC redefined by SWAT	SWAT code	% of total area
Agriculture close grown	AGRC	14
Range land	RNGE	16
Agriculture generic	AGRL	37
Barren land	BARR	0.0
Agricultural land row crops	AGRR	13
Forest evergreen	FRSE	0.0
Forest	FRST	1.2
Pasture	PAST	0.4
Forest deciduous	FRSD	18
Range arid land	SWRN	0.8
Water	WATR	0.0

Figure 6.12 presents the soil types in the catchment. There are six soil types in the catchment and the types and percentage coverage are provided in Table 6.4.

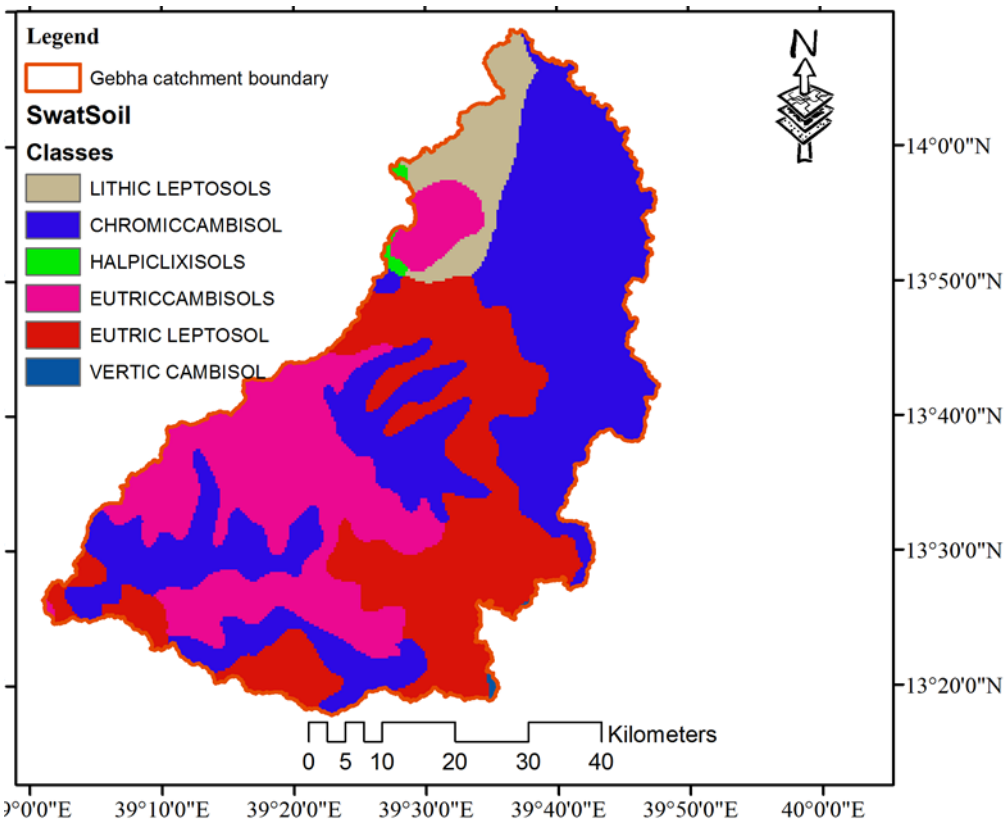

Figure 6.12. Soil map of Geba catchment with outlet at Adi Kumsi.

Table 6.4. Soil types of Geba catchment gauged at Adi Kumsi for SWAT model input.

Soil type	Area	
	km²	%
LithicLeptosols	221	5.69
Chromiccambisols	1676	43.15
Halpiclixisols	12	0.31
EutricCambisols	946	24.363
EutricLeptosols	1024	26.357
VerticCamisols	4.5	0.115

Topography and slope class definition were according to Figure 6.13 and Table 6.5, respectively.

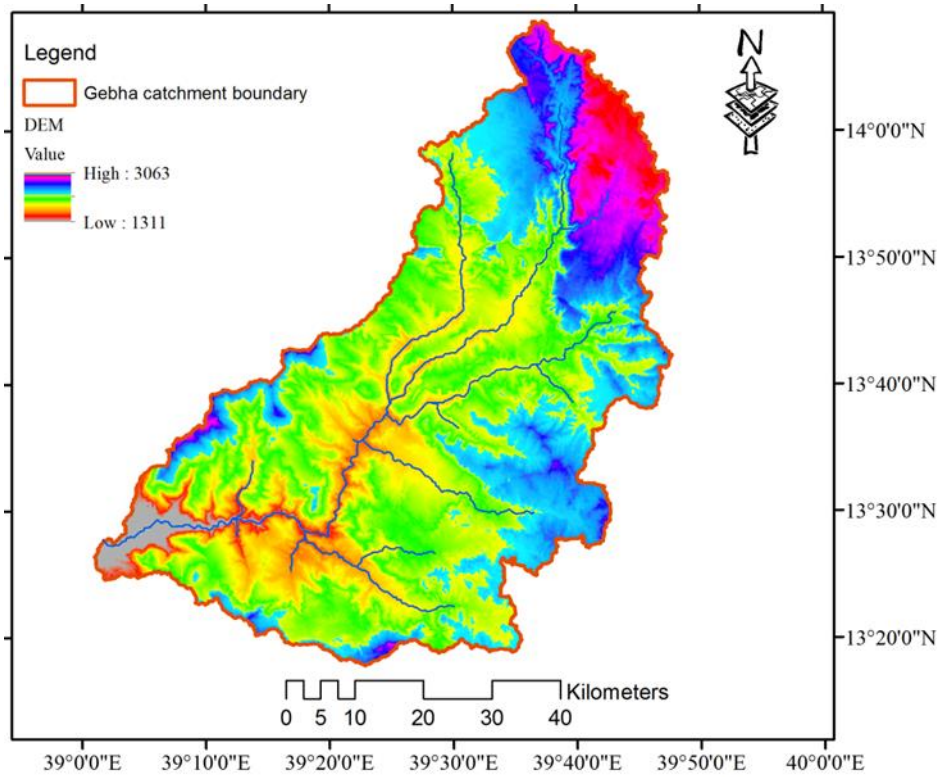

Figure 6.13. Topographic variation in the Geba Catchment with outlet at Adi Kumsi.

Table 6.5. Slope percentage distribution in Geba catchment gauged at Adi Kumsi.

S. No.	Slope class (%)	%of total area
1	0-5	15.6
2	5-15	46.0
3	15-30	28.6
4	30-45	9.8
5	>45	15.6

Finally, the spatial data, the land use map, the soil map and the topographic information (the slope classes) were overlaid to derive a total number of 673 HRUs with unique land cover/soil and slope classes. The land use, soil and slope datasets were imported overlaid and linked with the SWAT databases. To define the distributions of HRUs multiple HRU definition options were tested. For the final multiple HRU definition 10% land use, 10% soil and 5% slope thresholds were used.

6.6 Sensitivity analysis, calibration and validation

The SWAT model was calibrated against the observed discharge data from the Adi Kumsi station of the Geba River catchment, which forms part of the Tekeze River Basin. The calibrated model parameters were applied to the larger Tekeze Basin model, which included 11 target areas and to smaller scale models that included the remaining target areas (Figure 6.8).

6.6.1 Calibration of parameters

The streamflow data 1998-2004 were used for calibration and 2010-2013 were used for validation. Within a calibration period a warm up period was set to initialize the model for two years 1996–1998. Manual calibration was used to calibrate model parameters which represent the catchment runoff response to precipitation (Cibin et al., 2010; Moreira et al., 2018). The manual calibration was done by varying the values of the sensitive parameters within their permissible range (Table 6.6). It was carried out repeatedly by changing one of the most sensitive parameters in the model and then observing the corresponding changes in the simulated flow. Sensitivity analysis was carried out to identify the most sensitive parameters for the model calibration using One-factor-At-a-Time (LH-OAT), which is an automatic sensitivity analysis tool implemented in SWAT (van Griensven et al., 2006). Upon the completion of sensitivity analysis, the mean relative sensitivity (MRS) values of the parameters were used to rank the parameters, and their category of classification based on (Lenhart et al., 2002). If the MRS is in between 0 and 0.05 the sensitivity category is small to negligible. Medium sensitivity is given when the MRS values are in a range between 0.05 and 0.02; high sensitivity values categorized when the MRS values are in between 0.2 and 1.0 and the very high sensitivity values categorized when the MRS are greater than a value of 1.0.

Table 6.6. Sample of SWAT model parameters and their permissible ranges.

Parameters	Allowable range
CN2	±25%
ESCO	±25%
GWQMN	0-5000
SOL_Z	±25%
SOL_K	±25%
SOL_AWC	±25%

The parameter values giving the best results for simulated runoff in relation to observed runoff are given in Table 6.7. These parameters were subsequently used for extrapolation to the other SWAT models, including that of the Tekeze River Basin model.

Table 6.7. Optimised calibration parameter settings for the Geba River catchment, used for simulation of target area water balances. (CCMBS = Chromic cambisols; ELPS = Eutric leptosols)

Description of model parameters		Optimized values	Sub-basin	Land use	Soil	Slope classes	Hydrologic soil group
CN		82	All	AGRL, AGRC, AGRR	All	All	All
CN		62	All	FRST, FRSD	All	All	All
CN		72	All	RNGE	All	All	All
CN		85	All	BARR	All	All	All
CN		78	All	PAST	All	All	All
ESCO (-)		0.3	All	All	All	All	All
Sol_Z [mm]	Layer1	200	All	AGRL, AGRR, FRSD	CCMBS, ELPS, ECMBS	All	A,B,D
	2	400					
	3	2000					
Sol_Z	1	115	All	RNGE	All	All	A,D
	2	230					
	3	1150					
Sol_AWC	1	0.45	All	AGRC, AGRL, AGRR	CCMBS, ELPS	All	B,D
	2	0.144					
	3	0.144					
Sol_AWC	1	0.15	All	AGRL, AGRR, FRST, RNGE	ECMBS	All	A
	2	0.48					
	3	0.48					
SOL_K	1	0.0036	All	AGRL, AGRR, AGRC, FRSD	CCMBS	All	A
	2	8.03					
	3	7					
SOL_K	1	1.8	All	AGRL, AGRC, AGRR	ELPS	All	B
	2	4.59					
	3	2.5					
Alpha_BF [day^{-1}]		0.0001	All	All	All	All	All
GWDelay [day]		50	All	All	All	All	All
GWQMN [mm]		100	All	All	All	All	All
GWREVAP		0.02	All	All	All	All	All
REVAPMN [mm]		500	All	All	All	All	All
RCHRG_DP		0.1	All	All	All	All	All

6.6.2 Model performance evaluation

Two model performance evaluation methods, the Nash and Sutcliffe (1970) efficiency (E_{NS}), and the coefficient of determination (r^2) were used in both calibration and validation periods (see Equation 6.4 and Equation 6.5).

$$E_{NS} = 1 - \frac{\sum_{i=1}^{n}(q_{oi} - q_{si})^2}{\sum_{i=1}^{n}(q_{oi} - \bar{q}_o)^2} \quad (6.4)$$

$$r^2 = \frac{\left[\sum_{i=1}^{n}(q_{si} - \bar{q}_s)(q_{oi} - \bar{q}_o)\right]^2}{\sum_{i=1}^{n}(q_{si} - \bar{q}_s)^2 \sum_{i=1}^{n}(q_{oi} - \bar{q}_o)^2} \quad (6.5)$$

Where q_{si} is the simulated value, q_{oi} is the measured value, and $\overline{q_o}$ is the average observed flow. E_{NS} values range from 1.0 (best fit) to negative infinity.

A comparison of observed and simulated hydrographs of the Geba catchment, after calibration and validation, is shown in Figure 6.14. The comparison shows that the model performs reasonably in capturing the observed flow pattern and flow regimes. This is supported by a Nash and Sutcliffe efficiency coefficient and coefficient of determination values of 0.70 and 0.85 for calibration and 0.60 and 0.71 for the validation periods, respectively.

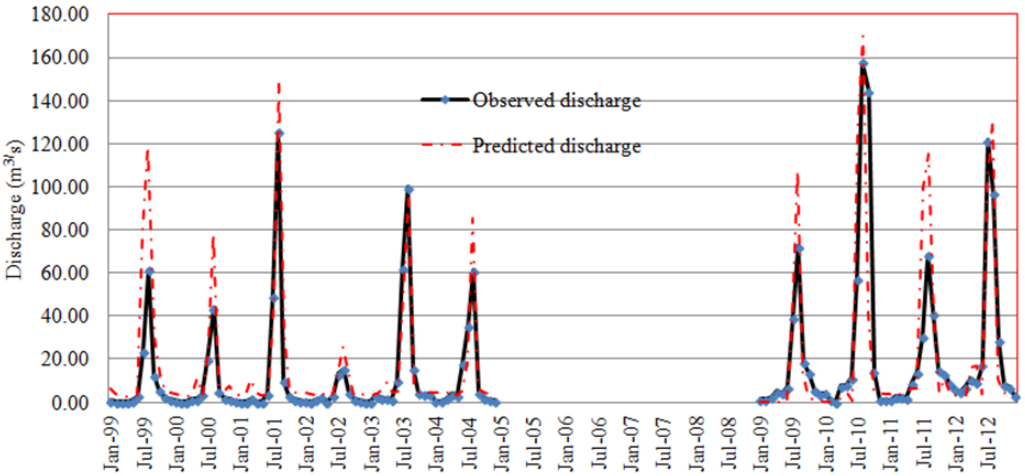

Figure 6.14. Comparison of simulated and observed river flows of the Geba RIver catchment following calibration for the 1999-2004 period and validation for the 2009-2012 period.

6.7 Basin and drainage network

The target areas with the identified boundaries, catchment areas and their location in the river basins are indicated in Table 6.8. The spatial location of the target areas are shown in Figure 6.15.

Table 6.8. Target areas and their locations in woredas, catchment areas and river basins.

S. No.	Target area short name	Area [km^2]	River name	Woreda name	Basin
1	BD1	18	-	Beyeda(Liware)	Located at foot of RasDashen mount/Tekeze
2	BD2	13	-	Beyeda(Abare)	Tekeze
3	TS2	220	Insua shet	MyAyne	Tekeze
4	TS3	165	Liag Shet	Tselemet(Dima)	Tekeze
5	OF1	56	Liliwa shet	Ofla(DenkaAshena)	Tekeze
6	OF2	93	Bel shet	Ofla(Adisham Bereket)	Tekeze
7	KT2-r	29	Chint shet	Kolatemben(Atakilte)	Tekeze
8	KT3	13	Tsalet	Kola Temben (Adiha)	Tekeze
9	HW4	14	Weri	Hawzen(Koraro)	Tekeze
10	HW2	16	Siluh	Hawzen(Digum)	Tekeze
11	ST3	19	Genfil	Saesi Tsdamba (Gula Ambina)	Tekeze
12	ML1	65	Mirsat sher	Mereb Leha(Adigebat)	Mereb
13	ML3	16	Dorena shet	Mereb Leha (Awet)	Mereb
14	ST2-r	93	Anza shet	Saesi Tsdamba (Sewin)	Denakil
15	ER2	35	Meareba shet	Erop(Ara)	Denakil
16	ER4-r	23	Berber	Erop(Ara)	Denakil
17	BE4-r	41	Fishe shet	Berehale(Sebana Dembale)	Denakil
18	BE1	12	Gemeru	Berehale (Lela Ala)	Denakil
19	AF1-r	170	Dabure	Afdera(Ayitura)	Denakil
20	AF4-r	250	Gordoh	Afdera(Debure)	Denakil
21	MG1	49	Meisha	Megale(Faro)	Denakil
22	MG2	55	Meisha	Megale(Adu)	Denakil
23	YL1	18	Kubi tobato shet	Yalo(GidaelanaMudalina Dirma)	Denakil
24	YL3	15	Kubi tobato shet	Yalo(Udeyla)	Denakil
25	KR1	96	Meleke shet	Kori(Meto Ariba)	Denakil
26	KR2	32	Gefunali shet	Kori(Silsa)	Denakil

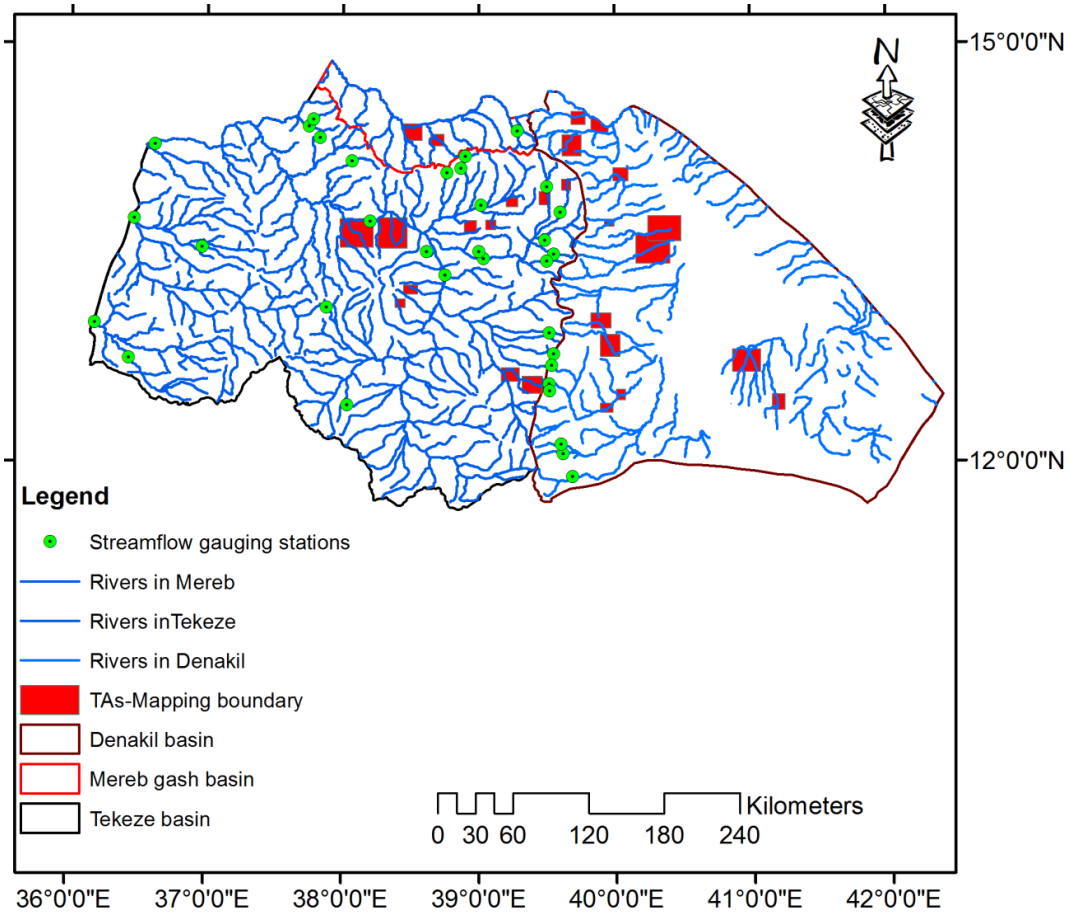

Figure 6.15. Drainage network and streamflow stations in the Tekeze basin region and target area boundaries.

6.8 Quick- and baseflow component separation

Master baseflow recession curves were made for the Geba River catchment at Adi Kumsi and for the larger Tekeze Basin at Emba Madre. The baseflow recession curve for Geba catchment at Adi Kumsi is shown in Figure 6.16. The recession constant of the slow linear reservoir is k = 0.02 day^{-1}. For Tekeze, considerable differences between years was observed in the baseflow recession constants, with the fastest baseflow recession in the period 1997-1998 and the slowest recession in 2003-2004 (k = 0.01 day^{-1}). This is shown in Figure 6.17.

The break in slopes between the fast reservoir and the subsequent slower draining reservoirs was used to separate quickflow from baseflow and determine the baseflow rise slope constants in the wet season. The slope of the line from the rise in streamflow until the recession of the intermediate reservoir for the Tekeze River Basin at Emba Madre varied between 0.021 and 0.030 mm d^{-1}, with an average of 0.0031 mm d^{-1}. For the Geba River, a lower baseflow increase slope of 0.0024 mm d^{-1} was calculated.

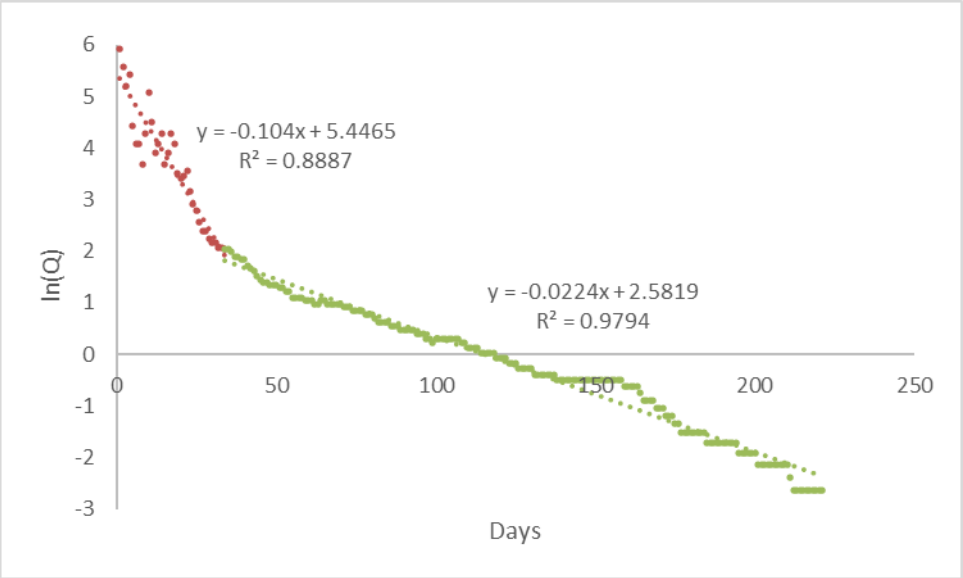

Figure 6.16. Master baseflow recession curve for the Geba River catchment at Adi Kumsi station as determined from baseflow recession data of 2000-2002. The fast reservoir (red) represents the quickflow component.

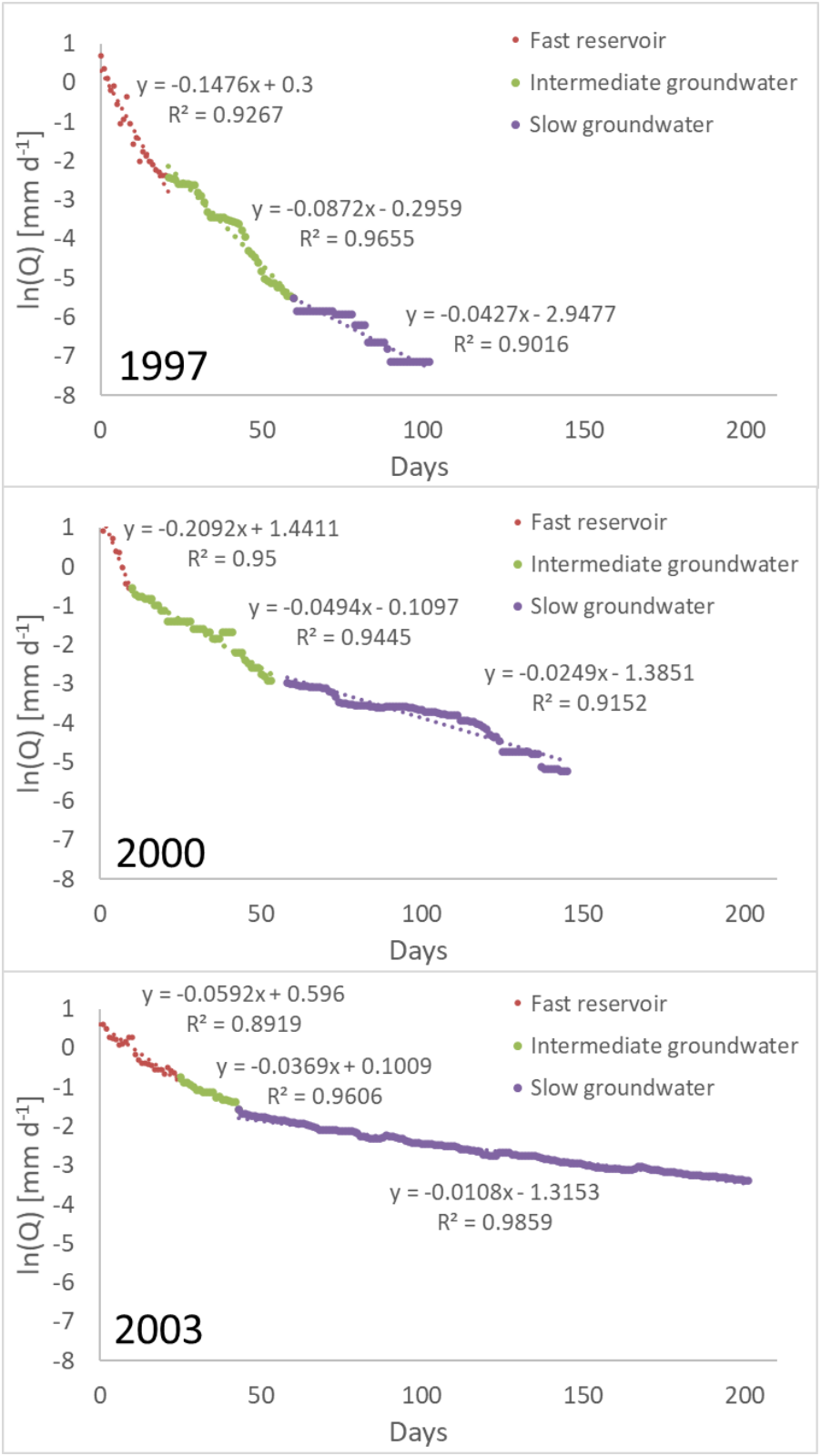

Figure 6.17. Master baseflow recession curves for the Tekeze River basin at Emba Madre station as determined from baseflow recession data of 1997-1998, 2000-2001 and 2003-2004. The fast reservoir represents the quickflow component.

The daily streamflow totals and corresponding baseflows for the Geba River catchment and Tekeze River basin in 2002 - 2003 are shown in Figure 6.18.

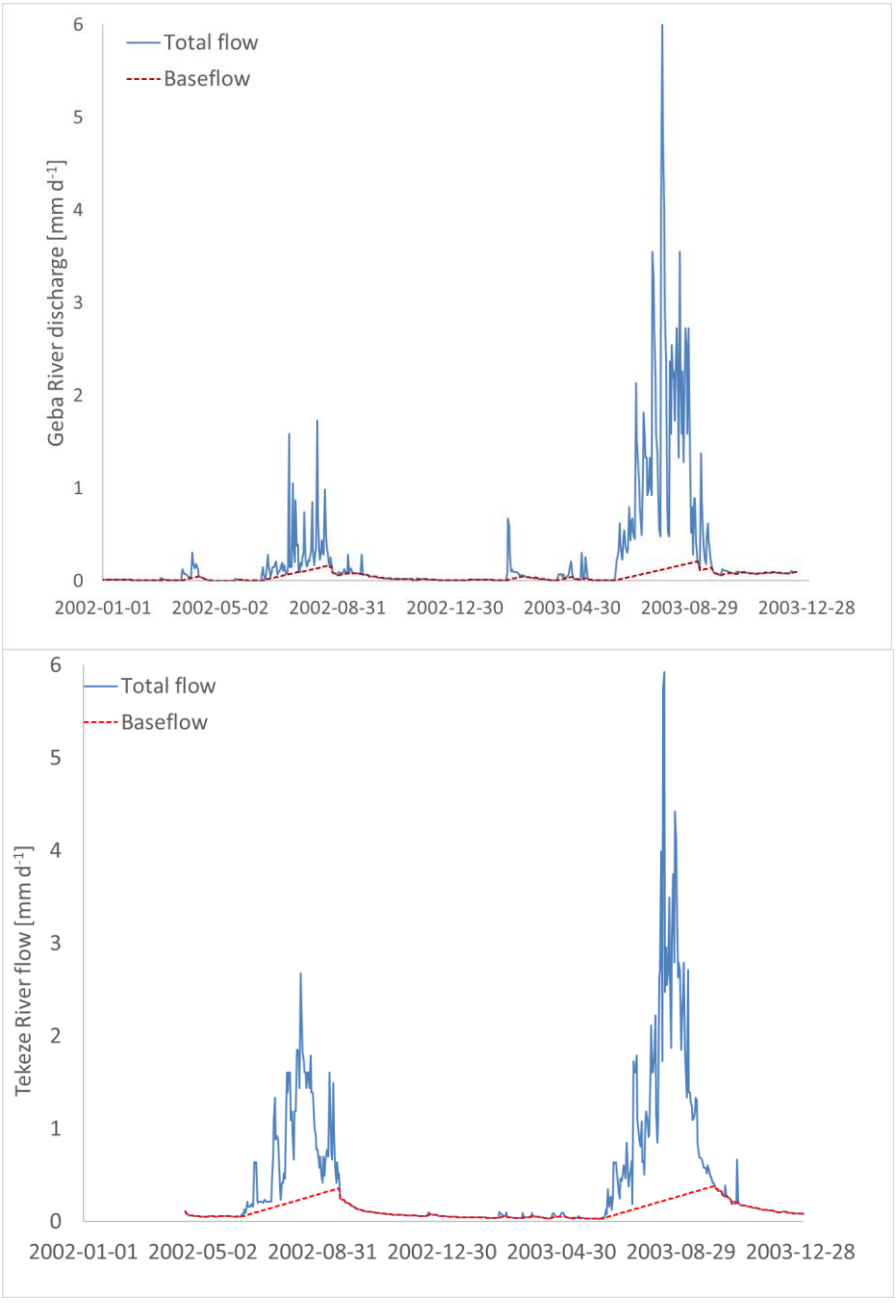

Figure 6.18. Daily streamflow totals and corresponding baseflow for the Geba (upper) and Tekeze (lower) rivers in the period 2002-2003.

The maximum daily flow was about 6 mm d^{-1} for both catchments, whereas the maximum baseflow amounted to 0.32 mm d^{-1} at Adi kumsi for the Geba River and was slightly higher at 0.41 mm d^{-1} for the Tekeze River at Emba Madre before the filling of the reservoir in 2008.

6.9 Demand analysis

6.9.1 Domestic water demand

Population density of the kebeles is expressed as the number of total inhabitants in 2030 per km^2. The population data are based on the census 2007 data (CSA, 2017) and was corrected for an average population growth of 2.46 % (CSA, 2013a, 2017). According to the WHO, basic access to water for health reasons should at least be at 20 l c^{-1} d^{-1}, whereas access at 50 l c^{-1} d^{-1} would represent a low level health concern (Howard and Bartram, 2003).

The domestic water demand [m^3 d^{-1}] per kebele is based on number of inhabitants and a daily per capita demand as defined in the GTP II (NPC, 2016). According to the GTP II water demand in rural areas would amount to 25 l c^{-1}d^{-1}. In urban areas water demand varies from 40 to 100 l c^{-1}d^{-1} (NPC, 2016), and a value of 50 l c^{-1}d^{-1} was taken for urban kebeles. Where urban or rural conditions are not clear 30 l c^{-1}d^{-1} was used.

6.9.2 Livestock water demand

A domestic water supply and livestock demand analysis was done to estimate the total water demand. The demands for the different human and livestock water user classes are provided in Table 6.9, with an estimated average per capita daily livestock unit water use at 25 l in Ethiopia (Sileshi et al., 2003).

Table 6.9. Water use for livestock classes under Sahelian conditions (Sileshi et al., 2003).

Class	Requirement [l d^{-1}]
Cattle	27.0
Sheep	5.0
Goats	5.0
Horses	20.0
Mules	16.0
Donkeys	16.0
Camels	45.0
Poultry	1.5
Beehives	1.8

Ideally, the livestock water demand would have been provided by the woreda offices. However, these data were not provided and the human and livestock population sizes and corresponding water demands were therefore estimated based on data provided by CSA (2021a, 2021b, 2013b). Use was made of data available at zonal level (Table 6.10).

Table 6.10. Human and livestock population (in thousands) by zone (CSA, 2021a).

Region	Zone	Population	Cattle	Sheep	Goats	Horses	Mules	Donkeys	Camels	Poultry	Beehives
Afar	Zone 1	392	917	2182	3924	0	0	125	472	0	0
Afar	Zone 2	401	62	413	1377	0	0	59	123	62	19
Afar	Zone 3	199	621	1090	1872	0	0	61	432	0	0
Afar	Zone 4	314	101	338	588	0	0	24	66	0	0
Afar	Zone 5	241	258	454	1083	0	0	39	165	0	0
Amhara	N Gondar	91	779	507	645	35	9	187	0	1304	96
Tigray	NW Tigray	1255	726	549	1110	0	0	179	11	1390	74
Tigray	E Tigray	658	467	615	195	0	0	146	0	971	79
Tigray	NW Tigray	769	1954	411	2357	0	0	268	18	2592	85
Tigray	S Tigray	1053	391	186	162	0	4	70	0	406	28
Tigray	W Tigray	333	848	101	679	0	0	73	7	871	39

The population at zonal level for the year 2021 was estimated from CSA census data using a growth rate of 2.46%, and the livestock ratio per capita was determined for nine livestock classes (Table 6.11).

Table 6.11. Distribution of livestock ratios per capita per zone for 2021.

Region	Zone	Cattle	Sheep	Goats	Horses	Donkeys	Camels	Poultry	Beehives
Afar	Zone 1	2.34	5.56	10.00	0.00	0.32	1.20	0.00	0.00
Afar	Zone 2	0.16	1.03	3.43	0.00	0.15	0.31	0.15	0.05
Afar	Zone 3	3.11	5.46	9.38	0.00	0.31	2.17	0.00	0.00
Afar	Zone 4	0.32	1.08	1.87	0.00	0.08	0.21	0.00	0.00
Afar	Zone 5	1.07	1.88	4.49	0.00	0.16	0.68	0.00	0.00
Amhara	N Gondar	0.27	0.17	0.22	0.01	0.06	0.00	0.45	0.03
Tigray	C Tigray	0.58	0.44	0.88	0.00	0.14	0.01	1.11	0.06
Tigray	E Tigray	0.71	0.93	0.30	0.00	0.22	0.00	1.48	0.12
Tigray	NW Tigray	2.54	0.53	3.07	0.00	0.35	0.02	3.37	0.11
Tigray	S Tigray	0.37	0.18	0.15	0.00	0.07	0.00	0.39	0.03
Tigray	W Tigray	2.55	0.30	2.04	0.00	0.22	0.02	2.62	0.12

Assuming that population / livestock class ratios remain constant for the next decade, estimates were made about the expected livestock population per woreda and kebele for the year 2030, using the projected population size as a reference. Table 6.12 lists domestic and livestock water demands for the 13 project woredas based on the data presented above.

Table 6.12. Region/zone details for different target woredas and estimated water demands for 2030.

Woreda	Region	Zone	Domestic [$m^3 d^{-1}$]	Livestock [$m^3 d^{-1}$]	Total [$m^3 d^{-1}$]	Area [Km^2]
Afdera	Afar	Zone 02	1,503	2,166	3,669	7882
Berehale	Afar	Zone 02	3,819	5,504	9,322	2483
Beyeda	Amhara	North Gondar	4,699	1,768	6,467	971
Erop	Tigray	Eastern Tigray	1,049	1,094	2,143	768
Hawzen	Tigray	Eastern Tigray	4,900	5,113	10,013	874
Kola Temben	Tigray	Central Tigray	5,789	5,149	10,938	1378
Kori	Afar	Zone 01	1,292	8,655	9,947	2870
Megale	Afar	Zone 02	1,437	2,071	3,508	1544
Mereb Leha	Tigray	Central Tigray	4,855	4,319	9,174	1254
Ofla	Tigray	South Tigray	5,741	2,570	8,312	1106
Saesi Tsadamba	Tigray	Eastern Tigray	5,282	5,512	10,793	960
Tselemt	Tigray	Northwestern Tigray	5,890	19,359	25,249	2609
Yalo	Afar	Zone 04	2,449	2,798	5,247	819

6.9.3 Industrial water demand

No data were available for the industrial (excluding livestock) water demands in the target areas. A report prepared for the Awash Basin Authority lists domestic, livestock and industrial water demands, with the annual industrial demand amounting to 7.4% of the corresponding domestic demand (Sahilu et al., 2018). For Addis Ababa water use by industry amounted to about 8% of domestic water demand, but when industries outside Addis Ababa were taken into account, the industrial use was estimated at 3.3% of domestic water use (Adeba et al., 2015). The average of these values, i.e. 5.4% of domestic water demand, was therefore used to estimate industrial water demand for the target areas.

6.9.4 Water for environmental flows

The environmental water requirement is related to the surface water flow regime that needs to be maintained for achieving maintenance of freshwater-dependent ecosystems. These objectives pose limitations on both high and low flows and environmental flow were estimated at 20-50% of mean annual river flow (Smakhtin et al., 2004). The target areas do not correspond to hydrological units where ephemeral or perennial river systems are present, and may depend for surface water flows on upstream areas, whereas groundwater abstractions in the target may influence baseflow rates and therefore have impacts on downstream ecosystems. For Awash Basin, the environmental flow requirement was estimated at 35% of the mean annual flow (Adeba et al., 2015), whereas a lower value of 22% was estimated for the Abay River (McCartney et al., 2008; Shiferaw and McCartney, 2009). A much higher value of 48-71% of mean annual runoff was modelled for the Omo-Gibe Basin in South Ethiopia to maintain natural habitats along the river (Tesfaye et al., 2020). This illustrates the need for a local assessment of river flow status and dependent freshwater ecosystems in the project areas. For this study, the environmental flow rate was taken as 25% of the mean monthly lateral and groundwater flow rates.

6.9.5 Daily water demand

An overview of the daily water demands for the target areas is given in Table 6.13. No agricultural cover was observed for eight areas and for these no irrigation demands have been listed.

Table 6.13. Estimates of daily demand for domestic water supply, livestock and irrigation water in the target areas.

Target Area	Area [km^2]	TA/Woreda area	Domestic [$m^3\ d^{-1}$]	Livestock [$m^3\ d^{-1}$]	Irrigation [$m^3\ d^{-1}$]	Total [$m^3\ d^{-1}$]
AF1-r	511	0.065	97	140	364	601
AF4-r	637	0.081	121	175		296
BD1	77	0.079	373	140	232	745
BD2	57	0.059	276	104	17	397
BE1	41	0.016	63	91		153
BE4-r	118	0.048	182	262	6	449
ER2	114	0.149	156	163	38	357
ER4-r	105	0.136	143	149		292
HW2	91	0.104	508	530	1099	2137
HW4	65	0.075	366	382	144	892
KR1	389	0.136	175	1173		1348
KR2	120	0.042	54	362		416
KR5	101	0.035	45	305		350
KT2-r	97	0.070	408	362	1720	2490
KT3	61	0.044	254	226	739	1219
MG1	187	0.121	174	250	73	497
MG2	262	0.170	244	351	31	626
ML1	188	0.150	728	648	2166	3541
ML3	93	0.074	360	320	31	711
OF1	158	0.143	820	367	1489	2676
OF2	212	0.192	1102	494	186	1782
ST2-r	253	0.264	1395	1455	826	3676
ST3	62	0.064	339	353	580	1272
TS2	583	0.224	1316	4327	826	6469
TS3	554	0.212	1250	4110	5356	10716
YL1	62	0.075	184	210		394
YL3	72	0.088	216	247		462

6.10 Monthly water balance modelling and demand

The calibrated SWAT model was run for the different catchments and the HRU / subcatchment water balance components (P, ET, Qlat, Qgw) were plotted on the target areas and the average monthly totals for each were target area are given below. The groundwater recharge in each target area consists of water percolating through the soil layers to the shallow aquifer, where it contributes to the dry season baseflow of the catchment, and a fraction that percolates to deeper aquifers that contribute to regional flow. This component is part of the water balance simulated for the HRUs and subcatchment by the SWAT model.

Scarcity of water occurs when the local demands for water cannot be met by the supply. As demands and supply both show spatial and temporal variations (e.g. irrigation needs and precipitation patterns). The water balance components provide information on the water supply status in the target areas, whereas water demand would be much more localized with a focus on the areas with higher population density (Boithias et al., 2014). The potential of a mismatch therefore exists between supply and demand areas in the target areas. The temporal variation issue may indicate a deficit in certain months of the year, whereas the overall annual-scale demand – availability ratio would not be cause for concern. In this study we have defined monthly and annual demand / availability Water Scarcity Indices (WSI, in %) to serve as indicators for water stress in a target area. The availability of water resources has been defined as the simulated water yield, which includes both surface and groundwater resources, of a target area minus the environmental 4flow requirements. Demand / water availability ratios above 100% clearly demonstrate an absolute shortage of water in a target area. However, due to non-uniform spatial distributions of water resources and demand centers, water scarcity can also be experienced at WSI values lower than 100%. A limit of the WSI of 40% (Balist et al., 2022; Vörösmarty et al., 2000) was therefore set as a criterium to assess the potential expansion of water resources, with a condition being that this limit should not be exceeded in any month of the year.

Eleven of the 26 target areas were located in the Tekeze River Basin. The river basin shows substantial variation in elevation, as shown earlier in Figure 6.3. The precipitation also shows considerable spatial variation and in precipitation inputs for the subcatchments are shown in Figure 6.19. The highest rainfall inputs are in the mountain areas in the western part, and to a lesser extend in those in the eastern part of the river basin. According to the CFSR data the center of the basin receives considerably less precipitation at values of less than 200 mm y^{-1}. The spatial variation of the lateral runoff component is shown in Figure 6.21 and shows that even under the low rainfall conditions in the center of the basin up to 30 mm y^{-1} of lateral flow is generated and contributes to the Tekeze River runoff. As the rainfall is highly seasonal, the smaller rivers in this central area may be ephemeral. Groundwater recharge in the Tekeze River basin is presented in Figure 6.22. The recharge pattern corresponds to the rainfall distribution over the river basin with low recharge rates (< 5 mm y^{-1}) in the central parts and much higher rates in the other parts of the basin.

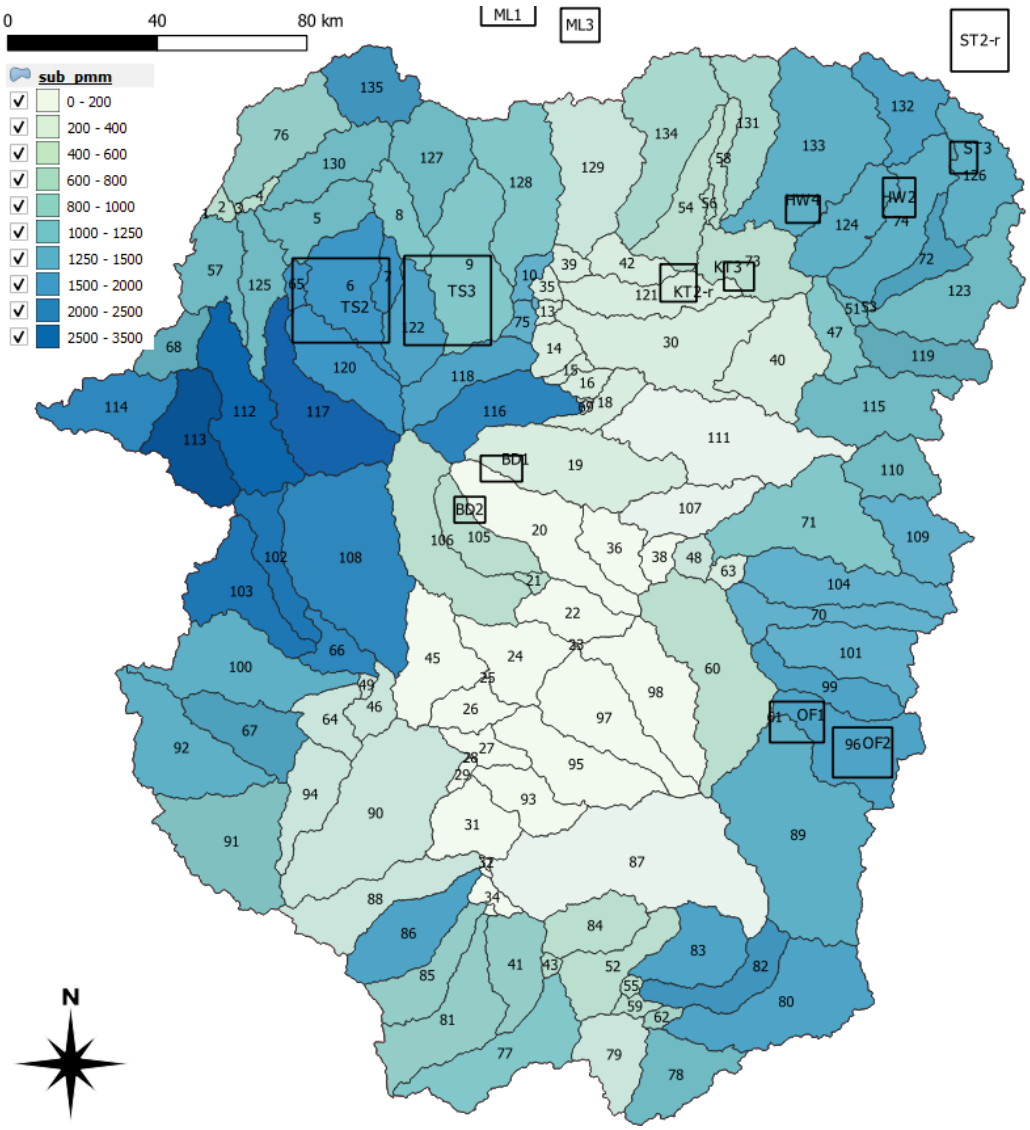

Figure 6.19. Annual average CFSR precipitation inputs [mm y^{-1}] into the Tekeze River basin distributed over the different subcatchments for the period 1994-2013.

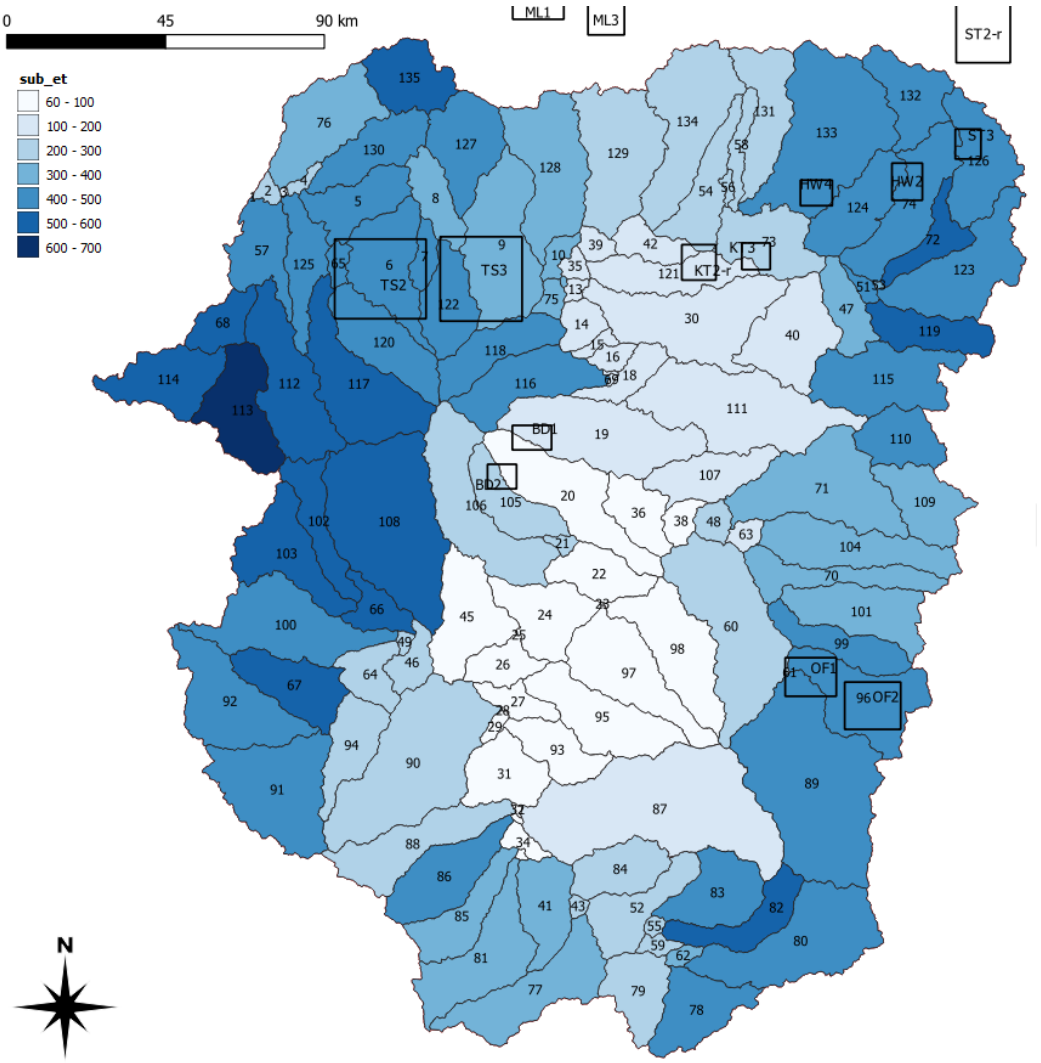

Figure 6.20. Spatial variation of the average actual evapotranspiration [mm y^{-1}] over the Tekeze River basin as modelled by SWAT for the period 1994-2013.

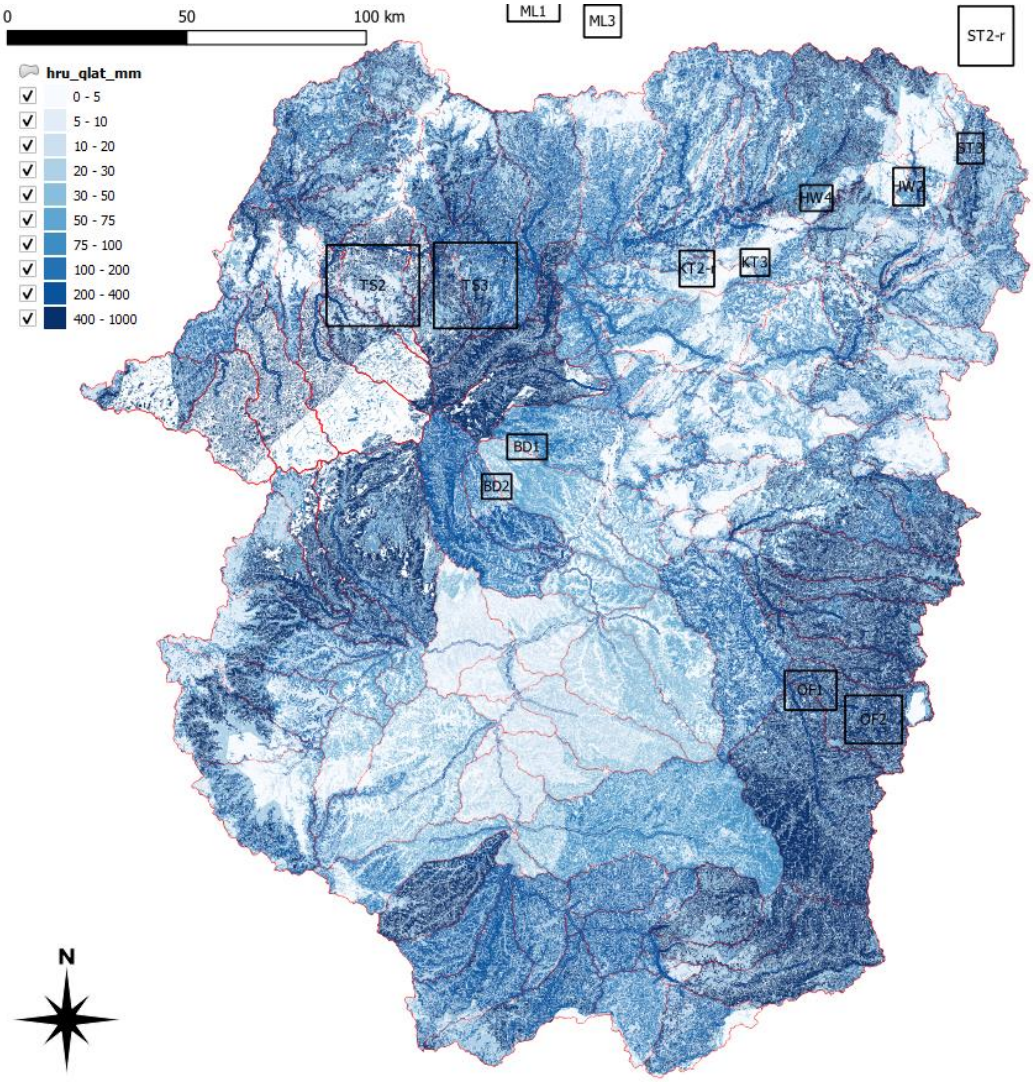

Figure 6.21. Spatial variation of lateral runoff [mm y^{-1}] in the Tekeze River basin as modelled with SWAT for the period 1994-2013 using CFSR weather data as input.

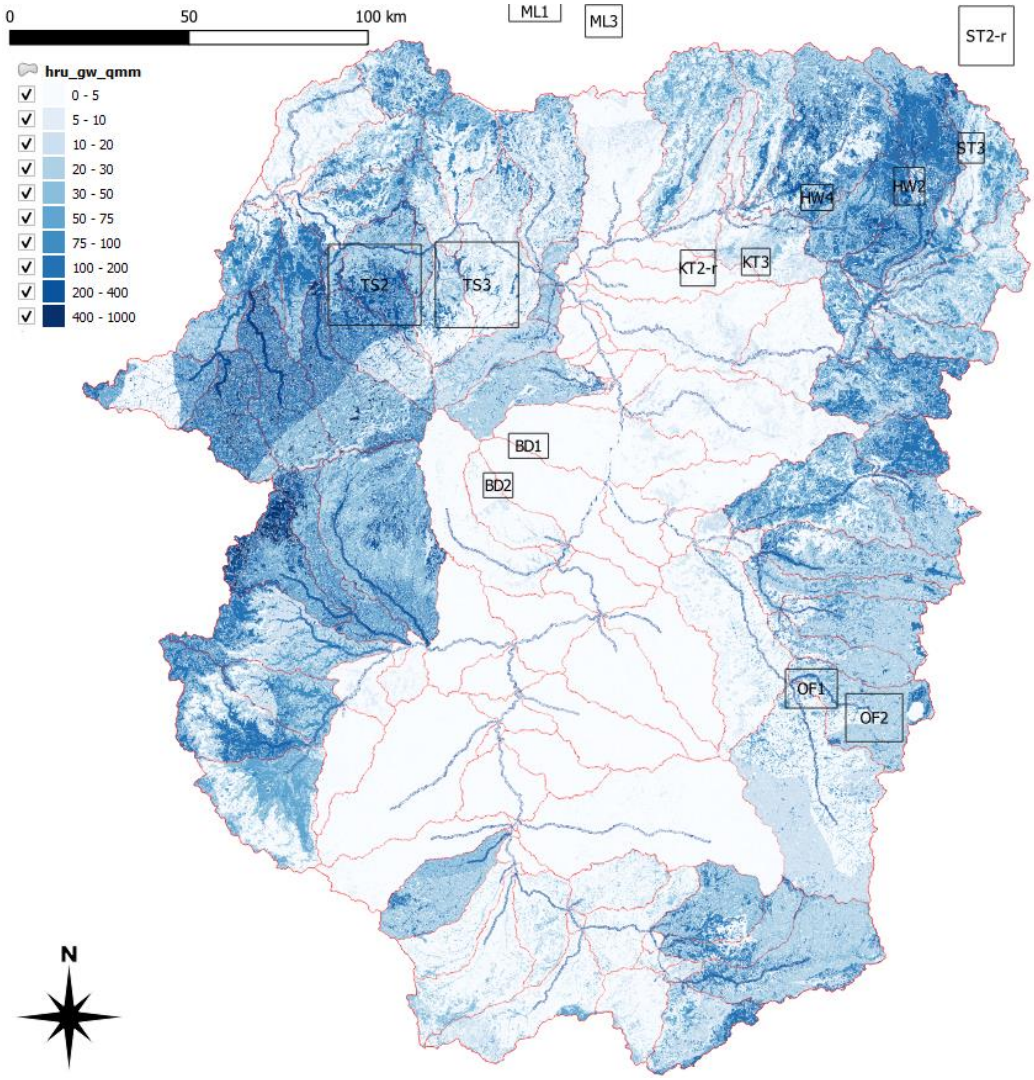

Figure 6.22. Spatial variation in the average annual groundwater recharge [mm y^{-1}] in the Tekeze River Basin as modelled with SWAT for the period 1994-2013.

6.11 Target areas

6.11.1 Target area TS2

Target area TS2 is much less dissected as neighboring TS3, and the remnants of a plateau can be seen in Figure 6.23. Both areas are transected by larger rivers, that seem to be mostly ephemeral in nature. The largest river may be perennial in the northeastern section of the area. A summary of the annual water balance components for TS2 is given in Table 6.14, whereas monthly overviews of water balance components and demands are presented in Table 6.15. Precipitation is high at an annual average of over 1800 mm y^{-1}, which leads to a total annual surface and groundwater yield of over 1000 mm y^{-1}. Land cover was classified as predominantly rangeland (47%), agricultural (43%) and trees growing on the steeper slopes. Water demand (4 mm y^{-1}) was dominated by livestock and agriculture on the plateau seemed to be mainly rainfed. In accordance with the high precipitation the WSI was low throughout the year. Groundwater exploration would be possible if the geological conditions would allow extraction of water from aquifers at depth.

Table 6.14. Annual water balance component values for target area TS2 as modelled with SWAT (1994-2013).

Water balance component	Value [mm y^{-1}]
PRECIP	1828.3
SURFACE RUNOFF	616.43
LATERAL SOIL	170.56
GROUNDWATER (SHAL AQ) Q	199.74
GROUNDWATER (DEEP AQ) Q	54.61
REVAP (SHAL AQ => SOIL/PLANTS)	36.75
DEEP AQ RECHARGE	53.58
TOTAL AQ RECHARGE	535.83
TOTAL WATER YLD	1041.35
PERCOLATION OUT OF SOIL	534.21
ET	514.9
PET	1837.7

The spatial variations of groundwater recharge of target areas TS2 and TS3 are shown in Figure 6.24. Although the areas are adjacent these belong to different subcatchments, with the TS2 catchment draining to the Northwest, and the TS3 catchment to the North. Area TS2 also has a higher fraction of flat area, which seems to enhance recharge rates and could reflect a difference in geology. Recharge in the TS2 area is high at values above 100 mm y^{-1} in the broad valleys in the central and southern part of the area and exceed 10 mm y^{-1} in the other parts of the target area.

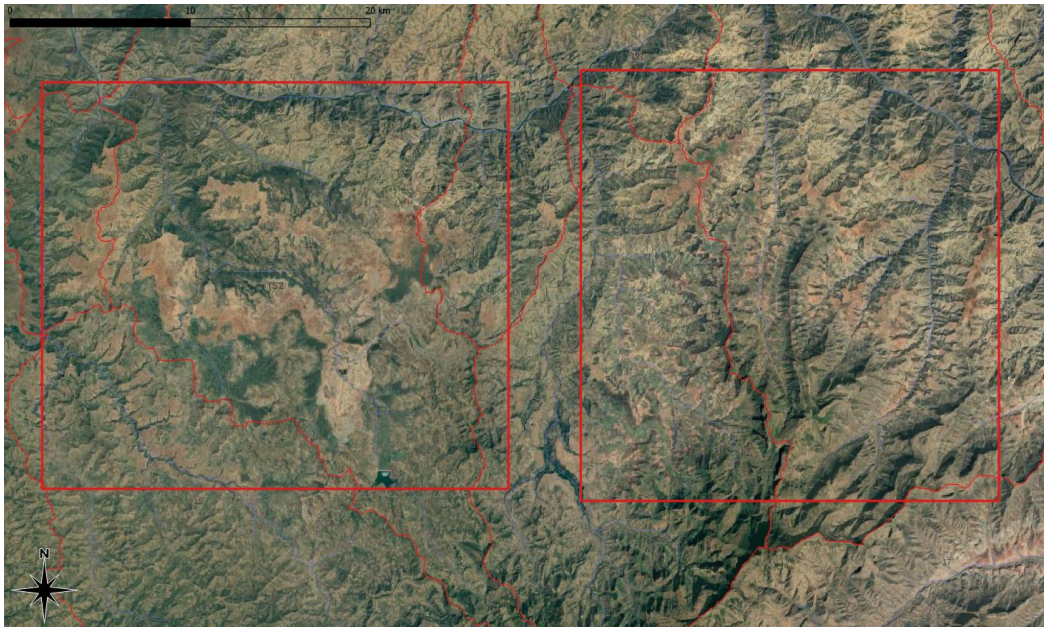

Figure 6.23. Google Earth satellite image of target areas TS2 (left) and TS3 (right).

Table 6.15. Average monthly water balance components for Target Area TS2 as modelled with SWAT and corresponding water demands. All values given in mm mo^{-1} or mm y^{-1}. SURFQ is the surface runoff, LATQ the lateral flow, WTYIELD the total of surface, lateral, groundwater recharge flows, ET the actual evapotranspiration, PET the potential evapotranspiration and EFR the environmental flow requirement. The WSI (Available Water Resources) represents the percentage of the total demand relative to the WTYIELD minus the EFR.

Month	Jan	Feb	Mar	Apr	May	Jun	Jul	Aug	Sep	Oct	Nov	Dec	Total
Rain	2.0	0.8	9.7	22.1	36.1	180.6	732.2	677.7	129.4	31.7	5.6	0.6	1828
SURFQ	0.0	0.0	0.3	1.9	0.8	26.8	271.9	279.7	27.2	7.4	0.5	0.0	616
LATQ	0.2	0.1	0.4	1.4	2.0	10.5	60.3	67.4	23.5	3.5	1.2	0.2	171
WTYIELD	22.6	19.2	20.8	21.9	21.4	54.7	350.5	368.3	74.5	36.6	26.2	24.5	1041
ET	3.2	1.6	29.3	67.3	63.7	51.6	75.1	82.0	76.9	39.2	19.0	6.0	515
PET	177	183	207	198	176	115	87	93	124	171	167	139	1836
EFR	5.6	4.8	5.2	5.5	5.4	13.7	87.6	92.1	18.6	9.1	6.5	6.1	260
Demand													
Domestic	0.070	0.064	0.070	0.068	0.070	0.068	0.070	0.070	0.068	0.070	0.068	0.070	0.825
Livestock	0.230	0.210	0.230	0.223	0.230	0.223	0.230	0.230	0.223	0.230	0.223	0.230	2.711
Irrigation	0.106	0.097	0.106	0.103	0.106	0.000	0.000	0.000	0.000	0.000	0.000	0.000	0.517
Industry	0.004	0.003	0.004	0.004	0.004	0.004	0.004	0.004	0.004	0.004	0.004	0.004	0.045
Total	0.410	0.374	0.410	0.397	0.410	0.294	0.304	0.304	0.294	0.304	0.294	0.304	4.097
WSI	1.8	1.9	2.0	1.8	1.9	0.5	0.1	0.1	0.4	0.8	1.1	1.2	0.4

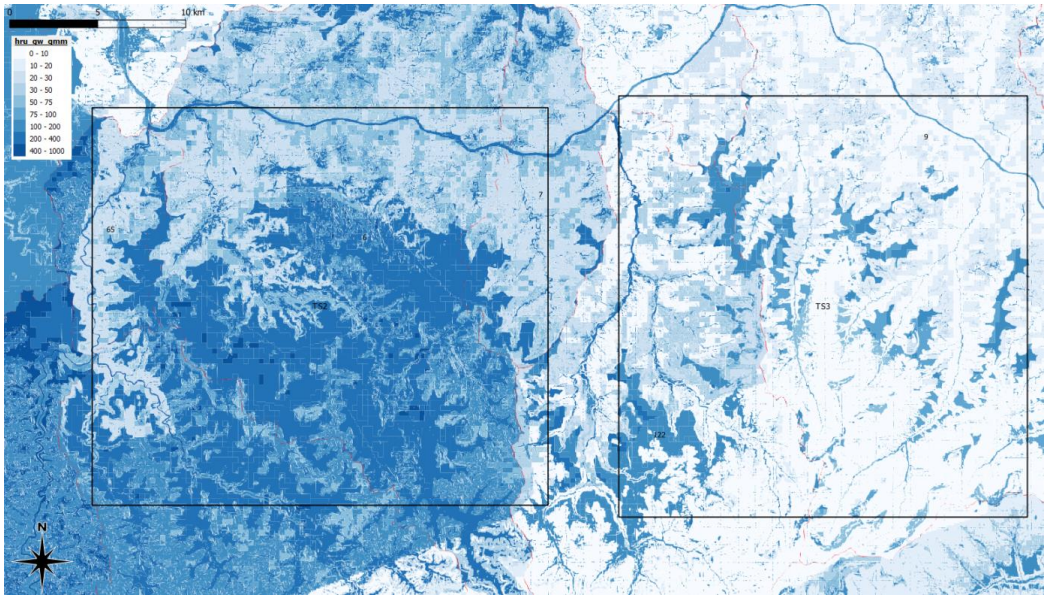

Figure 6.24. Spatial variation of the annual average groundwater recharge amounts [mm y^{-1}] in the TS2 (left) and TS3 (right) target areas.

6.11.2 Target area TS3

Precipitation in TS3 is well above 1000 mm y^{-1} and the larger rivers in the northern part seem to be perennial. A summary of the annual water balance components for TS2 is given in Table 6.16, whereas monthly overviews of water balance components and demands are presented in Table 6.17. River runoff is substantial and fed by surface runoff and throughflow components rather than through groundwater contributions. Land cover is largely agricultural (71%), tree cover (14%, on slopes; Figure 55) and rangeland (13%). The water demand is relatively high at over 7 mm y^{-1}, and dominated by irrigation and livestock water consumption. WSI remains below 10% throughout the year and as in its neighboring TS2 area, there may be potential for deep groundwater extraction under the right geological conditions as deep aquifer recharge was estimated at 36 mm y^{-1}.

Table 6.16. Annual water balance component values for TS2 as modelled with SWAT (1994-2013).

Water balance component	Value [mm y^{-1}]
PRECIP	1389
SURFACE RUNOFF	338.49
LATERAL SOIL	255.99
GROUNDWATER (SHAL AQ) Q	120.75
GROUNDWATER (DEEP AQ) Q	36.63
REVAP (SHAL AQ => SOIL/PLANTS)	32.74
DEEP AQ RECHARGE	36.58
TOTAL AQ RECHARGE	365.77
TOTAL WATER YLD	751.86
PERCOLATION OUT OF SOIL	365.66
ET	428.6
PET	1696.4

Table 6.17. Average monthly water balance components for Target Area TS3 as modelled with SWAT and corresponding water demands. All values given in mm mo^{-1} or mm y^{-1}. SURFQ is the surface runoff, LATQ the lateral flow, WTYIELD the total of surface, lateral, groundwater recharge flows, ET the actual evapotranspiration, PET the potential evapotranspiration and EFR the environmental flow requirement. The WSI (Available Water Resources) represents the percentage of the total demand relative to the WTYIELD minus EFR.

Month	Jan	Feb	Mar	Apr	May	Jun	Jul	Aug	Sep	Oct	Nov	Dec	Total
Rain	2.8	1.0	8.5	23.0	28.0	130.7	558.3	506.3	96.6	28.6	4.9	0.4	1389
SURFQ	0.0	0.0	0.0	1.0	0.6	16.8	157.2	143.9	13.7	5.1	0.1	0.0	338
LATQ	0.4	0.0	0.5	2.3	3.1	13.5	92.4	106.9	30.9	4.4	1.4	0.1	256
WTYIELD	14.1	11.7	12.8	14.7	15.0	40.9	260.9	264.1	59.7	25.8	16.9	15.3	752
ET	4.2	1.8	16.0	40.5	39.5	45.0	81.4	84.1	68.7	29.1	14.1	4.3	429
PET	152	163	184	185	171	111	91	92	118	160	149	119	1695
EFR	3.5	2.9	3.2	3.7	3.7	10.2	65.2	66.0	14.9	6.5	4.2	3.8	188
Demand													
Domestic	0.070	0.064	0.070	0.068	0.070	0.068	0.070	0.070	0.068	0.070	0.068	0.070	0.825
Livestock	0.230	0.210	0.230	0.223	0.230	0.223	0.230	0.230	0.223	0.230	0.223	0.230	2.711
Irrigation	0.724	0.660	0.724	0.701	0.724	0.000	0.000	0.000	0.000	0.000	0.000	0.000	3.532
Industry	0.004	0.003	0.004	0.004	0.004	0.004	0.004	0.004	0.004	0.004	0.004	0.004	0.045
Total	1.028	0.937	1.028	0.995	1.028	0.294	0.304	0.304	0.294	0.304	0.294	0.304	7.112
WSI	7.3	8.0	8.0	6.8	6.9	0.7	0.1	0.1	0.5	1.2	1.7	2.0	0.9

The spatial variations of groundwater recharge of target area TS3 has been presented in Figure 6.24. The area is strongly dissected with v-shaped valleys The highest values of over 100 mm y^{-1} were observed in valley areas with groundwater recharge on the hillslopes mostly being less than 10 mm y^{-1}.

6.12 Discussion

The target areas show a large variation in hydrological status, which is mainly related to the large differences in precipitation received by the areas. The annual average precipitation varies between 34 mm y^{-1} in AF1-r to 2093 mm y^{-1} in BD1. This impacts evapotranspiration rates, which are low in the low rainfall areas and level off to a maximum of about 600 mm y^{-1} in the high-rainfall areas, as shown in Figure 6.25. River runoff is also low when annual rainfall is less than 300 mm y^{-1} and then increases to above 1200 mm y^{-1} when rainfall exceeds 2000 mm y^{-1} (Figure 6.26). Groundwater recharge is low when precipitation is lower than 400 mm y^{-1} and increases to above 100 mm y^{-1} when average annual precipitation exceeds 1000 mm y^{-1} (Figure 6.27). The water demand also increases with increasing precipitation, as shown in Figure 6.28. These relations provide information that can be used to extrapolate the findings to other areas in the region. The difference in precipitation also impacts the land cover of the target areas, with the arid lands being used as rangelands and agriculture being an important land cover in the areas with precipitation above 1000 mm.

Based on the recharge values, three rainfall classes can be defined. Class I includes the areas with rainfall below 400 mm that experience very little recharge and where the demand for water is also low, being limited by the environmental conditions. Class II contains target areas with precipitation between 400 and 1000 mm y^{-1}. These areas experience groundwater recharge below 200 mm y^{-1} (Figure 6.27), similar moderate surface runoff values (Figure 6.26) and increasing water demand (Figure 6.28). Class III represents areas with average rainfall above 1000 mm y^{-1} where surface runoff exceeds

the groundwater recharge (>200 mm y^{-1}) and where demand is also higher to match the increased availability of water resources.

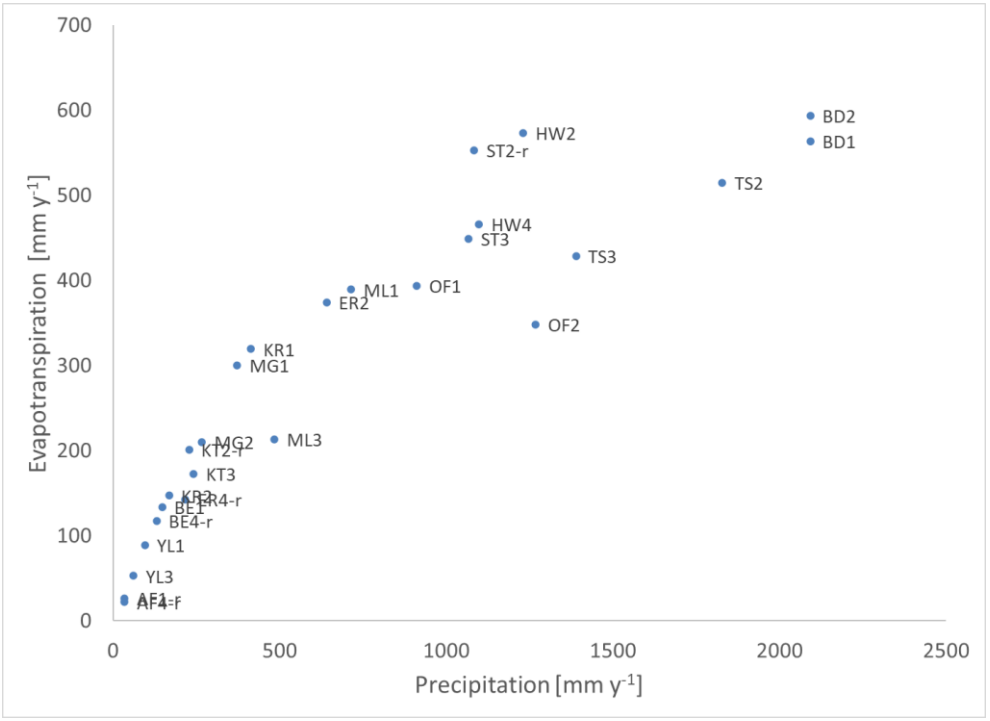

Figure 6.25. Relation between annual average precipitation and evapotranspiration for the various target areas.

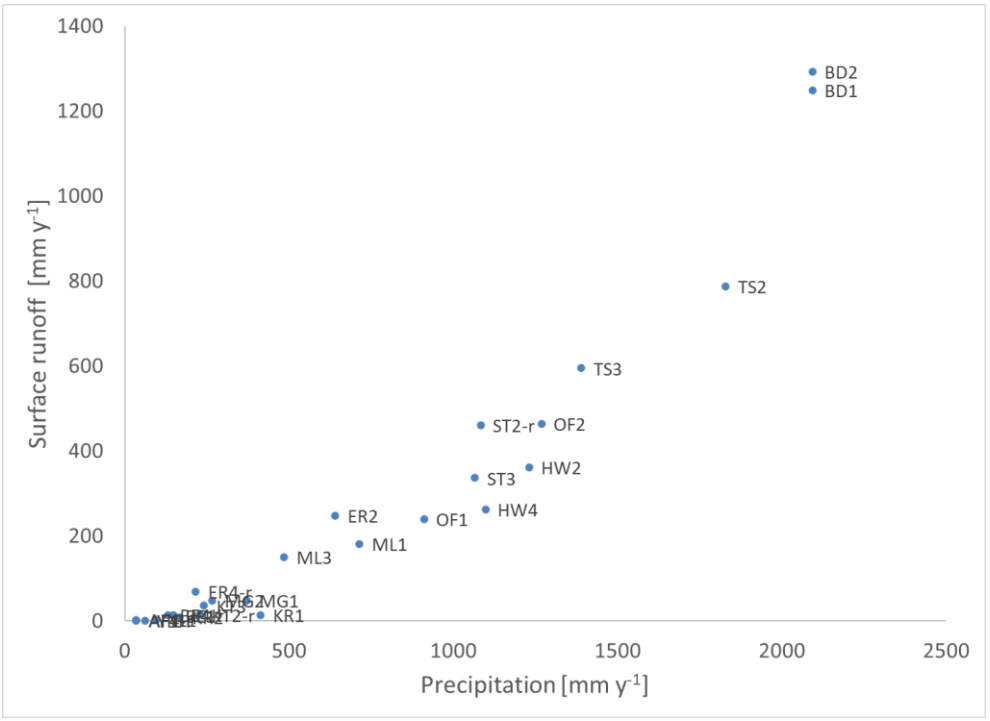

Figure 6.26. Relation between annual average precipitation and river runoff for the various target areas.

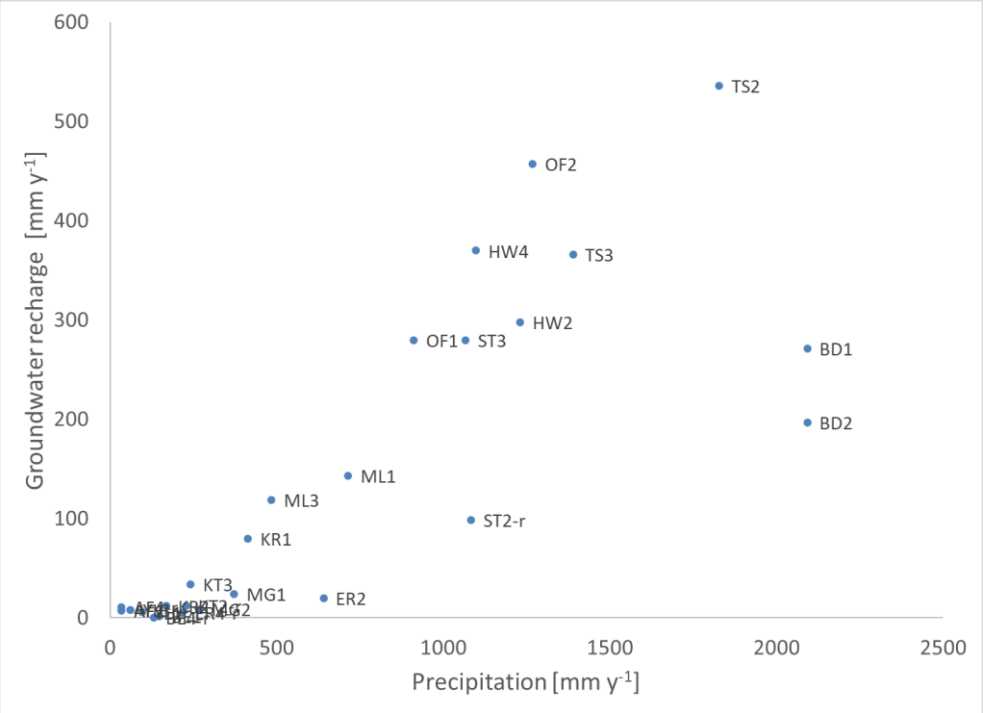

Figure 6.27. Relation between annual average precipitation and shallow and deep aquifer groundwater recharge for the various target areas.

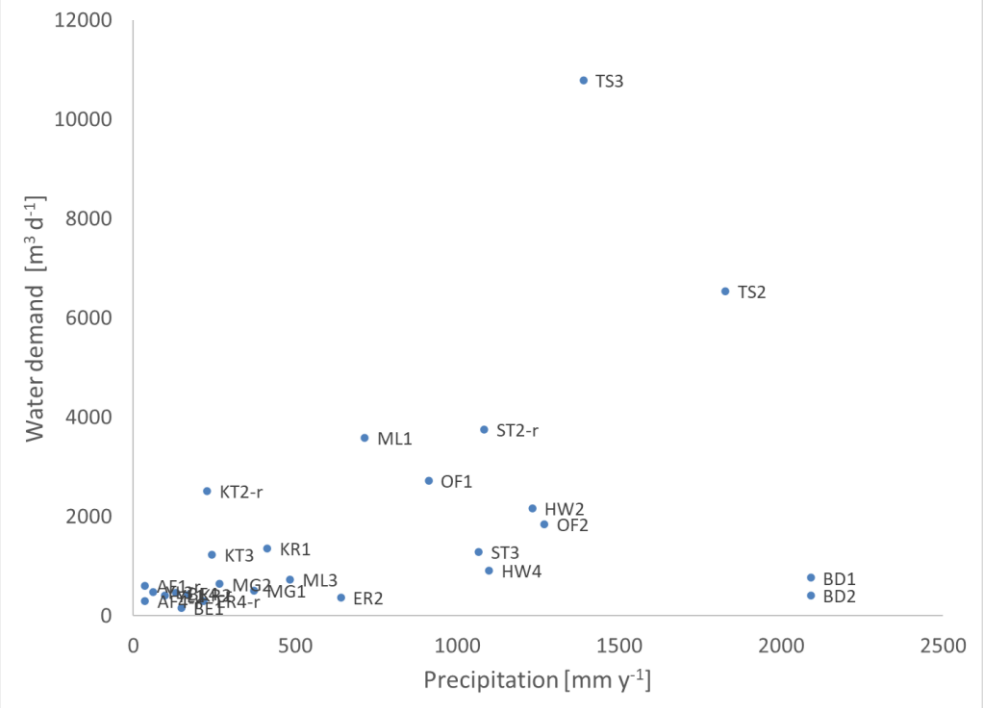

Figure 6.28. Relation between annual average precipitation and estimated target area total water demands.

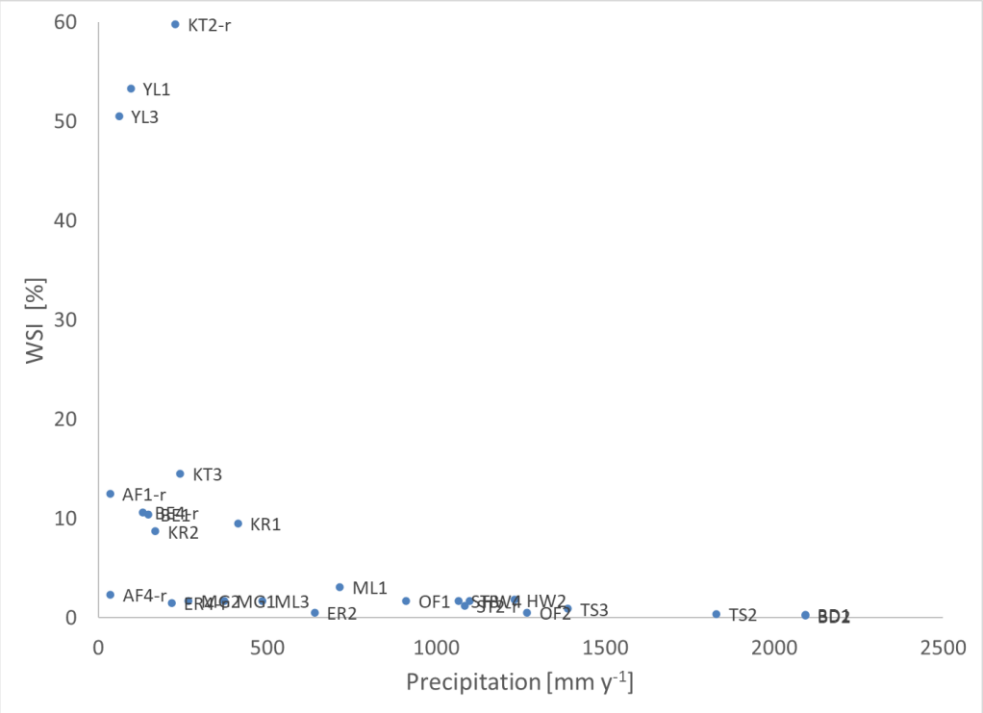

Figure 6.29. Relation between annual average precipitation and the water scarcity index (WSI) for the target areas.

Figure 6.29 shows the relation between the annual precipitation and the WSI. Target areas KT2-r, YL1 and YL3 have high WSI values and corresponding water shortage. Most of the Class I type have elevated WSI values and may also have monthly WSI values exceeding the limit. WSI values for Class II and Class III sites with rainfall above 400 mm y^{-1} remain low.

6.13 Conclusions and recommendations

Rainfall in the 26 target areas is highly variable ranging from less than 200 mm y^{-1} to over 2000 mm y^{-1}. This has a large impact on the water resources availability in the target area and the land use practiced. The more humid areas are used for agriculture, whereas the arid areas are used as rangeland, with livestock water demand probably being only in the wet season when pastoralists are present in the area. Water balances and demands have been calculated for the target areas. Target areas KT2-r, YL1 and YL3 show WSI values above the threshold of 40%, whereas the other areas have low WSI values, which suggests that there is potential for (ground)water resources development. Actual development of extraction points would depend on geological conditions and the local presence of aquifers that can be tapped.

The target area boundaries are not related to hydrological landscape units. This implies that increased (surface) water extraction upstream of target areas, or in the target areas will impact on the (downstream) water users, such as in the cases of target areas ML3 and ML1 and OF1 and OF2 that are linked through a major perennial river. In this sense, the current focus on the target areas has its limitations for evaluation of the potential for expansion of water extraction.

When interventions are being prepared a field reconnaissance visit should be made for verification the model simulations.

The Soil Water Assessment Tool was used to calculate the water balance and present the spatial variation of groundwater recharge in the target areas. The model output strongly depends on the land cover, soil and meteorological input to provide accurate information. The Globcover land cover data with 300 m resolution was observed not to match the ground land cover conditions in some of the target areas, where mosaic vegetation was mapped but agriculture observed. This could be related with the relatively small size of the fields, relative to the resolution of the data. Globcover did also not indicate irrigated agriculture in any of the target areas, whereas visual satellite image interpretation showed that irrigated agriculture was practiced. It is therefore important that land cover data are verified in the field to obtain accurate local information on the (agricultural) land cover in the area, including the fraction of irrigated land.

For better groundwater recharge estimates, the soil map should be modified to include geological information on where recharge is possible and enhanced, for instance in fracture zones, which could then be used to provide spatial variation in the groundwater parameters of the model. Such information is now available in this report but could not be incorporated in the modelling study.

The SWAT model was universally applied with calibrated parameters for the Geba River catchment. A comparison of simulated and observed discharge at Emba Madre station in the Tekeze River Basin showed that the model seemed to overestimate the surface runoff in the wet season. In addition, soil and land cover conditions are very different in the eastern target areas, which may impact the quality of the simulations. As such it would be advised to perform calibration of the model on different catchments in the region and use the calibration parameters to the target areas in these regions.

The study has been based mostly on public data and modelling. There was no direct data available for the target areas to allow assessment of fluxes of water travelling through the areas in larger rivers, the number and concentration centers of people in the areas, detailed land use maps showing locations of rainfed and irrigated agriculture and soil maps.

Discharge station data showed many gaps and missing data for the dry seasons. More information is needed on the surface water runoff, as well as on groundwater resources and annual variations in hydraulic heads in the aquifers. This requires the development of a monitoring network in these areas.

7 Hydrogeology of target areas in the Tselemt Woreda

The hydrogeology of the target areas TS3 (Tselemt 1) and TS2 (Tselemt 2) is inferred mainly from geological map, geomorphological features and structural setup. The area is drained by the middle catchment of the Tekeze River.

TS3 (Tselemt 1) target area falls between two streams flowing towards north to join the Tekeze River. It is characterized by mainly moderately productive Ashange basalt and Adigrat sandstone. The metavolcanic defined by Tsaliet group covers most of the northern half of the target area. This formation is found to be law productive because of the topographic setting it occupies. Several shallow and deep wells are drilled in the Ashange basalt and Adigrat sandstone. Among the moderate productive aquifer the Ashange basalt accounts more than 80 percent of surface area. The composition of this huge volcanic material is mainly basaltic. The high degree of fracturing and weathering and its topographic and geographic location makes it to serve as good aquifer and recharge zone.

TS2 (Tselemt 2) target area is part of the Tekeze basin, where both groundwater and surface water flows from south to north to join main the Tekeze River. A tributary of the Tekeze River divide the target area into two portions. Other major tributary of the Tekeze River flows along the eastern side of the target area. This drainage system and the major faults that follow the drainage pattern controls the groundwater storage and movement in this target area. The dominant hydro-lithologic units in the target area are Werii slate followed by Adigrat sandstone and Ashange basalt. Groundwater occurs in the Werii slate within weathered and fractured zones which can transmit and store water. Slates and phyllites have abundant quartz veins with fractures, and where they are crossed by groundwater movement they may hold considerable quantities of ground water.

The hydro-stratigraphic units in the Tselemt Woreda Target areas of TS3 (Tselemt 1) and TS2 (Tselemt 2) can be classified into three broad hydro-stratigraphic units:

- Low productive metavolcanic basement rocks represented by Tsaliet group;
- Moderately productive Adigrat sandstone;
- Moderately productive Ashange basalt.

TS3 (Tselemt 1) is mainly characterized by fractured and weathered Ashange basalt and adjoining Adigrat sandstone which are moderately productive. The northern portion is covered by metavolcanics characterized by low productivity. The degree of fracturing, grainsize and the topographic position they occupy determines the groundwater potential of this formations. The availability of the Ashange basalt and Adigrat sandstone in the target area is good sign of moderate groundwater potential. Several

shallow wells, hand dug wells and few deep wells are drilled in both target areas. The maximum well yield in this target area is not more than 1 l/sec indicating limited storage and permeability of the Ashange basalt and Adigrat sandstone. The maximum yield in TS2 (Tselemt 2) is obtained from a deep well near to a river drilled in the Werii slate.

7.1 Aquifer classifications

The hydro-stratigraphic units of Target area TS3 (Tselemt 1) and TS2 (Tselemt 2) can be grouped into the following aquifer classes:

- Low productive fissured aquifers (T = 0.1 – 1 m^2/d, q = 0.001– 0.01 l/s/m, Q = 0.05 – 0.5 l/s for wells and/or springs in which flow is mainly developed in irregular system of fissures & Weathered mantle of crystalline rocks. Moderate to highly productive in occasional cases in the fault fractures. These types of aquifers are mainly associated with the metavolcanic basement rocks;
- Moderately productive Fissured/porous aquifers (T = 1 – 10 m^2/d, q = 0.01 – 1 l/s/m, Q = 0.5 – 5 l/s for wells). This type of aquifers is represented by Adigrat sandstone;
- Moderately productive fissure aquifers (T = 1 – 10 m^2/d, q = 0.01 – 1 l/s/m, Q = 0.5 – 5 l/s for wells). It is mainly represented by Ashange basalt and Werii slate.

7.2 Groundwater occurrence and flow systems

The geology of both the Woreda and the target area is mainly characterized by the Ashange basalt, Adigrat sandstone, metasediments and metavolcanics. In target area TS3 (Tselemt 1) the elevated land on the southern side is characterized by highly dissected rugged Ashange basalt. The topographic gradient and the existing structures facilitate North ward movement of groundwater. The primary porosity and existing structures encourages northward flow of groundwater from southern side. Several springs, shallow wells and hand dug wells are aligned along SSE-NNW direction. Groundwater occurrence in the Ashange basalt is mainly attributed to the primary porosity during lava emplacement and secondary porosity associated with columnar joints and fracturing. The basalt plays an important role as groundwater reservoir in both target areas. Adigrat sandstone is found next to the basalt at lower elevation forming cliffs because of its resistance to weathering. Generally it plays an important role by recharging the downstream groundwater system, but under favorable topographic position it may yield sufficient amount of water to shallow and deep wells. The metavolcanic in Tselemt 1 target area has lower significance as aquifer because of limited fracturing and weathering. The maximum yield recorded in the target area is 6.5 l/s from wells drilled in Werii Slate. This implies the role that major structures play in groundwater occurrence. The Woreda receives high rainfall. The average annual rainfall at May Tsebri is about 1286 mm. Both target area receives direct recharge from rainfall facilitated by Fracturing, sandy soil and modest vegetation cover. Moreover both target areas are near to the foot of local hills, enabling them to receive recharge from floods during the rainy seasons. Generally the groundwater flow follows the topographic gradient.

7.3 Surface and groundwater interaction

The target areas in the Woreda are found near the mouth the Tekeze River tributaries namely. Though the area may not have a direct interaction the influence of the river can be traced in by existence of several shallow wells and springs near the rivers.

7.4 Groundwater resources potential estimates

The groundwater resource potential assessment of a given area can be approached by its availability, accessibility and sustainability. The Target area is mainly characterized by moderate productive weathered and fractured Hashange basalt, metasediments composed of werii slate, Metavolcanic defined by Tsaliet group and Adigrat sandstone. The woreda receives high rainfall. The average annual rainfall at May Tsebri is about 1286 mm. Both target area receives direct recharge from rainfall facilitated by Fracturing, sandy soil and modest vegetation cover. Moreover both target areas are near to the foot of local hills, enabling them to receive recharge from floods during the rainy seasons. Generally the groundwater flow follows the topographic gradient. The recharge is estimated using wetsSpass model resulting mean recharge value of 93 mm/year. The expected amount of annual groundwater recharge per target area is about 42041 m^3/day in TS3 (Tselemt 1) and 56054 m^3/day in TS2 (Tselemt 2).

7.5 Conceptual models

A conceptual (hydrogeological) model of a groundwater system is defined as “a descriptive representation of a groundwater system that incorporates an interpretation of the geological and hydrological conditions” (Barnett et.al, 2012; pp.24). Basically conceptual model consists of Physical and Hydrogeological framework. The hydroithologic characteristics and subsequent groundwater occurrence in the target area is explained in the previous section. The hydrogeological set up of the area favors diffuse or direct recharge mechanism. The three dimensional framework was analyzed from the geologic cross section to reveal that the groundwater movement is mainly controlled by topography and existing weathering and fracture features. As the dominant storage is in fractured and weathered mantle of ashange basalt and werii slate the groundwater flow system is assumed to be shallow (Figures 7.1 and 7.2).

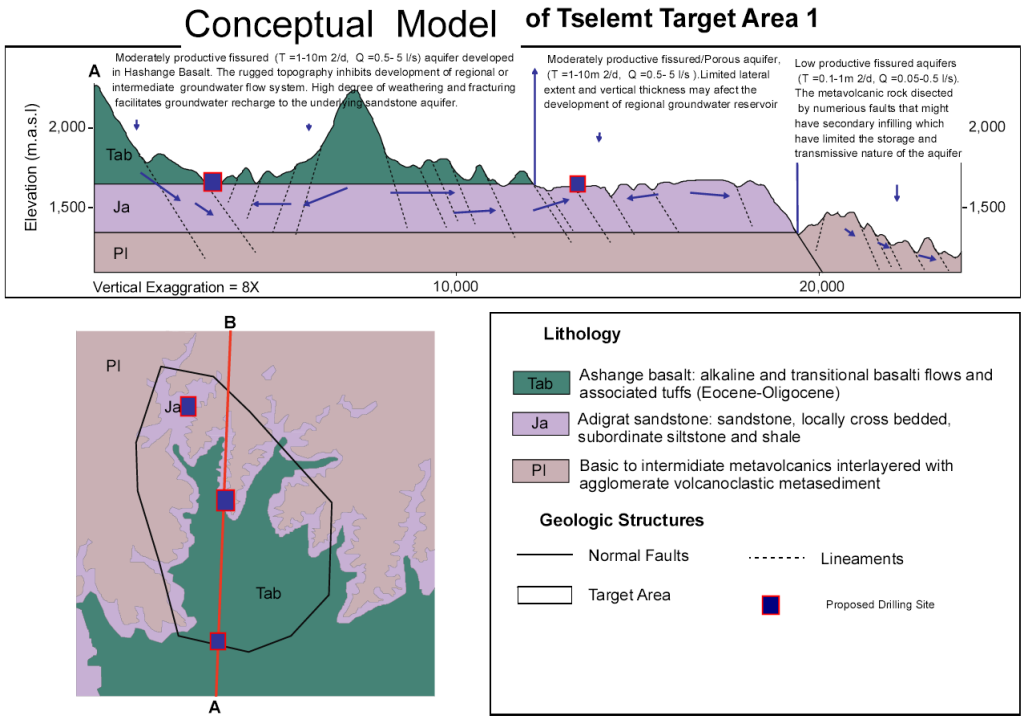

Figure 7.1. Conceptual model for target area Tselemt TS2.

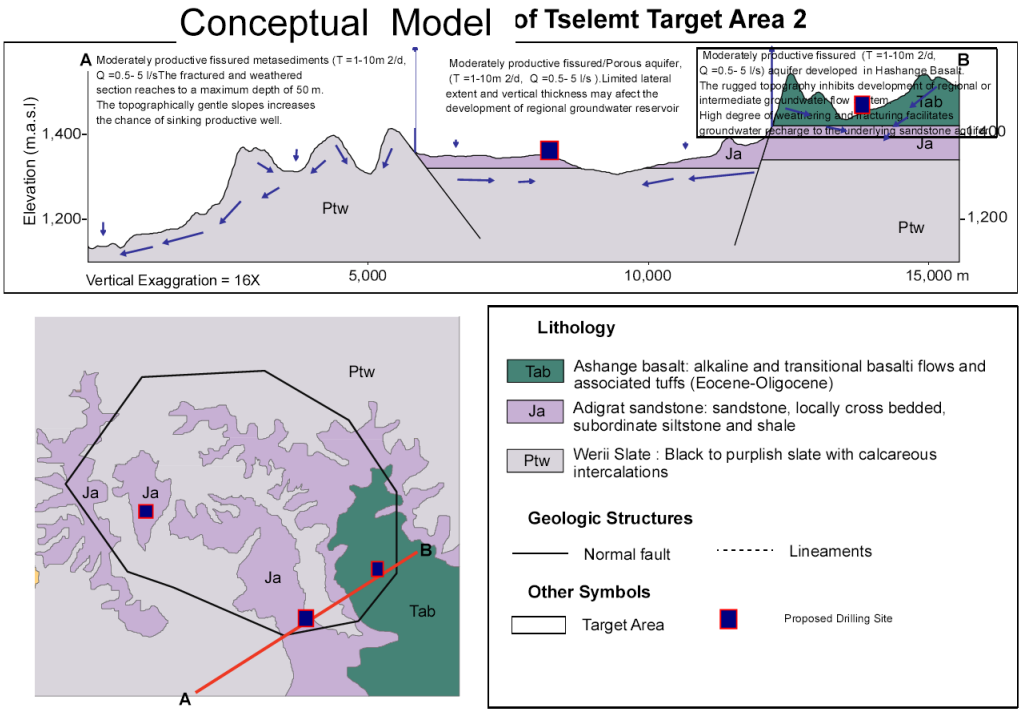

Figure 7.2. Conceptual model for target area Tselemt TS3.

7.6 Conclusions and recommendations

Though the area is characterized by mainline crystalline rocks careful application of existing information and previous field experiences has led us to select potential drilling sites for shallow well that might yield sufficient amount of water for communities.

8 Hydro-geochemistry

Previous studies conducted around the target area reveals that most of the shallow groundwater are fresh with total dissolved solid less than 1000 mg/l. Generally samples from metasediments have higher dissolved solids with electrical conductivity ranging from 180 to 940 µS/cm with mean value of 650. Adigrat sandstone, metavolcanics and the ashange basalt have relatively lower dissolved solids.

From previous analysis in the nearby area the groundwater is dominated by Calcium followed by Magnesium and sodium, while the dominant anion by far is Bicarbonate followed by sulphate and chloride. Generally the groundwater type from metasediments is mainly Mg-Ca-HCO3 whereas samples collected from metavolcanics and ashange basalt are Ca-Mg-HCO3 type. The piper diagram below shows distinction between samples collected from the metasediments and the other rock types. This is mainly governed by the possible dominance of carbonate minerals such as calcite in the metasediments.

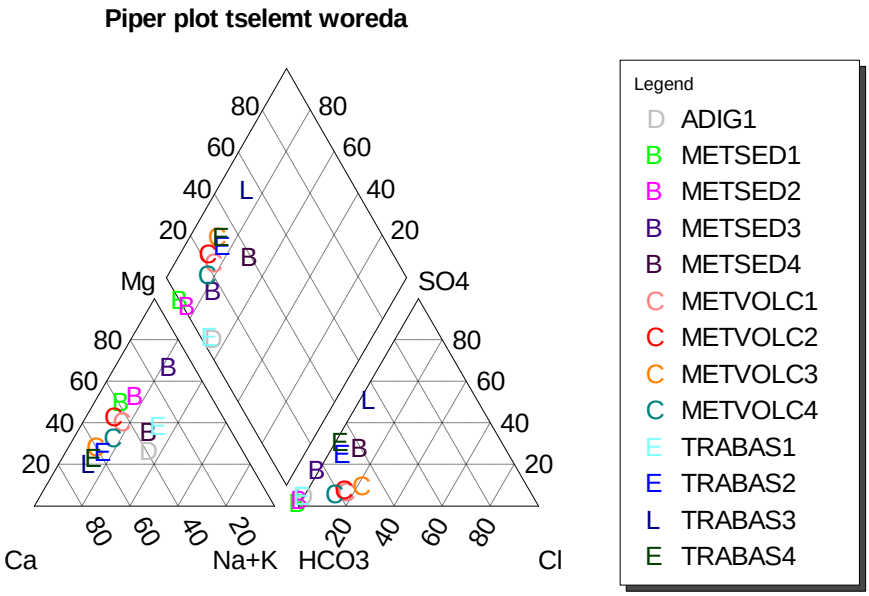

Figure 8.1. Piper diagram for the existing water sources in Tselemt woreda.

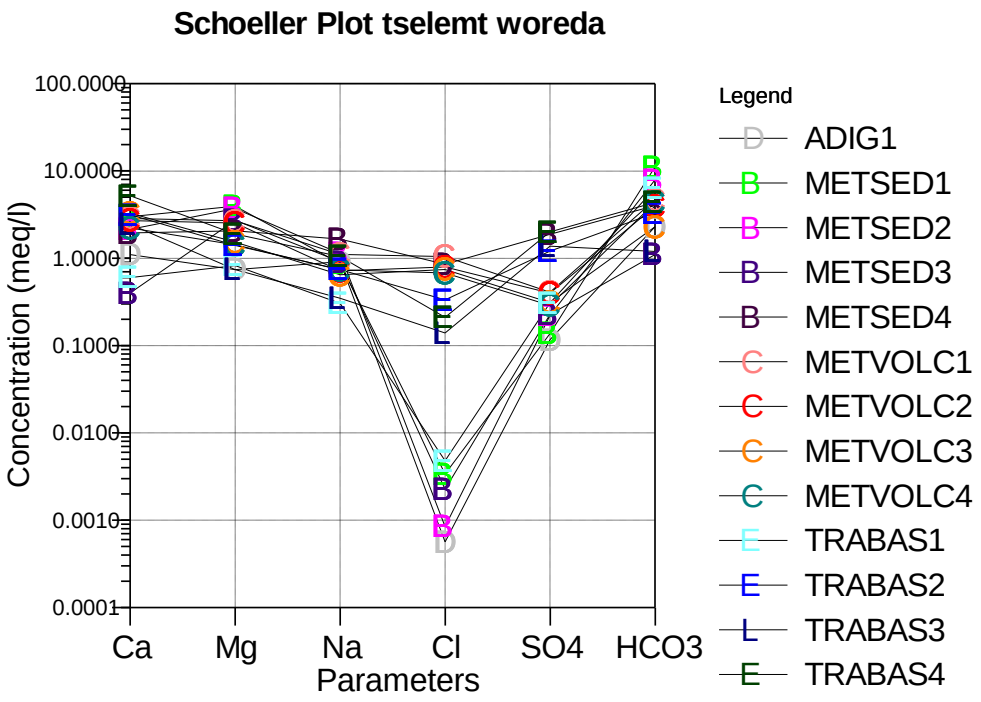

Figure 8.2. Schoeller diagram for existing water points in the Tselemt woreda.

Considering the above assessment the groundwater in the woreda have not shown major quality problems that surpasses the WHO standards.

9 Potential Drilling Sites

9.1 Location and Accessibility of Drilling Sites

In target area TS3 (Tselemt 1) and TS2 (Tselemt 2) based on the geology, hydrogeological characteristics and accessibility of the area four target drilling sites are selected. The reference ID's of the locations are shown in Table 9.1. Maps of the proposed target sites can be found in the Drilling Sites Annex.

Table 9.1. Proposed drilling sites in Tselemt target areas.

Target Area	Reference ID
TS3 (Tselemt 1)	TS-3-TW1
TS2 (Tselemt 2)	TS-2-TW1

9.2 Hydrogeological situation at the drilling sites.

The drilling sites selected for TS3 (Tselemt 1) is situated at the foot of a small hill near to stream flowing northward. The main lithology is Ashange basalt and Adigrat sandstone. The jointing, fracturing and weathering contributes for groundwater storage and movement that will enable to yield reasonably good amount of water to shallow well. The proposed well site for target area TS2 (Tselemt 2) is situated on near the bank of small stream flowing northward to the Tekeze River covered by mainly Adigrat Sandstone. Nearby faults, joints and intergranular porosity enhance groundwater storage and movement. Faults and local fissures contributes for the groundwater reservoir that will yield sufficient amount for shallow wells.

9.3 Well drilling

9.3.1 Depth and drilling diameter

Most shallow wells in the nearby area have an average depth of 50 meter. Therefore shallow wells with maximum depth of 60 meter is recommended in both sites.

9.3.2 Drilling methods

The drilling sites are mainly underlain by hard formations and; thus, the best drilling method would be DTH method. However, drilling situation such as collapsing layers may be encountered. Thus, a drilling rig with a combined capacity of both DTH and mud circulation system is proposed. The target areas are situated in water scarce areas and supply of drilling water would be the main challenge. Thus the drilling company has to have sufficient capacity to transport water for drilling from a long distance with water tanker/s.

9.3.3 Materials for casing and screens

The proposed drilling is deep and the water quality is not aggressive and thus, steel casings and screens are proposed. However, thick walled deep well uPVC casings if made available it is more advantageous.

9.3.4 Proposed well design

A detailed well design requires conducting Geophysical investigation on the particular drilling site. Therefore, only a generic well design can be given at this stage, which is shown below.

Generic design for a well with a depth of 60 meters:

- **Drilling depth:** Recommended drilling depth is 60 m;
- **Diameter of the well:** Recommended diameter of the well is 10";
- **Casing types and arrangement:**

Depth (m)	Thickness (m)	Casing		
		Type	Diameter (inch)	Length (m)
0 to 20	20	PVC blind casing	6	20
20 to 45	25	PVC screen casing	6	25
45 to 60	15	PVC blind casing	6	15

10 References

Adeba, D., Kansal, M.L., Sen, S., (2015). Assessment of water scarcity and its impacts on sustainable development in Awash basin, Ethiopia. Sustain. Water Resour. Manag. 1, 71–87. https://doi.org/10.1007/s40899-015-0006-7

Allen, R.G., Pereira, L.S., Raes, D., Smith, M., (1998). Crop evapotranspiration-Guidelines for computing crop water requirements-FAO Irrigation and drainage paper 56. Fao Rome 300, D05109.

Arısoy, M. Ö., Dikmen, Ü. (2013). Edge detection of magnetic sources using enhanced total horizontal derivative of the tilt angle.

Arnold, J.G., Moriasi, D.N., Gassman, P.W., Abbaspour, K.C., White, M.J., Srinivasan, R., Santhi, C., Harmel, R.D., Griensven, A. van, Liew, M.W. van, Kannan, N., Jha, M.K., (2012). SWAT: Model use, calibration and validation. Trans. ASABE 55, 1491–1508.

Asrat, A., Gleizes, G., Barbery, P., & Ayalew D. (2003). Magma emplacement and mafic-felsic magma hyberdiztion: Structural eviedence from the Pan-African Negash pluton, Northern Ethiopia. Journal of Structural Geology, 25(9), 1451-1469.

Awulachew, S.B., Erkossa, T., Namara, R.E., (2010). Irrigation potential in Ethiopia. Constraints and opportunities for enhancing the system. International Water Management Institute, Addis Ababa, Ethiopia.

Ayalew, D.& Yirgu, G., (2003). Crustal contribution to the genesis of Ethiopian plateau rhyolitic ignimbrites: basalt and rhyolite geochemical provinciality, J. geol. Soc. Lond., 160, 47–56.

Ayalew, D., Barbey, P., Marty, B., Reisberg, L., Yirgu, G. & Pik, R. (2002). Source, genesis and timing of giant ignimbrite deposits associated with Ethiopian continental flood basalts. Geochimica et Cosmochimica Acta, 66, 1429-1448.

Balist, J., Malekmohammadi, B., Jafari, H.R., Nohegar, A., Geneletti, D., (2022). Modeling the supply, demand, and stress of water resources using ecosystem services concept in Sirvan River Basin (Kurdistan-Iran). Water Supply ws2021436. https://doi.org/10.2166/ws.2021.436

Beiki, M. (2010). Analytic signals of gravity gradient tensor and their application to estimate source location. Geophysics, 75(6), I59–I74. https://doi.org/10.1190/1.3493639

Beyene, A. & Abdelsalam, M. (2005). Tectonics of the Afar Depression: A review and synthesis. J. African Earth Sci., 41, 41-59.

Beyth, M. (1972) “The geology of central and western Tigre, Ethiopia” Draft report, Ministry of Mines, Ethiopian Institute of Geological Surveys, Addis Ababa, Ethiopia.

Blakely, R. J. (1995). Potential Theory in Gravity and Magnetic Applications. Cambridge University, Cambridge. https://doi.org/10.1017/CBO9780511549816

Boithias, L., Acuña, V., Vergoñós, L., Ziv, G., Marcé, R., Sabater, S., (2014). Assessment of the water supply:demand ratios in a Mediterranean basin under different global change scenarios and mitigation alternatives. Sci. Total Environ. 470-471C, 567–577. https://doi.org/10.1016/j.scitotenv.2013.10.003

Boithias, L., Acuña, V., Vergoñós, L., Ziv, G., Marcé, R., Sabater, S., (2014). Assessment of the water supply:demand ratios in a Mediterranean basin under different global change scenarios and mitigation alternatives. Sci. Total Environ. 470-471C, 567–577. https://doi.org/10.1016/j.scitotenv.2013.10.003

Bosellini, A., Russo, A. & Assefa, G., (2001). The Mesozoic succession of Dire Dawa, Harar province, Ethiopia, J. Afri. Earth Sci., 32, 403–417.

Buchhorn, M., Smets, B., Bertels, L., Roo, B.D., Lesiv, M., Tsendbazar, N.-E., Li, L., Tarko, A., (2021). Copernicus Global Land Service: Land Cover 100m: version 3 Globe 2015-2019: Product User Manual. Zenodo. https://doi.org/10.5281/zenodo.4723921

Cibin, R., Sudheer, K.P., Chaubey, I., (2010). Sensitivity and identifiability of stream flow generation parameters of the SWAT model. Hydrol. Process. 24, 1133–1148. https://doi.org/10.1002/hyp.7568

Climate Hazards Centre, n.d. CHIRPS: Rainfall Estimates from Rain Gauge and Satellite Observations | Climate Hazards Center - UC Santa Barbara [WWW Document]. CHIRPS Rainfall Estim. Rain Gauge Satell. Obs. URL https://www.chc.ucsb.edu/data/chirps (accessed 4.10.20).

Cooper, G. R. J., Cowan, D. R. (2006). Enhancing potential field data using filters based on the local phase. Computers & Geosciences, 32(10), 1585–1591. https://doi.org/10.1016/j.cageo.2006.02.016

CSA, (2013a). Population Projections for Ethiopia 2007-2037. Central Statistical Agency, Addis Ababa, Ethiopia.

CSA, (2013b). Inter-censal Population Survey Report. Central Statistical Agency, Addis Ababa, Ethiopia.

CSA, (2017). Population Projection of Ethiopia for All Regions at Woreda Level from 2014 – 2017. Central Statistical Agency, Addis Ababa, Ethiopia.

CSA, (2021a). Agricultural sample survey. Volume II. Report on livestock and livestock characteristics (private peasant holdings). (Statistical Bulletin No. 589). Central Statistical Agency, Addis Ababa, Ethiopia.

CSA, (2021b). Population Size by Sex, Region, Zone and Woreda: July 2021. Central Statistical Agency, Addis Ababa, Ethiopia.

Davis, J. C., Sampson, R. J. (1986). Statistics and data analysis in geology (Vol. 646). Wiley New York et al.

Dinku, T., Funk, C., Peterson, P., Maidment, R., Tadesse, T., Gadain, H., Ceccato, P., (2018). Validation of the CHIRPS satellite rainfall estimates over eastern Africa. Quaterly J. R. Meteorol. Soc. 154, 292–312.

Dobrin, M. B. (1976). Introduction to geophysical prospecting Mc Graw-Hill Publ. Co., New York.

Ebinger, C.J., Yemane, T., WoldeGabriel, G., Aronson, J.L.& WalterR.C., (1993). Late Eocene–Recent volcanism and faulting in the southern main Ethiopian rift, J. geol. Soc. Lond., 150, 99–108.

Farr, T.G., Rosen, P.A., Caro, E., Crippen, R., Duren, R., Hensley, S., Kobrick, M., Paller, M., Rodriguez, E., Roth, L., Seal, D., Shaffer, S., Shimada, J., Umland, J., Werner, M., Oskin, M., Burbank, D., Alsdorf, D., 2007. The Shuttle Radar Topography Mission. Rev. Geophys. 45. https://doi.org/10.1029/2005RG000183

Fritz, H., Abdelsalam, M., Ali, K., Bingen, B., Collins, A., Fowler, A., Ghebreab, W., Hauzenberger, C., Johnson, P., Kusky, T., Macey, P., Muhongo, S., Stern, R., Viola, G., (2013). Orogen styles in the East African Orogen: a review of the Neoproterozoic to Cambrian tectonic evolution. Journal of African Earth Sciences 86, 65–106.

Garland, C.R. (1980). Geology of the Adigrat area. Ministry of Mines; Memoir, No. 1, Addis Ababa, Ethiopia.

Hagos, E.Y., (2005). Development and management of irrigated lands in Tigray, Ethiopia. (PhD Thesis). Wageningen University, UNESCO-IHE Institute for Water Education, Wageningen, The Netherlands.

Haile, G., G., T.G., Kifle, M., Gebremedhin, T., (2019). Effects of irrigation scheduling and different irrigation methods on onion and water productivity in Tigray, northern Ethiopia. https://doi.org/10.1101/790105

Hayward, N. J., & C. J. Ebinger (1996). Variations in the long-axis segmentation of the Afar rift system, Tectonics, 15, 244–257.

Hofman, C., Courtillot, V., Feraud, G., Rochette, P., Yirgu, G., Ketefo, E.& Pik, R., (1997). Timing of the Ethiopian flood basalt event and implications for plume birth and global change, Nature, 389(6653), 838–841.

Hofstetter, R., & Beyth, M., (2003). The Afar Depression: interpretation of the 1960–2000 earthquakes, Geophys. J. Int., 155, 715–732.

Howard, G., Bartram, J., (2003). Domestic Water Quantity, Service Level and Health (No. WHO/SDE/WSH/03.02). World Health Organization, Geneva, Switzerland.

Hunegnaw, A., Sage, L., & Gonnard, R., (1998). Hydrocarbon potential of the intra-cratonic Ogaden Basin SE Ethiopia: Journal of Petroleum Geology, v. 21, p. 401–425. Izzeldin, A.Y. Seismic, gravity and magnetic surveys in the central part of the Red Sea,

their interpretation and implications for the structure and evolution of the Red Sea. Tectonophysics 143 (1987), pp. 269–306.

Ibraheem, I. M., Gurk, M., Tougiannidis, N., Tezkan, B. (2018). Subsurface investigation of the Neogene Mygdonian Basin, Greece using magnetic data. Pure and Applied Geophysics, 175(8), 2955–2973. https://doi.org/10.1007/s00024-018-1809-x

Jacobsen, B. H. (1987). A case for upward continuation as a standard separation filter for potential-field maps. Geophysics, 52(8), 1138–1148. https://doi.org/https://doi.org/10.1190/1.1442378

Joint Research Centre (European Commission), Thiombiano, L., Yemefack, M., Van Ranst, E., Spaargaren, O., Micheli, E., Kilasara, M., Montanarella, Luca, Jones, R., Hallett, S., Dampha, A., Gallali, T., Deckers, J., Breuning-Madsen, H., Jones, A., Brossard, M., Jones, Arwyn, Le Roux, P., Dewitte, O., Jones, Robert, Montanarella, L., Zougmoré R, (2013). Soil atlas of Africa. Publications Office of the European Union, LU.

Kebede Hailemichael, Alemu, A., Fisseha, S. (2020). Upward continuation and polynomial trend analysis as a gravity data decomposition, case study at Ziway-Shala basin, central Main Ethiopian rift. Heliyon, 6(1), e03292. https://doi.org/10.1016/j.heliyon.2020.e03292

Kebede, B., Mammo, T. (2021). Processing and interpretation of full tensor gravity anomalies of Southern Main Ethiopian Rift. Heliyon, 7(4), e06872. https://doi.org/10.1016/j.heliyon.2021.e06872

Lenhart, T., Eckhardt, K., Fohrer, N., Frede, H.-G., (2002). Comparison of two different approaches of sensitivity analysis. Phys. Chem. Earth Parts ABC 27, 645–654. https://doi.org/10.1016/S1474-7065(02)00049-9

Lyngsie, S. B., Thybo, H., Rasmussen, T. M. (2006). Regional geological and tectonic structures of the North Sea area from potential field modelling. Tectonophysics, 413(3–4), 147–170. https://doi.org/https://doi.org/10.1016/j.tecto.2005.10.045

Mammo, T. (2010). Delineation of sub-basalt sedimentary basins in hydrocarbon exploration in North Ethiopia. Marine and Petroleum Geology, 27(4), 895–908. https://doi.org/10.1016/j.marpetgeo.2009.12.009

Mammo, T. (2013). Crustal structure of the flood basalt province of Ethiopia from constrained 3-D gravity inversion. Pure and Applied Geophysics, 170(12), 2185–2206. https://doi.org/10.1007/s00024-013-0663-0

McCartney, M.P., Shiferaw, A., Seleshi, Y., (2008). Estimating environmental flow requirements downstream of the Chara Chara weir on the Blue Nile River, in: Abtew, W., Melesse, A.M. (Eds.), Proceedings. Presented at the Workshop on Hydrology and Ecology of the Nile River Basin under Extreme Conditions, 16-19 June 2008. Sandy, UT, USA, Aardvark Global Publishing, Addis Ababa, Ethiopia, pp. 57–75.

Mengesha, T., Tadiwos, C., Workneh, H. (1996). The geological map of Ethiopia, 1: 2,000,000 scale. Ethiopia: EIGS Addis Ababa.

Mickus, K. L., Aiken, C. L. V, Kennedy, W. D. (1991). Regional-residual gravity anomaly separation using the minimum-curvature technique. Geophysics, 56(2), 279–283. https://doi.org/10.1190/1.1443041

Miller, H. G., Singh, V. (1994). Potential field tilt—a new concept for location of potential field sources. Journal of Applied Geophysics, 32(2–3), 213–217. https://doi.org/10.1016/0926-9851(94)90022-1

Mohr, P.A. & Zanettin, B. (1988). The Ethiopian flood basalt province. In: MacDougall, J.D. (ed) Continental Flood Basalts. Kluwer Academic, Dordrecht, 63-110.

Monteith, J.L., (1965). Evaporation and the Environment, in: Symposium of the Society of Experimental Biology No. 19. pp. 245–269.

Moreira, L.L., Schwamback, D., Rigo, D., Moreira, L.L., Schwamback, D., Rigo, D., (2018). Sensitivity analysis of the Soil and Water Assessment Tools (SWAT) model in streamflow modeling in a rural river basin. Rev. Ambiente Água 13. https://doi.org/10.4136/ambi-agua.2221

Moreira, L.L., Schwamback, D., Rigo, D., Moreira, L.L., Schwamback, D., Rigo, D., (2018). Sensitivity analysis of the Soil and Water Assessment Tools (SWAT) model in streamflow modeling in a rural river basin. Rev. Ambiente Água 13. https://doi.org/10.4136/ambi-agua.2221

Nash, J.E., Sutcliffe, J.V., (1970). River Flow Forecasting through Conceptual Models part I – A Discussion of Principles. J. Hydrol. 10, 282–290.

Neitsch, S.L., Arnold, J.G., Kiniry, J.R., Williams, J.R., (2011). Soil and Water Assessment Tool Theoretical Documentation Version 2009 (Texas Water Resources Institute Technical Report). College of Agriculture and Life Sciences, Texas A&M University, College Station, Texas, USA.

NPC, (2016). Ethiopia Growth and Transformation Plan II (GTP II) (Volume I No. 2015/16-2019/20). National Planning Commission, Federal Democratic Republic of Ethiopia, Addis Ababa, Ethiopia.

Saha, S., Moorthi, S., Pan, H.-L., Wu, X., Wang, Jiande, Nadiga, S., Tripp, P., Kistler, R., Woollen, J., Behringer, D., Liu, H., Stokes, D., Grumbine, R., Gayno, G., Wang, Jun, Hou, Y.-T., Chuang, H., Juang, H.-M.H., Sela, J., Iredell, M., Treadon, R., Kleist, D., Van Delst, P., Keyser, D., Derber, J., Ek, M., Meng, J., Wei, H., Yang, R., Lord, S., van den Dool, H., Kumar, A., Wang, W., Long, C., Chelliah, M., Xue, Y., Huang, B., Schemm, J.-K., Ebisuzaki, W., Lin, R., Xie, P., Chen, M., Zhou, S., Higgins, W., Zou, C.-Z., Liu, Q., Chen, Y., Han, Y., Cucurull, L., Reynolds, R.W., Rutledge, G., Goldberg, M., (2010). The NCEP Climate Forecast System Reanalysis. Bull. Am. Meteorol. Soc. 91, 1015–1058. https://doi.org/10.1175/2010BAMS3001.1

Sahilu, G., Abate, E., Tadesse, D., (2018). The Study of Water Use and Treated Wastewater Discharge Charge. Water Abstraction Charge Setting for Domestic and Non-Domestic Water Supply (Final report). School of Civil and Environmental Engineering Addis Ababa Institute of Technology (AAiT) Addis Ababa University., Addis Ababa, Ethiopia.

Salem, A. S. K., Campell, S., Derek, J. D., Dickinson, J., Murphy, C. (2011). Interpretation of Tensor Gravity Data Using an Adaptive Tilt Angle Technique. In 73rd EAGE Conference and Exhibition incorporating SPE EUROPEC 2011 (p. cp-238). European Association of Geoscientists & Engineers. https://doi.org/10.3997/2214-4609.20149566

Salem, A., Williams, S., Fairhead, J. D., Ravat, D., Smith, R. (2007). Tilt-depth method: A simple depth estimation method using first-order magnetic derivatives. The Leading Edge, 26(12), 1502–1505. https://doi.org/https://doi.org/10.1190/1.2821934

Shiferaw, A., McCartney, M.P., (2009). Investigating Environmental Flow Requirements at the Source of the Blue Nile River (No. H041853). Addis Ababa University and International Water Management Institute, Addis Ababa, Ethiopia.

Sileshi, Z., Tegegne, A., Tsadik, G.T., (2003). Water resources for livestock in Ethiopia: Implications for research and development, in: Proceedings. Presented at the MoWR/EARO/IWMI/ILRI international workshop, 2-4 December 2002, International Water Management Institute, Addis Ababa, Ethiopia, p. 14.

Smakhtin, V., Revenga, C., Döll, P., (2004). A Pilot Global Assessment of Environmental Water Requirements and Scarcity. Water Int. 29, 307–317. https://doi.org/10.1080/02508060408691785

Srinivasan, R., Zhang, X., Arnold, J., (2010). SWAT Ungauged: Hydrological Budget and Crop Yield Predictions in the Upper Mississippi River Basin. Trans. ASABE 53, 1533–1546. https://doi.org/10.13031/2013.34903

Stern, R.J. (1994). Arc assembly and continental collision in the Neoproterizoic East African Orogen—implication for the consolidation of Gondwanaland, Annual Review Earth Planetary Science 22, pp. 319–351.

Tadesse, T, Hoshino, M., Suzuki, K., & Iizumi, S. (2000). SmNd, RbSr and ThUPb zircon ages of syn- and post-tectonic granitoids from the Axum area of northern Ethiopia. Journal of African Earth Sciences, 30(2), 313–327.

Tadesse, T., (1996). Geology of the Axum area. Geological Survey of Ethiopia, Memoir 9, 192pp.

Tadesse, T., Hoshino, M., & Sawada, Y. (1999). Geochemistry of low-grade metavolcanic rocks from the Pan-African of the Axum area, northern Ethiopia. Precambrian Research, 96(1–2), 101–124.

Tallaksen, L.M., (1995). A review of baseflow recession analysis. J. Hydrol. 165, 349–370.

Tefera, M., Chernet, T., & Haro, W., (1996). Geological Map of Ethiopia: Ethiopian Institute of Geological Surveys, scale 1:2,000,000, 1 p.

Tesfaye, T.W., Dhanya, C.T., Gosain, A.K., (2020). Modeling the impact of climate change on the environmental flow indicators over Omo-Gibe basin, Ethiopia. Model. Earth Syst. Environ. 6, 2063–2089. https://doi.org/10.1007/s40808-020-00813-x

Thiessen, A.H., (1911). Precipitation for large areas. Mon. Weather Rev. 1082–1084.

Tibebe, D., Bewket, W., (2011). Surface runoff and soil erosion estimation using the SWAT model in the Keleta Watershed, Ethiopia. Land Degrad. Dev. 22, 551–564. https://doi.org/10.1002/ldr.1034

Tsegaye H. (1974). Geological map of Adi Arkay map sheet with explanatory side note. Unpublished document, Geological survey of Ethiopia.

UNICEF-UNESCO Report (2003). "Improving Available Information and Drilling Success rate in the Afar Regional State Government": Report and accompanying geological map of the Afar Depression, PP 41.

USDA-NRCS, (2004). Estimation of Direct Runoff from Storm Rainfall (Part 630 Hydrology No. Chapter 10), National Engineering Handbook. United States Department of Agriculture.

van Griensven, A., Meixner, T., Grunwald, S., Bishop, T., Diluzio, M., Srinivasan, R., (2006). A Global Sensitivity Analysis Tool for the Parameters of Multi-Variable Catchment Models. J. Hydrol. 324, 10–23. https://doi.org/10.1016/j.jhydrol.2005.09.008

Vörösmarty, C.J., Green, P., Salisbury, J., Lammers, R.B., (2000). Global Water Resources: Vulnerability from Climate Change and Population Growth. Science 289, 284–288. https://doi.org/10.1126/science.289.5477.284

Williams, J.R., (1969). Flood Routing With Variable Travel Time or Variable Storage Coefficients. Trans. ASAE 12, 0100–0103. http://dx.doi.org/10.13031/2013.38772

Williams, J.R., (1969). Flood Routing With Variable Travel Time or Variable Storage Coefficients. Trans. ASAE 12, 0100–0103. http://dx.doi.org/10.13031/2013.38772

Xie, H., You, L., Dile, Y.T., Worqlul, A.W., Bizimana, J.-C., Srinivasan, R., Richardson, J.W., Gerik, T., Clark, N., (2021). Mapping development potential of dry-season small-scale irrigation in Sub-Saharan African countries under joint biophysical and economic constraints - An agent-based modeling approach with an application to Ethiopia. Agric. Syst. 186, 102987. https://doi.org/10.1016/j.agsy.2020.102987

Yihun, Y.M., (2015). Agricultural water productivity optimisation for irrigated Teff (Eragrostic Tef) in water scarce semi-arid region of Ethiopia (PhD Thesis). Wageningen University, UNESCO-IHE Institute for Water Education, Delft, The Netherlands.

Zhao, C., Nan, Z., Cheng, G., (2005). Evaluating Methods of Estimation and Modelling Spatial Distribution of Evapotranspiration in the Middle Heihe River Basin, China. Am. J. Environ. Sci. 1, 278–285. https://doi.org/10.3844/ajessp.2005.278.285

van Hogendorpplein 4
2805 BM Gouda

Telephone: +31(0)182 – 686 424
Internet: www.acaciawater.com
Email: info@acaciawater.com